# ALGORITHMS FOR BED TOPOGRAPHY RECONSTRUCTION IN GEOPHYSICAL FLOWS

---

A thesis submitted in partial fulfilment of the requirements for the Degree of Doctor of Philosophy in Mechanical Engineering in the University of Canterbury

by **Alelign Fekade Gessese**

UNIVERSITY OF CANTERBURY
*Te Whare Wānanga o Waitaha*
CHRISTCHURCH NEW ZEALAND

**University of Canterbury**

November 2013

---

# Abstract

Bed topography identification in open channel and glacier flows is of paramount importance for the study of the respective flows. In the former, the knowledge of the channel bed topography is required for modelling the hydrodynamics of open channel flows, fluvial hydraulics, flood propagation, and river flow monitoring. Indeed, flow models based on the Shallow Water Approximation require prior information on the channel bed topography to accurately capture the flow features. While in the latter, usable bedrock topographic information is very important for glacier flow modellers to accurately predict the flow characteristics. Experimental techniques to infer the bed topography are usually used but are mostly time consuming, costly, and sometimes not possible due to geographical restrictions. However, the measurement of free surface elevation is relatively easy. Alternative to experimental techniques, it is therefore important to develop fast, easy-to-implement, and cost-effective numerical methods.

The inverse of the classical hydrodynamic problem corresponds to the determination of hydraulic parameters from measurable quantities. The forward problem uses model parameters to determine measurable quantities. New one-shot and direct pseudo-analytical and numerical approaches for reconstructing the channel bed topography from known free surface elevation data is developed for one-dimensional shallow water flows. It is shown in this work that instead of treating this inverse problem in the traditional partial differential equation (PDE)-constrained optimization framework, the governing equations of the direct problem can be conveniently rearranged to obtain an explicit PDE for the inverse problem. This leads to a direct solution of the inverse problem which is successfully tested on a range of benchmark problems and experimental data for noisy and noiseless free surface data. It was found that this solution approach creates very little amplification of noise.

A numerical technique which uses the measured free surface velocity to infer the channel bed topography is also developed. The one-dimensional shallow water equations along with an empirical relationship between the free surface and the depth averaged velocities are used for the inverse problem analysis. It is shown that after a series of algebraic manipulation and integration, the equation governing the inverse problem simplifies to a simple integral equation. The proposed method is tested on a range of analytical and experimental benchmark test cases and the results confirm that, it is possible to reconstruct the channel bed topography from a known free surface velocity distribution of one-dimensional open channel flows.

Following the analysis of the case of one-dimensional shallow water flows, a numerical technique for reconstructing the channel bed topography from known free surface elevation data for steep open channel flows is developed using a modified set of equations for which the zero-inertia shallow water approximation holds. In this context, the shallow water equations are modified by neglecting inertia terms while retaining the effects of the bed slope and friction terms. The governing equations are recast into a single first-order partial differential equation which describes the inverse problem. Interestingly, the analysis shows that the inverse problem does not require the knowledge of the bed roughness. The forward problem is solved using MacCormack's explicit numerical scheme by considering unsteady modified shallow water equations. However, the inverse problem is solved using the method of characteristics. The results of the inverse and the forward problem are successfully tested against each other.

In the framework of full two-dimensional shallow water equations, an easy-to-implement and fast to solve direct numerical technique is developed to solve the inverse problem of shallow open channel flows. The main underlying idea is analogous to the idea implemented for the case of one-dimensional reconstruction. The technique described is a

"one-shot technique" in the sense that the solution of the partial differential equation provides the solution to the inverse problem directly. The idea is tested on a set of artificial data obtained by first solving the forward problem.

Glaciers are very important as an indicator of future climate change or to trace past climate. They respond quickly compared to the Antarctica and Greenland ice sheets which make them ideal to predict climate changes. Glacier bedrock topography is an important parameter in glacier flow modelling to accurately capture its flow dynamics. Thus, a mathematical technique to infer this parameter from measured free surface data is invaluable. Analogous to the approaches implemented for open channel flows, easy-to-implement direct numerical and analytical algorithms are developed to infer the bedrock topography from the knowledge of the free surface elevation in one space dimension. The numerical and analytical methods are both based on the Shallow Ice Approximation and require the time series of the ablation/accumulation rate distribution. Moreover, the analytical method requires the knowledge of a non-zero glacier thickness at an arbitrary location. Numerical benchmark test cases are used to verify the suitability and applicability of the algorithms.

The following papers, based on sections of this thesis, have appeared in international journals or conference proceedings:

1. **Gessese, A. F., M. Sellier, E Van Houten, G. Smart. (2011).** "Reconstruction of river bed topography from free surface data using direct numerical approach in one-dimensional shallow water flow." Inverse Problems **27**.
2. **Gessese, A. F., M. Sellier, E Van Houten, G. Smart. (2011).** "Inferring channel bed topography from known free surface data." 34th World Congress of the International Association for Hydro-Environment Engineering and Research (IAHR), Brisbane, Australia.
3. **Gessese, A. F., G. Smart, C. Heining, M. Sellier, (2012).** "One-dimensional bathymetry based on velocity measurements." Inverse Problems in Science and Engineering (iFirst): 1-17.
4. **Gessese, A., K. Mawanzi Wa, M. Sellier. (2012).** "Bathymetry reconstruction based on the zero-inertia shallow water approximation." Theoretical and Computational Fluid Dynamics (Online First).
5. **Alelign Gessese and Mathieu Sellier, (2012).** "A direct solution approach to the inverse shallow water problem." Mathematical Problems in Engineering, 2012 Hindawi Publishing
6. **Sellier, M., Gessese, A. and Heining, C. (2012).** "Analytical and numerical bedrock reconstruction in glacier flows from free surface elevation data." 23rd International Congress of Theoretical and Applied Mechanics (ICTAM2012), 19-24 Aug 2012, Beijing, China.

# Acknowledgements

I would like to express my deepest appreciation to my supervisor Dr. Mathieu Sellier for giving me the opportunity to do this PhD study and his invaluable supervision, advise, guidance, and encouragement throughout the course of this study. My appreciation also goes to my co-supervisor Dr. Elijah Van Houten for his involvement in the early stages of this research work.

During the course of this study, I have had a chance to work with Dr. Graeme Smart from the National Institute of Water and Atmospheric Research (NIWA), Christchurch, New Zealand. Thus, I would like to thank Dr. Graeme Smart for his several insightful ideas, supervision and involvement in this project.

The financial support from the Departmental Premier Scholarship from the Department of Mechanical Engineering helped me to carry out this research. Without this support, this study would not have been possible.

The collaboration work with Dr. Christian Heining from Bayreuth University, Germany, and the financial support from the New Zealand Royal Society is also acknowledged. It helped me to gain experience to work with experts of fluid mechanics.

I like to express my appreciation to my office mates for creating friendly working environment and fellow students, Kabila Mawanzi Wa and Yannick Muller who have been working with me during their internship in the Department of Mechanical Engineering.

Lastly, my special thanks go to my family (Tatawa, Truye, and Abebe and others), my wife (Firehiwot), and my friends for their continual encouragement and support during my study.

# Table of Contents

# List of figures

# 1. Introduction

## Contents

## 1.1. Background

Geophysical flows are environmental flows characterized by the transfer of mass, momentum and energy which occur in nature. These flows range from, but are not restricted to, large scale atmospheric flows such as atmospheric currents, ocean currents and glacier flows to small scale flows which include small scale buoyancy driven flows, flows involving the interaction of elastic solids and viscous fluids, [1].

On the large scale frame work, these flows encompass the most important part of natural flows and can provide paramount information about the environmental health: glaciers are good indicators of the climate change; river flows are associated with environmental hazards due to flooding or drought; the study of debris flows may indicate the level of the damage that can result [2]; and the study of tsunami flows indicates the extent of inundation and can facilitate tsunami warnings and the evacuation procedures. On a small scale, the importance of geophysical flows is pronounced in engineering applications: interaction of droplets and buoyancy driven bubble flows, for example.

River flows may indicate the health of the environment. The health of river ecosystems can be determined by various factors like; discharge, physical structure and topography of the channel and riparian zone, level of exploitation, water quality [3, 4], nutrient distribution, and amount of sediment transport. Well explored river flow systems are, most of the time, influenced by humans to achieve specific predefined economical, social and ecological objectives, [4]. This may include dams for hydropower, bridges for transport, and irrigation channels. This calls for appropriate waterways management to achieve optimal economical output while maintaining minimal ecological effect on the water body. To achieve this appropriate management of river flows, models may require substantial data related to river flows under investigation.

Experimental assessment techniques for river flow management may range from flood impact assessment to more specific flow parameter measurement. These assessments, although not always possible, provide guidance for management and pre and post-alteration of rivers. Wide and shallow channels, for example, are more sensitive in their wetted perimeter to inflow rate changes than narrow and deep rivers. The assessment results may contain information that can be used to define the minimum environmental flow of a particular river flow system to preserve the health of its ecosystem, [4]. Current research issues at the National Institute for Water and Atmospheric Research (NIWA) of New Zealand show that the extraction of water from a river system may affect an ecosystem at large. Rules are suggested to set abstraction while satisfying the requirement of minimal environmental flow (NIWA Website). However, defining the minimal environmental flow for a particular river is difficult and calls for the knowledge of many variables.

River flow assessment techniques are not only restricted to the definition of minimal environmental flows, but also incorporate many other aspects which are directly or indirectly related to the river. These may include: the study of flood plains, river flow monitoring, parameter measurement, and past, present, and future flood studies. The river flow parameters, discharge, flow area, depth of the flow, quantity of sediment transport, and riverbed and bank topographic shapes will ultimately define the river flow condition. River flow modellers make use of these parameters to identify the ecological, social and economical impact of a river. This is not an easy task and calls for a complex, integrated, system study.

Shallow waters constitute significant proportion of all fresh water bodies. The study of shallow water flows plays an important role in watershed management, flood forecasting, and design of hydrodynamics structures for irrigation purposes. Substantial advancements

of theoretical and numerical modelling, laboratory experimentation and *in-situ* data acquisition of shallow water flows have taken place in the past several decades. Shallow water hydrodynamic modelling requires flow parameters in order generate useful data for a better understanding of the flow dynamics. These parameters may be identified and calibrated experimentally with the help of measurement techniques and numerically with the help of hydrodynamic modelling tools. Many numerical models were developed using the Navier-Stokes or approximate governing equations. The Shallow Water Equations have been used to investigate the shallow water flow dynamics since their first derivation, see e.g. [5, 6] and will be used in part-I of this thesis.

The study of open channel flows requires an understanding of the hydrodynamics of the flow in order to accurately capture its characteristics. Designing and studying engineering projects on rivers, understanding the hydraulic phenomena of the watercourse for water quality control, and prediction of exceptional natural events associated with water flow constitute the three main objectives of the study of open channel flow simulation, [5]. All modelling studies of such applications require well established governing equations along with predefined parameters, boundary conditions and initial conditions. Previous studies show that there has been tremendous progress in the field of hydraulic modelling of open channel flows. However, the representation of accurate channel bed topography is still a challenge, [7-9] . Parameters such as bed elevation and roughness coefficients are required prior to the implementation of the simulation open channel flows. The level of discrepancy in these data will have a direct effect on the simulation results. Thus, in order to accurately predict the hydrodynamics of open channel flows, precise bed topographic elevation data and other hydraulic parameters are required. In [10] and references therein, it is stated that some hydrological models contain conceptual parameters that usually cannot be assessed by *in-situ* data measuring techniques. On the contrary, some models

only use measurable parameters from field surveys. But the procedure is often long and expensive because it is difficult to determine parametric values at each computational grid point of the flow domain.

There have been significant developments in experimental techniques to measure river bathymetry and flow depths. Examples of these techniques for river bathymetry include: interferometric synthetic aperture radar (SAR) digital photogrammetry [9, 11] used for the North Ashburton River, New Zealand; LiDAR and ground survey [7] used for the Yakima and Trinity River Basins in the USA to assess its ability to map bathymetry. However, most experimental techniques to identify the bed elevation can be time consuming [9, 12] and expensive [7, 10] especially for wide, gravel bed and long reach rivers.

Another component of geophysical flows is associated with glacier flows. Glaciers of the world have come to rapidly change with climate variation, [13]. Valley glaciers in mountainous regions have significant effect on people's activities and their economical importance is high when the downstream melt water is used for hydroelectric power generation and irrigation purposes. The other benefit of glaciers for local economies is tourism [14]; this is also true for New Zealand glaciers (Fox and Frank Joseph glaciers). Conversely glaciers may have side effects. Glacier avalanches and outburst of glacier-dammed lakes may cause considerable downstream catastrophes with excessive destruction [15]. At a smaller scale, glacier fluctuations may also have local effects like road washouts.

Glaciers usually react differently to climate changes depending on their size and geographical locations, [14] which makes the generalization of their sensitivity a difficult process. However, most glaciers have similar trends of response to global warming, [13,

15]. Thus glaciers are useful not only for the aforementioned purposes but also for meteorological and climate change studies which are indicators of environmental health. The studies of glaciers may range from historical, climatic, and biological tracing, to specific study of the mechanics and dynamics of glacier flow. In Farinotti, [16, 17], it is shown that glaciers play an important role in the sea-level rise. The volume and spatial ice coverage changes of glaciers are manifestations of the current climate changes. However, instantaneous changes are imperceptible and for most glaciers the dynamical change can only be noticed over periods of decades. This lagged response requires a full ice-flow numerical model to extend the possibility of inferring past climate changes, see e.g. [15, 18]. Thus, glacier flow models should incorporate respective parameters depending on the nature of the glacier [14]. For example, smaller mountain glaciers are characterized by relatively fast response with higher ice velocities. Therefore, there is an increasing interest in modelling glacier flows to accurately identify their relevance in climate change prediction. To do this, it is important to understand the glacier flow dynamics, derive its governing equations, and identify the parameters involved.

Many mass balance and ice flow models have been developed for two main purposes: (1) in order to study the effect of particular climatic conditions on the glacier shape and flows, and (2) to determine the climatic signal from glacier fluctuations and thus use it for meteorological study. The former constitutes the forward problem while the later is the inverse problem in this particular scenario. However, more specific and detailed models are being developed to study the dynamics of glaciers. Glaciers are rivers of ice which are characterized as incompressible flow governed by the Stokes equations. Simplification of the Stokes equations provides more specific models with limited applicability. Examples are Higher-Order approximation and Shallow Ice approximation, see e.g. [19] . Albeit it is a simplified form of the Stokes equation, the Shallow Ice approximation (SIA) equation

has a wide range of applicability and it will be used for glacier bedrock reconstruction in part-II of this thesis.

In glaciology, the knowledge of the bedrock is directly related to the ice thickness distribution, i.e. a known ice thickness means a known glacier bedrock if the corresponding free surface elevation data exists. Thus, the knowledge of the bedrock is as important as the knowledge of ice thickness distribution not only as an input to glacier flow models but also for future and past climate change analysis [20].

Parameters that are commonly used to characterise glaciers are spatial lengths, aspect ratios, slope, depth distribution, bedrock topography, free surface elevation, velocity fields, and ice ablation/accumulation rates. Remote sensing techniques such as aerial photography, satellite imaging, airborne laser altimetry with digital elevation models, synthetic aperture radar (SAR), and Light Detection and Ranging (LiDAR) are widely used to monitor glacier parameters. Keller et al. [21] used airborne laser altimetry with a digital elevation model (DEM) to identify glacier thinning trends. Free surface elevation, spatial lengths and surface velocity can be determined from these aerial surveys [16]. However, very few measurement techniques provide the possibility to measure the ice thickness distribution. Christensen and his co-workers, [20], showed that airborne laser altimetry with kinematic global positioning system (GPS) allow the measurement of the ice thickness distribution, however, it calls for complex signal processing techniques. Thus *in-situ* data acquisition techniques which are restricted to a small number of glaciers [17] are required to capture the topological description of glaciers. Current *in-situ* techniques include radio-echo sounding and borehole measurements are laborious and costly.

Both shallow water and glacier flows, albeit their dynamics are distinct, play an important, yet identical, role in the indication of environmental health if their dynamics is well understood. The study of their dynamics, eventually, calls the knowledge of parameters prior to numerical and computational modelling of flows. Different approaches ranging from analytical to experimental techniques are being used to determine the relevant parametric values which are essential for further study of both flows. Experimental, analytical, and numerical study of these flows has been an area of research interest. Numerical modelling has evolved not only to support the experimental studies but also to enable researchers to determine some experimentally impossible parameters and to perform more detailed study.

In the context of numerical modelling of shallow water and glacier flows, both share the requirement of bed topographic elevation data prior to analysis in order to understand and accurately capture the respective flow dynamics.

### *1.1.1. The shallow water approximation*

The shallow water equations model a variety of atmospheric and geophysical flows, see e.g. [5, 22] . Despite the increased use of the full Navier-Stokes equations for the modelling of free surface flows due to the availability of more complex computational fluid dynamics packages, the shallow water equations are yet the most famous and most widely used governing equations to model the hydrodynamics of shallow water flows. They are derived from the Navier-Stokes equations for incompressible free surface flows by depth averaging the flow under hydrostatic pressure assumption. The shallow water equations form a set of non-linear partial differential equations which relate the inertia terms, the effect of the topographic elevation of the channel bed, and the channel flow resistance. Detailed representation of the equations will be presented in chapter 2.

Over several decades, shallow water equations have been used to study the flow characteristics of shallow water flows. Analytical solutions of particular flow scenarios have been previously developed. Many numerical approaches have been implemented to address different aspects of the solution such as accuracy, variable dependency, numerical cost, and practical applicability. While some other methods have been developed to assess different flow scenarios like steady and unsteady river flows, flood modelling, dam beak problems, braided rivers, tsunamis, and subcritical, transcritical and supercritical open channel flows, see e.g. [6, 22, 23]. The last but not the least purpose of these equations can be explained in their applicability for the inverse problem analysis to identify unknown parameters from the measured ones, see e.g. [24]. The inverse problem approach based on the shallow water approximation can be twofold: a direct numerical reconstruction approach and the conventional optimization based reconstruction technique which calls for the use of cost functions to minimize it, see e.g. [25, 26]. The former approach is implemented in this thesis for the study of bed topography reconstruction from measured free surface data in open channel flows.

### *1.1.2. The shallow ice approximation*

Analogous to the shallow water approximation, the SIA equation is the approximation of the Stokes equation which governs a gravity driven non-Newtonian incompressible fluid (glaciers in this case) flow. This equation was introduced by Kolumban Hutter, [13] , in 1983 after simplifying the Stokes equations under the set of assumptions. Some of the assumptions of the simplification process include: (1) neglected longitudinal stress and (2) small aspect ratio (the depth of the glacier is much smaller than the other length scales). The SIA equations are commonly used for ice sheet modelling [27, 28] although they have accuracy restrictions for anisotropic ice where the directional properties are different. The derivation of the equations will be presented in chapter 7.

The SIA equation is a non-linear partial differential equation which relates the effect of the bed topographic elevation, mass balance on the glacier surface (ablation/ accumulation), and momentum flux. Typical glacier flow is characterized by a line of equilibrium which separates the accumulation and ablation zones. For a steady glacier, the addition of mass in the accumulation zone is balanced by the downward flow and the ablation of ice in the respective zone. Thus, steady glaciers, experience continuous addition of ice in the accumulation zone and continuous flow of ice towards the snout. However, if one of the parameter experiences change due to climate changes, the glacier will respond accordingly making it transient.

Recent developments have demonstrated the limitations of SIA applicability while the higher-order and full Stokes models are deemed to have a wider range of applicability [19]. However, the ease of coding and the low computational requirement make the SIA model a popular choice in glacier modelling [29-31]. To solve SIA-based governing equation, different numerical approaches have been proposed: explicit finite difference scheme [29], semi implicit scheme [32], alternating-direction-implicit (ADI) method [33], or finite volume scheme On the other hand, the use of the SIA for inverse problem analysis is paramount for parameter identification from measured glaciological data either with the help of conventional optimization techniques or direct numerical techniques, see e.g. [17, 35-37]. The direct numerical technique to infer the bedrock topographic elevation from known glacier surface elevation data in one dimension is presented in part-II of the thesis.

## 1.2. The forward and inverse problems

Mathematical models, which arise from the physical theories of particular phenomena, allow engineers, scientists, and modellers to predict the values of measurable parameters

based on the model equations which describe the physical system. These mathematical models require a set of parameters to determine and study the physics of a system. This is called the forward problem, which constitutes in determining the effect of a particular cause. As an example, consider the study of a dam break problem which requires priori information on the size of the dam, downstream bathymetry, wetness of the downstream landscape, and the reach depth. Given these parameters and with the help of the governing equations, the water level, velocity and flow rate can be determined as a function of time. In this example, the causes are the model parameters (dam size, water level in the dam, and downstream topography and wetness) while the effects are the output parameters (water levels at the upstream and downstream positions of the dam, velocity and flow rate of the flow).

On the other hand, an inverse problem consists of using actual results of some measurement to infer the values of unknown model parameters which characterize the system, see e.g. [38]. In other words, it is an approach to determine the cause of a particular effect. It is thus, an opposite of the forward problem. To demonstrate this, in the abovementioned example, the determination of downstream bed topography from the water level and other measured parameters can be considered as the inverse problem.

In the area of the focus of this thesis, the inverse problem constitutes the determination of bed topography from known free surface data in open channel and glacier flows. To perform this task, few approaches of the inverse problem analysis are possible among them: the direct solution approach and the partial differential equation (PDE) constrained optimization based approach.

### *1.2.1. The optimization based solution approach*

An optimization based solution approach is well known for solving inverse problems. In this approach, a minimization function is defined to determine the model parameters iteratively. The following steps are involved to perform this solution approach for parameter identification.

i. Solve the forward problem to determine measurable parameters from known model parameters. This is an important step because the minimization function (objective function) requires a reliable solution approach for the forward problem.
ii. Define a minimization function which relates the observed and calculated data and determines their difference.
iii. Guess a value of a model parameter based on the experimental observation of the system and compute the objective function.
iv. Estimate the sensitivity to find a direction in the parameter space which leads to a decrease of the objective function.
v. Take the largest possible step in that direction and update the value of the unknown parameter and continue the iteration until the limit of the error is achieved. The resulting value of the model parameter which minimized the minimization function is then regarded as the solution of the inverse problem.

In the context of open channel flows, the optimization based approach is implemented by many authors. To mention some: references [26, 39-41] have implemented this approach for the determination of bed topography and [42-48] for the evaluation of channel roughness of open channels and other flow parameters [49] in open channel flows. While, in the context of glacier flows, some techniques on the inverse problems are implemented, see [35, 36] for example.

The above mentioned steps are essential steps for the inverse problem analysis based on the optimization solution approach. However, the details and other required steps of this solution approach are not covered in this thesis, as the other approach, the direct solution approach, is implemented for the study covered in this research.

### *1.2.2. The direct solution approach*

The direct solution approach of the inverse problem is not a common way of solving an inverse problem which is embedded in the framework of the very few inverse problems in the literature. This solution approach uses the governing equations of the forward problem to solve for the model parameters with the help of equation rearrangement if necessary. The process is analogous to the determination observable parameters in the forward problem analysis. However, this approach is not always possible. The governing equations of the forward problem should allow us to conveniently rearrange them for the determination of the unknown model parameters. Thus, this approach is restricted to some inverse problems. The steps involved in this solution approach are given below

i. Solve the forward problem to determine measurable parameters from known model parameters. In this step, previously implemented solution approaches can be used to produce numerical test cases whenever necessary.
ii. Rearrange the governing equation/s in such a way that model parameters can be evaluated from measured parameters.
iii. To validate the approach, solve for the unknowns and compare the results against experimental or numerical test cases.

This direct solution approach is, for example, well implemented in [50-53] for substrate shape identification from the known free surface data in thin film flows. In this research, this approach is implemented to determine bed elevation data from known free surface

data in open channel and glacier flows. The whole solution strategy can be seen in the subsequent chapters of the thesis to achieve the following predefined set of objectives of the research.

## 1.3. Focus of the present work

The shallow water and the SIA approximations are the basis of the work presented in this thesis. These approximations and equations are formulated and presented in chapters 2 and 7, respectively. Specifically, the former is applied to the analysis of bed topography reconstruction of shallow water flows in open channels from known water free surface elevation data and measured velocity distribution. While the latter, in a similar context, is applied to the bedrock reconstruction of glaciers from known glacier surface topographic elevation data. Both problems are very important as the knowledge of bed topographies not only play a vital role in the modelling of these flows but also constitute information to study the environmental health of the accompanying region.

The application of numerical modelling techniques to environmental problems is hampered by the nonlinearity of the governing equations, and the lack of actual data on model parameters, see e.g. [54]. Numerical modelling of flow and sediment transport, design and construction of hydraulic structures, and prediction of flood inundation all rely upon the prior knowledge of essential hydraulic parameters like the roughness coefficient, the bed slope, spatially distributed bed topographic information of rivers, flood plains, estuaries, and manmade open channels, [55]. All these parameters and their accurate representation play paramount role in the numerical and computational analysis of free surface flows to accurately predict measurable hydraulic parameters involved in the flow analysis. Thus, there is a growing need to efficiently and accurately represent the river channel topography at high resolution, see e.g. [8]. There has been considerable

development in the measurement techniques of bed topographic elevation in river flows. Numerical based channel bed reconstruction algorithms are very important as conventional aerial imagery techniques (conventional LiDAR, for example) do not penetrate water bodies. Thus, the determination the underlying riverbed profile of a river requires underwater data gathering to complete the river bathymetry. Sufficient data is not always obtained because *in-situ* data gathering is extremely expensive and time consuming. Therefore, the implementation of numerical techniques will further assist in providing sufficient bathymetry data.

On the other hand, there is a lack of algorithms to reconstruct the bedrock topographic elevation from known glacier free surface data. This task has important applications to predict ice-shelf evolution and its possible melting due global warming. Measurement of ice thickness has a vital role in determining the volumetric change of glaciers, predicting the effects of global warming and future climate change. But it requires ground surveys as well as aerial imagery. These are costly and time consuming operations if even at all possible.

Therefore, both problems have strong similarities which motivate this combined study where it is believed that this work has addressed the following important questions.

1. Can we develop direct analytical and numerical algorithms to infer the bed topography from the known free surface elevation?
2. How sensitive is the reconstruction algorithm to noise in the measured data?

In line with addressing the above mentioned questions, the objectives of this work are

- ✓ To develop an algorithm for the determination of the channel bed profile from the knowledge of free surface elevation data of shallow water flows. The model may help in gaining a complete understanding in the hydrodynamics of shallow water

flows. Identification of parameters required for the reconstruction process, in addition to the free surface elevation data, is addressed.

- ✓ To develop a solution methodology for the reconstruction of channel bed topography of open channel flows from the measured velocity distribution in one-dimensional flow. This solution procedure is based on the one-dimensional shallow water equations and additional parameters required for the identification of the bathymetry are determined.
- ✓ To develop an algorithm for the reconstruction analysis of the bedrock profile from the known free surface data of glaciers. This algorithm will be based on the one-dimensional SIA equation and will give a better understanding of glacier flows.

## 1.4. Outline of the thesis

The thesis mainly constitutes two major parts. In Part-I, the solution approach for the reconstruction of bed topography from the free surface data in open channel flows is presented. The free surface data constitutes the free surface elevation and the free surface velocity. However, the reconstruction analysis based the two-dimensional shallow water flow from know free surface velocity is not included in this research. In Part-II, the glacier bedrock reconstruction approach from the known free surface elevation data based on the one-dimensional SIA equations is presented.

Each chapter of the thesis addresses different aspects of the study which are directly and indirectly related to the inverse problem. Chapter 2 presents the derivation of shallow water equations from the Navier Stokes equations under a set of approximations and assumptions. This chapter is a framework for the subsequent chapters because the inverse problem analysis for the open channel flows is based on the governing equations presented in this chapter.

Chapter 3 presents the one-dimensional analytical and numerical direct solution approach of the inverse problem which is inferring the channel bed topography from known free surface elevation data in one-dimensional shallow water flows. In this approach, one-dimensional shallow water equations are rearranged such that the unknown model parameter, bed topography, will be directly evaluated by solving the coupled sets of equations. In this chapter, the forward problem is solved by using an upwind conservative numerical scheme [56] to generate canonical test cases which will be used for the validation of the inverse problem results. Quantitative comparisons of the results along with the assessment of the effect of noise in measurable quantities on the inferred bedrock topography are presented this chapter.

In chapter 4, a numerical technique which uses the measured flow velocity to infer the channel bed topography is presented. The depth-averaged one-dimensional shallow water equations along with an empirical relationship between the free-surface and the depth-averaged velocities are used for the inverse problem analysis. It is shown that after a series of algebraic manipulation and integration, the equation governing the inverse problem simplifies to a simple integral equation. The proposed method to solve the inverse problem along with a range of analytical and experimental benchmark test cases are presented in this chapter.

In chapter 5, the two-dimensional shallow water equations are modified by neglecting inertia terms while retaining the effects of the bed slope and friction terms. A numerical technique is presented for reconstructing the channel bed topography from given free surface elevation data for steep open channel flows for which the zero-inertia shallow water approximation holds. It is shown that by algebraic manipulation, the governing equation can be rewritten into a single first-order partial differential equation which describes the inverse problem. For the respective forward problem, a MacCormack

explicit numerical scheme is used by considering unsteady modified shallow water equations. However, the inverse problem is solved using the method of characteristics. As shown in this chapter, the results of the inverse and the forward problem are successfully tested against each other on two different test cases.

Chapter 6 presents a numerical technique to identify the underlying bed topography from given free surface elevation data in two-dimensional shallow open channel flows. The full two-dimensional shallow water equations are used to solve the inverse problem directly. The idea is tested on a set of artificial data obtained by first solving forward problem governed by the two-dimensional shallow water equations using the MacCormack numerical scheme. The inverse problem is solved by using the backward difference explicit numerical scheme. The method is tested against the forward problem counterparts with noise free and noisy free surface elevation data.

In chapter 7, widely used governing equations which dictate the flow of glaciers and ice-sheets are presented. Starting from the Stokes equations, the derivation of SIA equations are also presented.

Chapter 8 presents the glacier bedrock reconstruction approaches from known free surface data using one-dimensional SIA equation. Both analytical and numerical reconstruction techniques are presented. In line with the inverse problem solution, the forward problem solution based on an explicit numerical scheme is also presented. An implicit numerical scheme is used for the numerical reconstruction of the glacier bedrock.

Lastly, the concluding remarks of this research and recommendations for related future work are presented in chapter 9.

# PART- I

# CHANNEL BED RECONSTRUCTION IN SHALLOW WATER FLOWS

# 2. Mathematical model: derivation of the field equations

## Contents

## 2.1. Introduction

Gravity-driven shallow water flows frequently arise in nature. Such flows are well represented by the Saint Venant's shallow water equations, [57]. These governing equations are the most commonly used mathematical model to simulate open channel flows which are derived by vertical integration of the Navier-Stokes equations assuming a small aspect ratio (where the depth is conveniently very small compared to the other length scales), a hydrostatic pressure distribution in the flow, and wind shear stress on the water surface is neglected, see e.g. [5, 6, 26, 58]. These equations are commonly applied for the simulation of unsteady and steady, one and two-dimensional shallow water flows.

The shallow water equations are well known and describe incompressible free surface flows. Both explicit and implicit numerical methods have been extensively used for the computation of their numerical solution. Even though implicit schemes are stable for CFL (Courant, Fredrichs, Lewy) numbers greater than 1, they lead to the solution of large non-linear algebraic systems, and the computational effort grows very quickly with the number of cells, see e.g. [59]. Conversely, the explicit methods are relatively easy-to-implement but have problems associated with numerical stability and they are known to produce spurious results, see e.g. [6]. However, if the CFL number is less than 1, these methods can produce results with acceptable errors, see e.g. [6, 60].

The study of shallow water flows in the context of inverse and forward problem requires a good understanding of the governing equations. These equations will be used for both problems, thus it is important to know the derivation of the equations from the Navier-Stokes equations under the aforementioned assumptions.

## 2.2. The derivation of shallow water equations

### *2.2.1. Background*

The Navier-Stokes Equations are the cornerstone of all fluid mechanics, [61]. All forms of fluid flow studies use these famous equations to solve many engineering problems of vast application. However, the Navier-Stokes equations may be required to be approximated based on the nature of the flow and with the help of acceptable assumptions such that a solution with less computational effort can be obtained. The better the approximation, the closer the governing equations to the Navier-Stokes equations, the more realistic the solutions.

Like most engineering fluid mechanics problems, the study of free surface flows call for the frequent use of the Navier-Stokes equations (or geophysical approximate equations) for better understanding of the flow hydrodynamics. Free surface flows include: river and stream flows, flows through irrigation channels, floods, flow downstream of partially or fully breached dams, estuarine flows and tsunami flows. These flows, even though they have different hydrodynamic natures, have similar set of governing equations, which are the shallow water equations. The one-dimensional form of the shallow water equations have been widely used to model such flows under a one-dimensional flow assumption. However, with the help of fast computers in recent times, two-dimensional shallow water flow equations have become a popular choice for the simulation of shallow water flows. But the popularity is hampered by the computational cost, especially for long reach open channel flows. Thus, in spite of the fact that the solution of the two-dimensional equations should give more accurate results, one-dimensional flow equations are still a popular choice by many researchers and modellers.

In recent years, unlike the conventional use of these equations, attempts have been made to develop a solution approach to use the shallow water equations for an inverse analysis where unknown parameters can be identified from the given hydraulic data. In this regard the use of these shallow water equations is twofold and thus the understanding of their characteristics and the derivation is very important in order to employ fast, easy, and reliable inverse problem solution approaches. For this purpose, the derivation and the characteristics of the shallow water equations are given in the following section.

The continuity equation which expresses the conservation of fluid mass and the momentum equations govern the fluid flow of free surface flows. The conservation of energy, for the course of the study, is left aside as its effect on the present work is not included.

Let $\rho$ be the density of the fluid under consideration having a velocity field $\vec{U}$ whose components are $(U,V,W)$. The continuity and momentum equations written below constitute the conservative form of the Navier-Stokes equations.

Conservation of mass:

$$\frac{\partial \rho}{\partial t} + div(\rho \vec{U}) = 0 \qquad (2.1)$$

Momentum equation:

$$\frac{\partial (\rho \vec{U})}{\partial t} + \nabla (\rho \vec{U} \otimes \vec{U}) = div(\underline{\underline{\sigma}}) + \rho \vec{g} + \rho \vec{F} \qquad (2.2)$$

Where $\underline{\underline{\sigma}}$ is the stress tensor, $\vec{g}$ and $\vec{F}$ are the acceleration of gravity and other external forces respectively.

The above equations can also be written in a non-conservative form, but this form is not used in the following. Rewriting the conservation equations for a Newtonian

incompressible free surface flow in Cartesian coordinates will lead to the following equations.

Conservation of mass:

$$\frac{\partial U}{\partial x}+\frac{\partial V}{\partial y}+\frac{\partial W}{\partial z}=0 \tag{2. 3}$$

Conservation of Momentum:

$$\begin{aligned}
&\frac{\partial U}{\partial t}+U\frac{\partial U}{\partial x}+V\frac{\partial U}{\partial y}+W\frac{\partial U}{\partial z}=-\frac{1}{\rho}\frac{\partial p}{\partial x}+\nu\Delta(U)+F_x\\
&\frac{\partial V}{\partial t}+U\frac{\partial V}{\partial x}+V\frac{\partial V}{\partial y}+W\frac{\partial V}{\partial z}=-\frac{1}{\rho}\frac{\partial p}{\partial y}+\nu\Delta(V)+F_y\\
&\frac{\partial W}{\partial t}+U\frac{\partial W}{\partial x}+V\frac{\partial W}{\partial y}+W\frac{\partial W}{\partial z}=-\frac{1}{\rho}\frac{\partial p}{\partial z}-g+\nu\Delta(W)+F_z
\end{aligned} \tag{2. 4}$$

Where $p$ is the pressure, $\nu$ is the kinematic viscosity of the fluid. In these equations there are four equations with four unknowns $U,V,W \text{ and } p$ and as there is no hypothesis for the pressure, these equations are referred to as the incompressible Navier -Stokes equations, [61] .

These equations are always accompanied by boundary conditions which may vary depending on the complexity of the flow. For numerical modelling of open channel flows, these boundary conditions may include the bottom features, side walls like river banks, free surface features, upstream & downstream limits of the domain, and boundaries of hydraulic structures.

For free surface flows, the hydrostatic pressure hypothesis along with Boussinesq approximation will provide a relationship for the pressure terms in the momentum equation. This approximation simplifies the z-momentum equation by neglecting the

effect of diffusion along the vertical direction, [61]. The pressure in the vertical direction of the fluid flow with a fluid having density variation can be determined by

$$p = p_{atm} + \rho_o g(\psi - z) + g\int_z^{\psi} \Delta\rho dz' \tag{2. 5}$$

Where $p_{atm}$ is the atmospheric pressure and $\psi$ is the elevation of the free surface

This implies that pressure term in the momentum equations can be substituted by the hydrostatic pressure. Thus the Navier-Stokes equations with the hydrostatic pressure assumption can be written as:

Mass conservation

$$\frac{\partial U}{\partial x} + \frac{\partial V}{\partial y} + \frac{\partial W}{\partial z} = 0 \tag{2. 6}$$

Momentum conservation

$$\begin{aligned} \frac{\partial U}{\partial t} + U\frac{\partial U}{\partial x} + V\frac{\partial U}{\partial y} + W\frac{\partial U}{\partial z} &= --g\frac{\partial \psi}{\partial x} + \nu\Delta(U) + F_x \\ \frac{\partial V}{\partial t} + U\frac{\partial V}{\partial x} + V\frac{\partial V}{\partial y} + W\frac{\partial V}{\partial z} &= -g\frac{\partial \psi}{\partial y} + \nu\Delta(V) + F_y \end{aligned} \tag{2. 7}$$

Pressure

$$p = p_{atm} + \rho_o g(\psi - z) + \rho_o g\int_z^{\psi} \frac{\Delta\rho}{\rho_o} dz' \tag{2. 8}$$

In these equations, the effect of buoyancy due to density gradient and the effect of atmospheric pressure gradient are included in the source terms $F_x$ and $F_y$ of equation (2.7).

The source terms and the body forces included in the above equations are: the bottom friction, wind force, Coriolis force, centrifugal forces, buoyancy and atmospheric pressure gradient effects.

The bottom friction is the most important body force in the analysis of open channel flows. It is created due to the bottom shear stress to oppose the flow of fluid which results in energy dissipation. The bottom shear stress acting on a fluid is equal and opposite to the stress applied on the bottom by the flowing fluid due to bottom friction. This stress is expressed as

$$\vec{\tau} = -\mu \frac{\partial \vec{U}}{\partial n} \tag{2. 9}$$

and requires the knowledge of the flow. Based on turbulence models, the shear stress can be written in the form where the shear stress velocity is apparent. Analogous to the one-dimensional expression, $\tau = -\rho(U^*)^2$, the two-dimensional shear stress can be expressed as:

$$\vec{\tau} = -\frac{1}{2}\rho\, C_f \sqrt{U^2 + V^2}\, \vec{U} \tag{2. 10}$$

Where $U^*$ is the shear velocity, $C_f$ is a dimensionless friction coefficient and the relationship assumes that $\vec{U}$ is sufficiently far from the wall, [61]. The relationship can be rewritten as

$$\nu \frac{\partial \vec{U}}{\partial n} = \frac{1}{2}\rho\, C_f \sqrt{U^2 + V^2}\, \vec{U} \tag{2. 11}$$

The bottom shear stress term can thus be computed by two possible approaches. One is with a turbulence model which can provide a formula for the shear stress based on the friction coefficient $C_f$ and the flow in the immediate vicinity of the wall. In most

turbulence models either the value of $C_f$ or the shear stress velocity is given. The second approach is by the knowledge of the friction coefficient and its associated flow velocity $\vec{U}$ based on the laws of bottom shear stress in two-dimensions. The velocity will be the depth averaged average velocity (the friction coefficient on the bottom will thus be the same in two and three dimensions). This is the case of the Chezy, Strickler, and Manning formula, [6, 61].

The Chezy formula with $C$ as a Chezy coefficient can be expressed as

$$C_f = \frac{2g}{C^2} \tag{2. 12}$$

The Strickler formula with $S$ as a Strickler coefficient can be expressed as

$$C_f = \frac{2g}{h^{1/3} S^2} \tag{2. 13}$$

The Manning formula with $n$ as a Manning coefficient can be expressed as

$$C_f = \frac{2g\, n^2}{h^{1/3}} \tag{2. 14}$$

Wind forcing appears in the equations through the two-dimensional conditions on the free surface of the flow which can be given by equation (2.15)

$$\nu \frac{\partial \vec{u}_H}{\partial n} = \frac{\rho_{air}}{\rho} a_{wind} \vec{w} \left\| \vec{w} \right\| \tag{2. 15}$$

Where the terms $\vec{u}_H$, $a_{wind}$ and $\vec{w}$ are the horizontal velocity at the surface, dimensionless number, and speed of the wind 10m above the fluid free surface, respectively. The coefficient $a_{wind}$ is dependent on the speed of the wind which accounts for a complex phenomenon on the free surface due to the effect of the wind. For instance, the influence of wind depends on the surface roughness of the flow and the surface roughness itself

depends on the wind and the distance over which it is applied. However, for the course of this study, the effect of wind is neglected.

The Coriolis and the centrifugal forces are the forces generated due to the effect of earth rotation. These forces are important for the study of oceanic or atmospheric areas where their effect is significant. However, for small water bodies like rivers, streams, and lakes these forces are negligible. Thus, for the geophysical flows of the current study, the expressions to determine these forces are not included in the governing Navier-stokes equations.

### *2.2.2. The Saint Venant equations*

The French scholar, Jean-Claude Adhemar Barre, Count of Saint-Venant presented two papers to the Academie des Sciences on the theoretical mechanics and the dynamics of fluids in 1834 which were used as the basis for the "Barre de Saint-Venant equations", published in 1871, [57]. These equations, also known as "the shallow water equations" are today the most important equations for the study of maritime and fluvial hydraulics. As mentioned above, these equations are obtained from the Navier-Stokes equations with the help of simplifying hypotheses. The approximations to derive the shallow water equations from the Navier-Stokes equations are:

i. The pressure, as mentioned above, is hydrostatic and the momentum equations will have terms associated with the depth of the flow. If the vertical density variation is neglected the hydrostatic pressure is expressed as:

$$p(x,y,z,t) = p_{atm} + \rho g(\psi(x,y,t) - z(x,y,t)) \tag{2. 16}$$

ii. The vertical velocity of the flow is neglected, thus the z-momentum equation disappears in the shallow water equations. This approximation goes with the

hydrostatic pressure hypothesis according to which the vertical acceleration of the flow should be negligible.

iii. The free surface and the bottom of the channel are assumed to impermeable where there will be no mass transfer through, i.e. the water particles situated between these two interfaces will remain there. Thus the permeability conditions are:

$$\frac{\partial \psi}{\partial t} - \vec{U}^s . \vec{n}_s = 0 \Big|_{at\ the\ free\ surface} \quad \text{and} \quad \frac{\partial Z_b}{\partial t} - \vec{U}^b . \vec{n}_b = 0 \Big|_{at\ the\ bottom} \tag{2. 17}$$

iv. The Navier-Stokes equations are vertically averaged from the free surface to the bottom with a hydrostatic pressure and constant density. This is done by averaging all the hydrodynamic parameters over the depth of the flow.

$$u = \frac{1}{h} \int_{Z_b}^{\psi} U dz \quad \text{and} \quad v = \frac{1}{h} \int_{Z_b}^{\psi} V dz \tag{2. 18}$$

These averages of the velocity vector $\vec{U}$ are the velocity components of the depth averaged velocity vector $\vec{u}$ .

**Averaging the continuity equation**

$$\int_{Z_b}^{\psi} \left( \frac{\partial u}{\partial x} + \frac{\partial v}{\partial x} + \frac{\partial w}{\partial x} \right) dz = 0 \tag{2. 19}$$

Applying the Leibnitz rule and taking the permeability conditions into account, the depth averaged continuity equation will be:

$$\frac{\partial h}{\partial t} + div( h\vec{u} ) = 0 \tag{2. 20}$$

In this equation, the divergence term is calculated in two directions.

**Averaging the momentum equations**

Averaging the momentum equation can be done by applying the same technique to each term of the momentum equation.

The time derivative term:

$$\int_{z_b}^{\psi} \frac{\partial U}{\partial t} dz = \frac{\partial (hu)}{\partial t} \tag{2. 21}$$

The advection terms:

$$U\frac{\partial U}{\partial x} + V\frac{\partial U}{\partial y} + W\frac{\partial U}{\partial z} \quad \text{or} \quad \frac{\partial (UU)}{\partial x} + \frac{\partial (UV)}{\partial y} + \frac{\partial (UW)}{\partial z} \tag{2. 22}$$

$$\int_{z_b}^{\psi} \left( \frac{\partial (UU)}{\partial x} + \frac{\partial (UV)}{\partial x} + \frac{\partial (UW)}{\partial x} \right) dz = \frac{\partial (huu)}{\partial x} + \frac{\partial (huv)}{\partial y} \tag{2. 23}$$

However, on the right hand side of these terms there is additional non-zero term arising from the fluctuation of diffusion against the average values which are called dispersion terms, i.e. when there is non-zero vertical velocity fluctuation.

The diffusion term:

$$\int_{z_b}^{\psi} \nu \Delta(U) dz = div(h\nu\ grad(u)), \quad \int_{z_b}^{\psi} \nu \Delta(V) dz = div(h\nu\ grad(v)) \tag{2. 24}$$

The pressure terms for a constant density along the flow domain are integrated as

$$\begin{aligned} \int_{z_b}^{\psi} -\frac{1}{\rho}\frac{\partial}{\partial x}\left[\rho g(\psi - Z_b)\right] dz &= -hg\frac{\partial \psi}{\partial x}, \\ \int_{z_b}^{\psi} -\frac{1}{\rho}\frac{\partial}{\partial y}\left[\rho g(\psi - Z_b)\right] dz &= -hg\frac{\partial \psi}{\partial y} \end{aligned} \tag{2. 25}$$

The averaging of the source and body terms is simple if the source term is constant. For a constant body force the terms are averaged by multiplying each

component of the source term by the water depth $h$. Thus $F_x$ and $F_y$ give $hF_x$ and $hF_y$ respectively.

The final form of the depth averaged momentum equations in $x$ and $y$ directions are:

$$\begin{aligned}
&\frac{\partial(hu)}{\partial t}+\frac{\partial(huu)}{\partial x}+\frac{\partial(huv)}{\partial y}=-gh\frac{\partial \psi}{\partial x}+hF_x+div(h\nu_e\ grad(u)),\\
&\frac{\partial(hv)}{\partial t}+\frac{\partial(huv)}{\partial x}+\frac{\partial(hvv)}{\partial y}=-gh\frac{\partial \psi}{\partial y}+hF_y+div(h\nu_e\ grad(v))
\end{aligned} \qquad (2.\ 26)$$

Where the term $\nu_e$ is the effective viscosity which includes the turbulent viscosity and dispertion.

v. The restrictive assumption of the shallow water equations is that the wavelength of the surface waves should be much larger that the depth of the flow, meaning that the shallow water equations, from its name, are more applicable to water bodies having smaller aspect ratio (ratio of depth to other length scales).

Thus the final forms of the shallow water equations are

$$\begin{aligned}
&\frac{\partial h}{\partial t}+div(h\vec{u})=0\\
&\frac{\partial(hu)}{\partial t}+\frac{\partial(huu)}{\partial x}+\frac{\partial(huv)}{\partial y}=-gh\frac{\partial \psi}{\partial x}+hF_x+div(h\nu_e\ grad(u))\\
&\frac{\partial(hv)}{\partial t}+\frac{\partial(huv)}{\partial x}+\frac{\partial(hvv)}{\partial y}=-gh\frac{\partial \psi}{\partial y}+hF_y+div(h\nu_e\ grad(v))
\end{aligned} \qquad (2.\ 27)$$

These equations form coupled non-linear partial differential equations. The terms $F_x$ and $F_y$ account for different body forces other than gravity and pressure if they are considered for the calculation. These forces may include; bottom friction, drag force and head loss,

the coriolis force, the influence of wind, effect of atmospheric pressure, sources of momentum, spatial variation of density, and tide generating forces.

Friction on the bottom is a very important phenomenon in the study of open channel flows. The term expressing the friction on the bottom is often an unknown environmental parameter and friction laws are mostly empirical. These laws include; Chezy's Law, Strickler's Law, and Manning's Law, see Equations 2.12-2.14. The selection of a particular friction law depends on the particularity of the problem and the experience of the numerical modeller. For the course of this study, Manning's friction law is considered. But the methods described in the following would easily apply to other laws,

Although the shallow water equations allow the use of other body forces and the effect of the diffusion and dispersion, the terms accounting these effects are neglected in the course of this study.

Thus, the final forms of the shallow water equations which are used for the current study are:

$$H_t + E_x + F_y + S = 0$$

$$H = \begin{pmatrix} h \\ uh \\ vh \end{pmatrix} \quad E = \begin{pmatrix} uh \\ u^2h + \frac{1}{2}gh^2 \\ uvh \end{pmatrix} \quad F = \begin{pmatrix} uh \\ uvh \\ v^2h + \frac{1}{2}gh^2 \end{pmatrix} \quad S = \begin{pmatrix} 0 \\ -gh(S_{ox} - S_{fx}) \\ -gh(S_{oy} - S_{fy}) \end{pmatrix} \qquad (2.28)$$

$$S_{fx} = \frac{n^2 u\sqrt{u^2+v^2}}{C_o h^{4/3}} \qquad S_{fy} = \frac{n^2 v\sqrt{u^2+v^2}}{C_o h^{4/3}}$$

$$S_{ox} = -\frac{\partial z_b}{\partial x} \qquad S_{oy} = -\frac{\partial z_b}{\partial y}$$

These equations, along with the boundary conditions which will be imposed in the study of a particular open channel flow, govern the shallow water flows. A whole hierarchy of

simplified models have been derived and analyzed from these equations in the past in an attempt to simplify calculations yet capture the main flow characteristics. The simplifications and the modifications, however, impose additional restrictions to the applicability of the resulting equations.

# 3. Bed topography reconstruction using one-dimensional shallow water flows

## Contents

## 3.1. Introduction

Once introduced, the one-dimensional shallow water equations became popular and have been widely used for the modelling of open channel flows. Their application includes flood inundation modelling, river flow modelling, estuarine modelling, sediment transport analysis, and partial dam break flow analysis. In the past several decades, different one-dimensional based numerical method have been developed: HEC-RAS [62]; LISFLOOD-FP [63]; RiverFLO-2D [64]; and ISIS [65] are some worthy of mention. These models make use of shallow water equations along with appropriate boundary and initial conditions to study open channel flows.

The use of shallow water equations in disaster prevention is vital as most inundation models incorporate these equations for the purpose of flood modelling, see e.g. [66], and predictions of extreme changes in river and coastal environments. The continuous river catchment topological and topographical change makes flood analysis difficult as conditions change with time. Dynamically changing river catchments can result from human alterations for increased resource needs. The downstream gravel excavation of Waimakariri River in Canterbury region of New Zealand can be mentioned as a good example, [67]. Human alterations coupled with sediment transport require the use of river catchment management to reduce the level of potential flood hazards which in turn, frequently requires the use of hydrological models. These hydrological models use one or two-dimensional shallow water equations to study the flow characteristics and flood behaviour, see e.g. [68, 69] .

In the context of sediment transport, the one-dimensional shallow water flows are also important due to the fact that most sediment transport models use these equations along with a diffusion model, [70]. The one-dimensional shallow water equations model the hydrodynamics of the flow while the diffusion model or the morphodynamical component

models the transport in a coupled manner, see e.g. [71]. The popularity of these equations in the modelling of sediment transport arise from the one-dimensional nature of the flow which calls for relatively less computational effort as compared to two-dimensional models where the application for long reach rivers is limited.

The one-dimensional shallow equations approximate the spanwise flow variations which may result in considerable amount of deviation from the actual flow characteristics. However, in spite of this deviation, the solutions for the modelling of different water bodies have been accepted for over a century.

The application of numerical modelling techniques to environmental problems is hampered by the nonlinearity of the governing equations, and the lack of actual data on model parameters, see e.g. [54]. These model parameters include channel roughness coefficient, bed slope, spatially distributed bed topographic information of open channel flows [55]. Thus, there is a growing need to efficiently and accurately represent the river channel topography at high resolution to study fluvial environments for flow hydraulics, flood routing and monitoring of geomorphological changes, see e.g. [8]. This is mainly true for the study of long river reaches where field data gathering techniques are not suitable due to costly operation and time constraint. Hilldale and Raff [7] assessed the quality of bathymetric airborne LiDAR surveys from the perspective of its application towards creating accurate, precise and complete streambed topography of the Yakima and Trinity river basins in the USA. They compared the results of ground surveys of the riverbed with airborne LiDAR based data. Systematic error between the two indicates a consistent bias in the data but random error falls within values of expected precision.

The importance of efficient algorithms for riverbed reconstruction in river flows is paramount because *in-situ* data gathering is extremely expensive and time consuming. Conventional aerial imagery techniques (such as LiDAR) do not usually penetrate water

bodies. Thus field based determination of the riverbed topography requires underwater data gathering to complete the river bathymetry. Smart and co-workers [39] have used airborne LiDAR returns with an optimization based hydraulic model to reconstruct the riverbed topography.

Other ways or techniques to determine the bed topographic elevation and other easily measureable hydraulic parameters have been proposed in recent years. Roux and Dartus [24] for example, presented a methodology to reconstitute information about the geometry of the river from top sight and also performed a sensitivity analysis to build a framework for parameter optimization in open channel flows. Castaings and co-workers [26] attempted to reconstruct riverbed topology from free surface information with the help of adjoint method/technique. They have shown an efficient methodology to predict the actual shape of an underlying obstacle. Honnorat and co-workers [72] have shown a variational data assimilation based optimization technique to retrieve channel topography from a known steady state solution of the forward problem.

In a slightly different context, Sellier studied the inverse problem of reconstructing the substrate topography from known free surface data in thin film flows, [50]. Heining and Aksel also studied the reconstruction of the bottom topography of steady state thin-film flow, [52]. They used a direct approach, analogous to the approach used in Sellier [50] for solving the governing equations to reconstruct the bottom topography for weakly and strongly undulated free surfaces. Yahia-Djouadi et al. [73] used an implicit function theorem to prove the existence of an obstacle on the bottom of a channel where the upper bound of the flow is known.

In this chapter of the thesis, one-dimensional Saint Venant Equations are used to reconstruct the underwater bed topography from known free surface elevation data analogous to the approaches implemented by Sellier [50], where a direct analytical and

numerical implementation is used to find a solution for the unknown parameter unlike the conventional optimization based reconstruction approaches.

## 3.2. The governing equations

The one-dimensional Saint-Venant equations which govern unsteady incompressible flow in an open channel in the form of continuity and momentum equations are considered in the reconstruction process of this one-dimensional flow study.

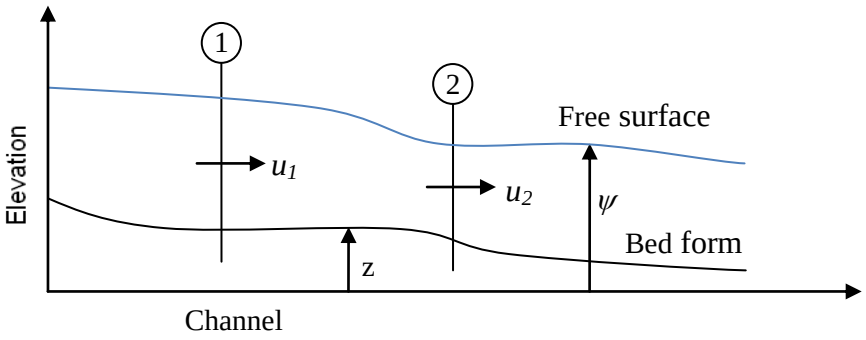


Figure 3. 1: Description of open channel flow

These equations, written in a different form, are derived from the general shallow water equations discussed above.

$$\frac{\partial A}{\partial t}+\frac{\partial Q}{\partial x}=0 \tag{3. 1}$$

$$\frac{\partial Q}{\partial t}+\frac{\partial (Q^2/A)}{\partial x}+gA\frac{\partial (z+h)}{\partial x}+gAS_f=0 \tag{3. 2}$$

Where $Q$ is the flow rate ($m^3/s$), $A(x,t)$ is the cross-sectional area in ($m^2$), $z(x)$ is the bed topography which is known to solve the forward problem, $h(x,t)$ is the depth of the flow, $S_f$ is the frictional slope (frictional resistance) and g is the acceleration due to gravity. The frictional slope $(S_f)$ can be given by the Manning formula

$$S_f=\frac{n^2Q|Q|}{R^{4/3}A^2} \tag{3. 3}$$

where $R$ is the hydraulic radius ($R=A/P$) and $P$ the wetted perimeter of the channel.

## 3.3. The forward problem

The solution of the one-dimensional Saint Venant equations is developed to allow a better understanding of the hydrodynamics of flow and to generate free surface data for the inverse problem. The determination of the water level, flow velocities, and depth of the flow for a given bed topography and spatially distributed Manning's coefficient constitutes the forward problem.

These governing equations are discretized over temporal and spatial grids using a cell centred method in the spirit of that described in [56] as shown in Figure 3.2. The conserved variables are defined at the cell centres and represent the average value over each cell, while the fluxes are calculated at the interfaces between cells.

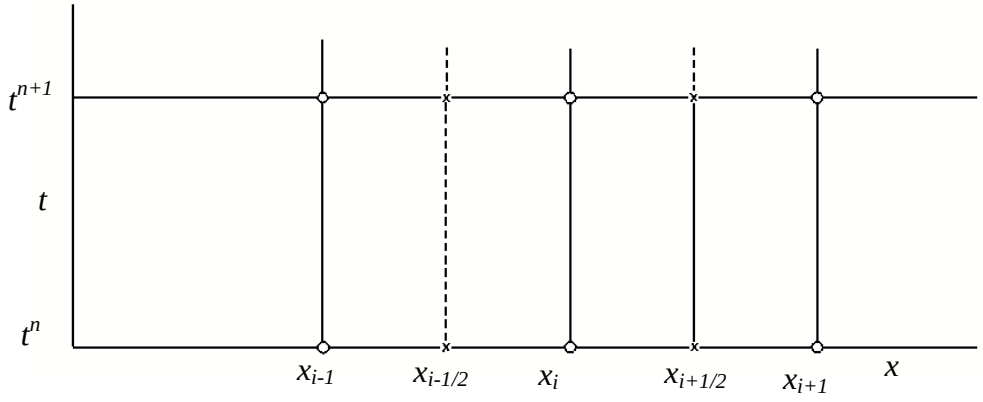


Figure 3. 2: A spatially staggered grid used for the discretization of the governing equations

Integrating Equations (3.1) and (3.2) over the $i^{th}$ cell with the length of $\Delta x$ and applying Greens theorem, following the approach of [56], yields the discretized form of the equations.

$$A_i^{n+1} = A_i^n - \frac{\Delta t}{\Delta x}(Q_i^n - Q_{i-1}^n) \tag{3. 4}$$

$$Q_i^{n+1} = Q_i^n - \frac{\Delta t}{\Delta x}\left(\frac{(Q_i^n)^2}{A_i^n} - \frac{(Q_{i-1}^n)^2}{A_{i-1}^n}\right) - \Delta t\left(gA_i^{n+1}\left[w_1\left(\frac{(z_i - z_{i-1})}{\Delta x} + \frac{(h_i^{n+1} - h_{i-1}^{n+1})}{\Delta x}\right) + w_2\left(\frac{(z_{i+1} - z_i)}{\Delta x} + \frac{(h_{i+1}^{n+1} - h_i^{n+1})}{\Delta x}\right)\right] - g\frac{n^2 Q_i^n |Q_i^n|}{(R_i^n)^{4/3} A_i^n}\right) \quad (3.5)$$

where $w_1$ and $w_2$ are weighting factors for the upwind and downwind fluxes of the water surface and they are evaluated by the following expressions.

$w_1 = 1 - \sqrt{Cr_{down}}$ and $w_2 = \sqrt{Cr_{up}}$

where $Cr_{down} = \frac{\Delta t}{\Delta x}\frac{u_{i+1} + u_i}{2}$ ; $Cr_{up} = \frac{\Delta t}{\Delta x}\frac{u_i + u_{i-1}}{2}$ and $u$ is the depth averaged velocity of the flow.

The flow rate $Q$ and cross sectional $A$ can be written as functions of depth averaged velocity $u(x,t)$, the depth of the water $h(x,t)$, and the width of the channel $B(x)$ according to

$$Q_i^n = u_i^n h_i^n B_i^n$$
$$A_i^n = h_i^n B_i^n \quad (3.6)$$

Substitution of Equation (3.6) into (3.1) and (3.2) allows the governing equations to be rewritten as functions of $u(x,t)$, $h(x,t)$ and $B(x)$. The resulting discretized forms of the governing equations are solved explicitly with the help of a MATLAB script written to solve for the water depth $h(x,t)$ and velocity $u(x,t)$. As given in [56], this scheme is conditionally stable with a stability condition of $Max\left[\frac{\Delta t}{\Delta x}(|u_i|) + \sqrt{gh_i}\right] \le 1$. The boundary conditions are treated by introducing a ghost grid point outside the domain where the conserved quantities and their gradients are specified.

The discretized governing equations result in algebraic equations which can easily be advanced in time. To examine the performance of this scheme, numerical results are

compared with existing analytical solutions for some benchmark test cases which can be found in, [56, 74, 75]. These test cases include: the idealized dam break problem with a dry bed; the idealized dam break problem with a wet bed and subcritical and transcritical steady flow over a horizontal open channel with a bump. The numerical implementation has been extensively validated on the following benchmark test cases. The results of the steady state test cases will later be used for the analysis and validation of the inverse problem.

### *3.3.1. Test case I: Idealized dam break problem in a rectangular channel with dry bed*

A 1200m long rectangular frictionless channel with unit width is considered with a dam located 500m from the upstream end of the channel. Initially the upstream water depth is 10m and the downstream channel is dry. The dry bed is treated by specifying the depth of the water as a very small number $h_{dry} \le 10^{-10}$ m to avoid numerical problems associated with division by zero. In the computation, a spatial grid size $\Delta x = 2$ m and a temporal grid size $\Delta t = 0.01$ s are used. Assuming the dam breaks at time $t = 0$, then the numerical results are generated 30 seconds after the dam failure. Figures 3.3 - 3.5 show comparisons of the numerically computed water depth, flow rate and velocity variations with the exact solution.

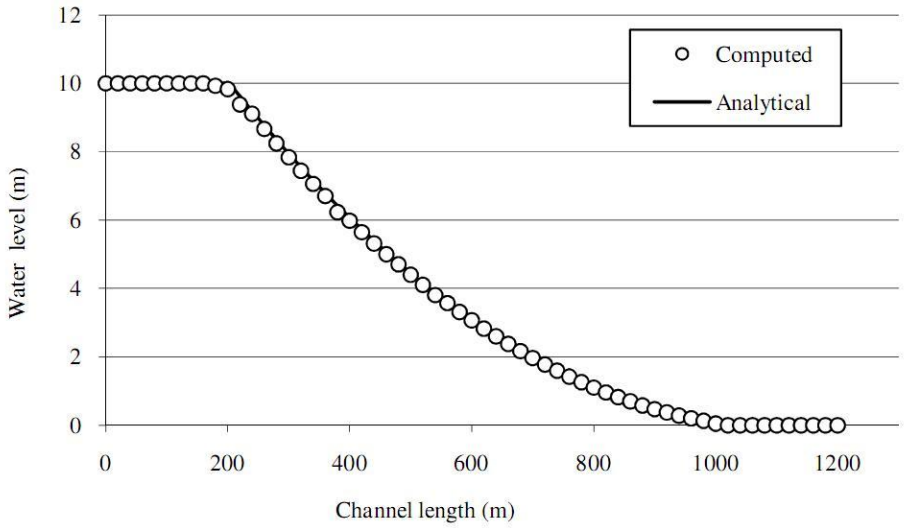


Figure 3. 3: Water level variation along a channel of the idealized dry bed dam break problem after 30 seconds.

The depth of the water varies parabolically from the undisturbed upstream edge and the dry bed. Three regions can be clearly seen in the flow; the undisturbed stationary region; the moving water front region and the dry bed region. The positive wave travels downstream on the dry bed, while a negative wave travels upstream into the undisturbed region. The depth of the flow towards the upstream direction reduces with time as a result of the flow mass flowing downstream.

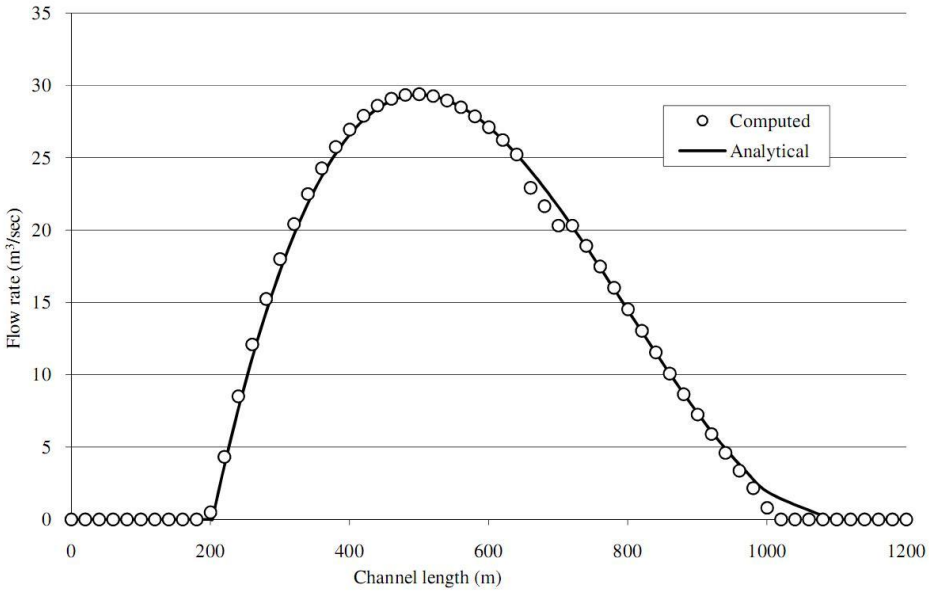


Figure 3. 4: Flow rate variation along the channel of the idealized dry bed dam break problem after 30 seconds.

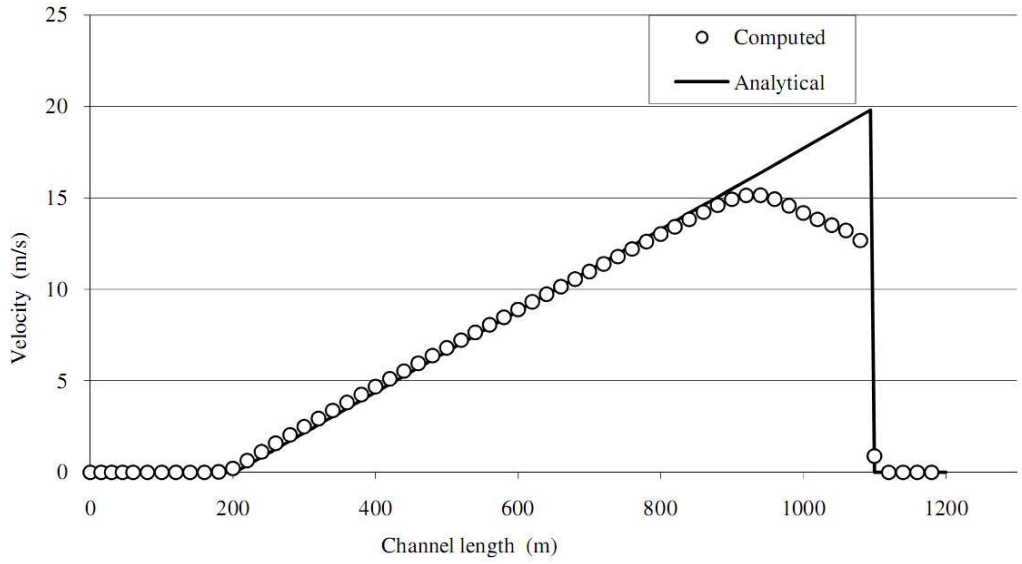


Figure 3. 5: Velocity variation along the channel of the idealized dry bed dam break problem after 30 seconds.

As can be seen in the comparisons above, the numerical results are in good agreement with the exact solution. In Figure 3.5, it can be seen that the velocity near the leading edge of the flow is under predicted. Many numerical models have difficulties in predicting the exact values of the velocities near the wave front edge, as the water depth in the area is very small [56] but as the focus of the present work is on the inverse problem, the quality of the numerical solution is deemed satisfactory for our purposes.

### *3.3.2. Test case II: Idealized dam break problem in a rectangular channel with wet bed*

In this test case the initial downstream water depth is set to 2 m while the domain and the numerical conditions are set to be similar as that of test case I. This test case is used to investigate the performance of the numerical scheme for a flow with discontinuities in the domain. The numerical results are generated 30 seconds after the dam failure. Water depth, flow rate, and velocity variations are compared with the exact solution in Figures 3.6 - 3.8.

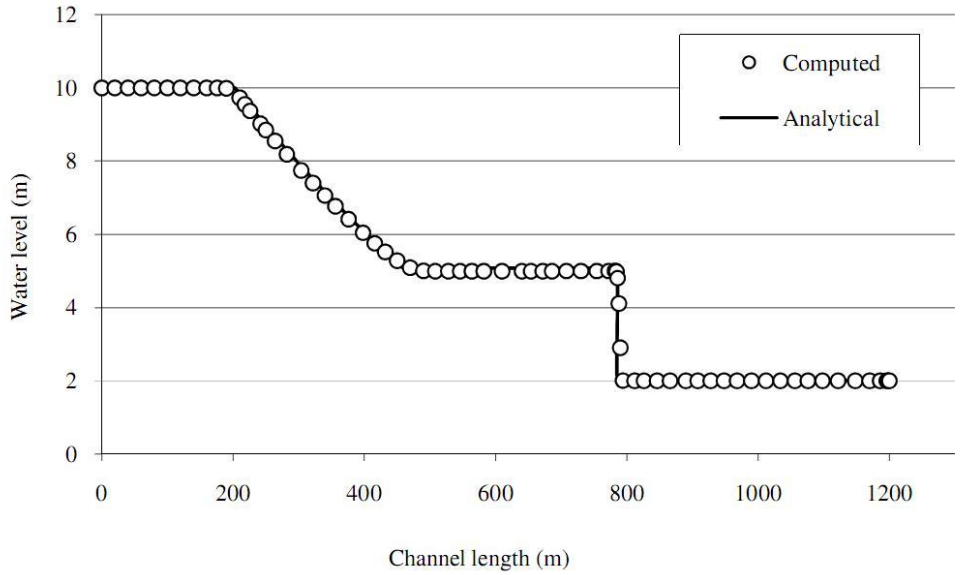


Figure 3.6: Water depth versus distance for the idealized wet bed dam break problem after 30 seconds.

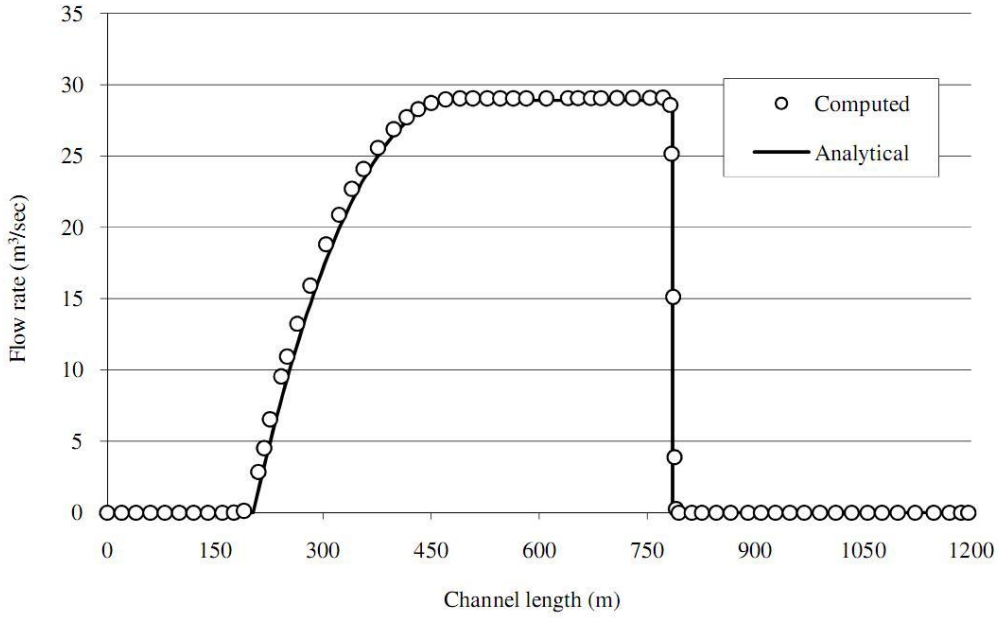


Figure 3.7: Flow rate versus distance for the idealized wet bed dam break problem after 30 seconds.

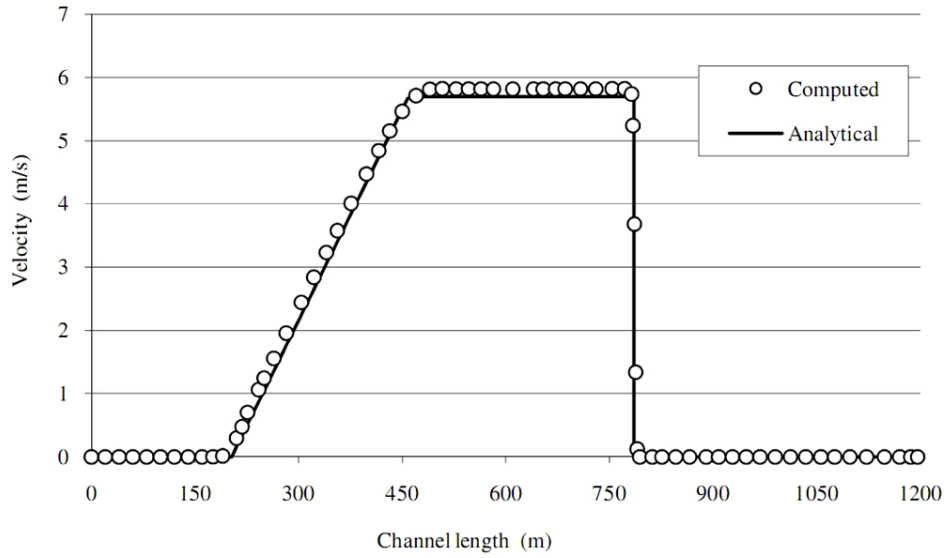


Figure 3.8: Velocity of the flow versus distance for the idealized wet bed dam break problem after 30 seconds.

As can be seen from the above Figures, there is good agreement between the computed results and exact solutions. Due to the presence of stationary water downstream of the dam, there exists a discontinuity at the interface of the moving front and the undisturbed downstream stationary water. The numerical scheme has accurately handled the discontinuity, at the moving wave front of the flow. The upstream depth of the water reduces with time in a similar fashion as in the case of the dry bed.

The above two test cases are presented for the sole purpose of evaluating the capability of the numerical scheme to solve unsteady shallow water flows. The test cases used to generate the free surface data for the inverse problem are described in the following section.

### *3.3.3. Test case III: Steady flow in a frictionless rectangular channel with a bump*

A 1m wide, 25m long channel is considered to test transcritical flow over a bump. The frictionless channel bed is assumed to have a rectangular cross section and a bump. The bed topography is defined by

$$z = \begin{cases} 0 & x < 8 \ \ and \ \ x > 12 \\ 0.2 - 0.05(x-10)^2 & 8 \le x \le 12 \end{cases} \tag{3. 7}$$

The depth at the downstream boundary is set as $h = 0.33\,\text{m}$ and the water inflow condition is specified as $Q = 0.18\,\text{m}^3/\text{s}$. This test is used to study the convergence of the numerical solution towards steady-state flow conditions and confirm the conservation of discharge along the channel. A spatial grid size $\Delta x = 0.1\,\text{m}$ and a temporal grid size $\Delta t$ = *0.01* s are used. Steady-state results have been generated and the flow rate over the domain was conserved after 400 seconds in the numerical computation. Figure 3.9 shows the comparison of computed water level with the analytical solution.

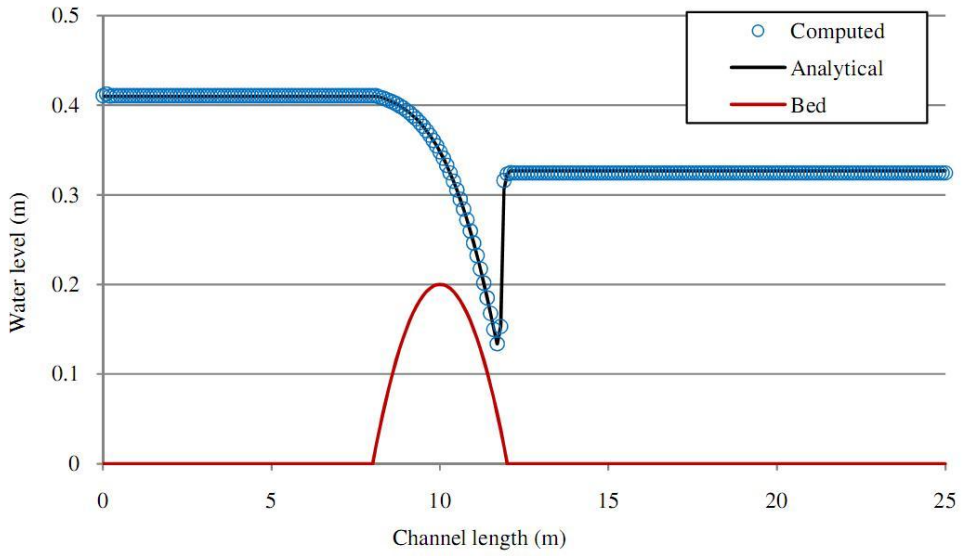


Figure 3. 9: Water level variations along a channel with transcritical flow

As an additional test case for the flow over the same bed topography, subcritical flow conditions of $Q = 4.42\,\text{m}^3/\text{s}$ at the upstream boundary and $h = 2\,\text{m}$ at the downstream boundary are imposed. This test case is performed to evaluate the performance of the scheme in predicting the steady-state water level for subcritical flow. The computed steady-state free surface profile is compared with its analytical solution in Figure 3.10.

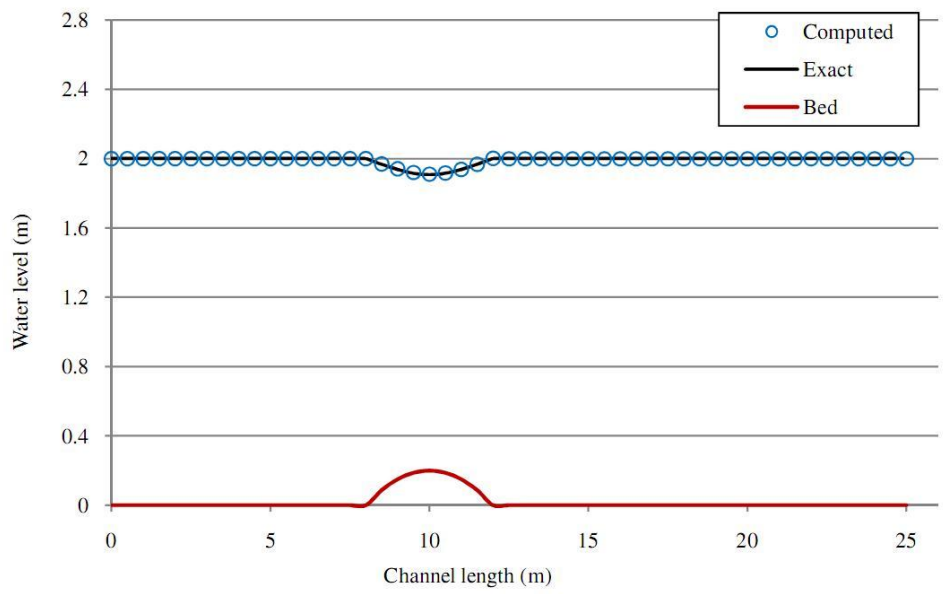


Figure 3. 10: Water level variations along the channel with subcritical flow

It can be seen that the numerical results are in good agreement with the analytical solution which can be obtained by applying the Bernoulli equation for the points outside the hydraulic jump in the domain. The jump region in the transcritical flow case has been modelled with the help of conservation of momentum. These results are also in a good agreement with the results presented in [56, 74, 75].

From the forward problem analysis, it is now established that the numerical scheme is capable of modelling steady and unsteady; subcritical and transcritical shallow water flows. Wetting and drying fronts numerical implementation is omitted due to the ranges of applicability of the whole solution approach presented in this thesis.

## 3.4. The inverse problem

The inverse problem for one dimensional flow is solved by two approaches: Numerical and Pseudo-Analytical approaches. Both approaches are easy-to-implement and fast to run. Those are presented below in detail.

A direct numerical approach is applied to solve the shallow water flow inverse problem. In order to solve the inverse reconstruction problem, the Saint-Venant equations are first rearranged to obtain an explicit partial differential equation which governs the inverse problem. The rearrangement is best understood by the variable $\psi = z + h$, which corresponds to the free surface elevation. The governing equations for the inverse problem are given by the equations.

$$\frac{\partial A}{\partial t} + \frac{\partial Q}{\partial x} = 0 \tag{3.8}$$

$$\frac{\partial Q}{\partial t} + \frac{\partial (Q^2 / A)}{\partial x} + gA\frac{\partial (\psi)}{\partial x} + gAS_f = 0 \tag{3.9}$$

The definitions of terms are as given in the previous section. The use of the free surface variable ($\psi$) reduces the complexity of the momentum equation which governs the inverse problem as the term $\frac{\partial h}{\partial x} + \frac{\partial z}{\partial x}$ is replaced by $\frac{\partial \psi}{\partial x}$. However, the bed topography is an unknown parameter which will be computationally determined from the discretized governing equations. The discretized equations take the same form as the one used in the forward problem, i.e.

$$A_i^{n+1} = A_i^n - \frac{\Delta t}{\Delta x}(Q_i^n - Q_{i-1}^n) \tag{3.10}$$

$$Q_i^{n+1} = Q_i^n - \frac{\Delta t}{\Delta x}\left(\frac{(Q_i^n)^2}{A_i^n} - \frac{(Q_{i-1}^n)^2}{A_{i-1}^n}\right) - \Delta t\left(gA_i^{n+1}\left[w_1\left(\frac{(\psi_i - \psi_{i-1})}{\Delta x}\right) + w_2\left(\frac{(\psi_{i+1} - \psi_i)}{\Delta x}\right)\right] - g\frac{n^2 Q_i^n |Q_i^n|}{(R_i^n)^{4/3} A_i^n}\right) \tag{3.11}$$

Substituting Equation (3.6) into (3.10) and (3.11) leads to the following set of algebraic equations.

$$h_i^{n+1} = h_i^n - \frac{\Delta t}{\Delta x}(h_i^n u_i^n - h_{i-1}^n u_{i-1}^n) \tag{3.12}$$

$$u_i^{n+1} = \frac{1}{h_i^{n+1}} \left\{ \begin{array}{l} h_i^n u_i^n - \frac{\Delta t}{\Delta x}\left( \frac{(h_i^n u_i^n)^2}{h_i^n} - \frac{(h_{i-1}^n u_{i-1}^n)^2}{h_{i-1}^n} \right) \\ - \Delta t\left( g h_i^{n+1}\left[ w_1\left( \frac{(\psi_i - \psi_{i-1})}{\Delta x} \right) + w_2\left( \frac{(\psi_{i+1} - \psi_i)}{\Delta x} \right) \right] - g \frac{n^2 h_i^n u_i^n \,|h_i^n u_i^n|}{(R_i^n)^{4/3} h_i^n} \right) \end{array} \right\} \tag{3.13}$$

where $w_1$ and $w_2$ are weighting factors for the upwind and downwind fluxes and they are evaluated by the following expressions.

$w_1 = 1 - \sqrt{Cr_{down}}$ and $w_2 = \sqrt{Cr_{up}}$

where $Cr_{down} = \frac{\Delta t}{\Delta x}\frac{u_{i+1} + u_i}{2}$ ; $Cr_{up} = \frac{\Delta t}{\Delta x}\frac{u_i + u_{i-1}}{2}$

The hydraulic radius $R_i^n$ is also evaluated simultaneously from the evaluated spatially distributed depth of the flow $h_i^n$. The Manning's friction coefficient is set identical as the forward problem test cases.

Equations (3.12) and (3.13) are solved iteratively and simultaneously for $(h)$ and $(u)$ using a MATLAB script given the initial and boundary conditions depending on the benchmark test cases used in the forward problem. Once the depth of the flow $(h)$ is determined from the above set of equations, the bed elevation $(z)$ is determined by simply subtracting $(h)$ from the given free surface elevation ($\psi$). Although unsteady governing equations are solved, the steady solution for steady boundary conditions is found after a finite number of iterations.

On the other hand by considering the steady state flow equations, it is shown that a pseudo-analytical solution exists to reconstruct the bed topography in shallow water flows. The steady state governing equations can be written as

$$\frac{dQ}{dx} = 0, \tag{3.14}$$

$$\frac{d(Q^2/A)}{dx} + gA\frac{d\psi}{dx} + gAS_f = 0. \tag{3.15}$$

Equation (3.14) depicts the conservation of mass in the flow showing that there exists a constant flow rate along the channel length. For a known continuous function $\psi$, the term $\frac{d\psi}{dx}$ is known by differentiating with respect to the independent variable $x$. However, in practice, the free surface data measurement is discrete and noisy and a curve fitting technique is required to obtain reliable gradients of the free surface. Simplifying Equation (3.15) and substituting into Equation (3.14) results in

$$\frac{Q^2}{A^3}\frac{dA}{dx} = g\frac{d\psi}{dx} + gS_f, \tag{3.16}$$

Equation (3.16) is a simple ordinary differential equation which can be solved by simple integration.

$$\int \frac{Q^2}{A^3} dA = \int g\left(\frac{d\psi}{dx} + S_f\right)dx, \tag{3.17}$$

$$\frac{Q^2}{2A^2} = -g\psi - g\int S_f dx + C_0, \tag{3.18}$$

Where $C_0$ is a constant of integration to account for the indefinite integral that can be determined from known boundary condition. For a known area of the flow, steady flow rate, and Manning's friction coefficient, the term $S_f$ can be determined.

If a frictionless channel is considered, the corresponding value of $C_0$ can be evaluated by

$$C_0 = \frac{Q^2}{2A_0^2} + g\psi_0, \tag{3.19}$$

Substituting the value of $C_0$ and introducing the friction term in the equation results in

$$\frac{Q^2}{2A^2} + g\psi + g\int S_f\, dx = \frac{Q^2}{2A_0{}^2} + g\psi_0\,, \tag{3.20}$$

Equation (3.20) is the energy equation which governs one-dimensional open channel flows with kinetic energy, potential energy, and loss of energy due to channel friction terms, respectively. This can be illustrated in Figure 3.1. The sum of the energies at point 1 is equal to the sum of the kinetic and potential energies at point 2 and the energy lost due to friction when the fluid particles experiences flow from 1 to 2.

The frictional energy loss between given points in a flow can be evaluated by considering an infinitesimal channel length over which we can conveniently assume a constant frictional loss. Hence, equation (3.20) can be rewritten between grid point (*i*) and (*i*-1) in the computational domain which relates the change in free surface elevation, kinetic energy, and frictional energy loss between these grid points. Accordingly,

$$\left(\frac{Q^2}{2A^2}\right)_i - \left(\frac{Q^2}{2A^2}\right)_{i-1} + g\left(\psi_{(i)} - \psi_{(i-1)}\right) + g\Delta x\left(S_{f(i)} - S_{f(i-1)}\right) = 0, \tag{3.21}$$

Substituting equation (3.6) into (3.20) produces the following simplified form.

$$u^2{}_i - u^2{}_{i-1} + 2g\left(\psi_{(i)} - \psi_{(i-1)}\right) + 2g\Delta x\left(S_{f(i)} - S_{f(i-1)}\right) = 0. \tag{3.22}$$

Thus by applying a marching approach from the upstream to the downstream boundary, we can solve for $(u)$ and then for $(h)$ from the continuity equation to generate a pseudo-analytical solution for the channel bed topographic elevation in the one-dimensional context.

Equation (3.22) and continuity equation for the steady flows will be solved for ($u_i$) and ($h_i$) simultaneously. The channel bed topographic elevation is then evaluated using ($z_i = \psi_i - h_i$) to complete the pseudo-analytical approach.

The known free surface profiles used in the following test cases are the results obtained from the forward problem solution. The discretized free surface elevation data are used as input parameters for the solution of the inverse problem.

In practice, measured free surface data obtained from experiments will be noisy. Thus to account for this issue, noise is introduced as a percentage of the total depth of the flow in the free surface profile to simulate realistic measurement conditions. In the inverse problem solution, the noisy free surface data is smoothed in order to avoid unbounded gradient levels within the free surface. The requirements of the curve matching all data points and possessing a continuous first derivative can be satisfied by cubic spline fitting as it generates curves with continuous first and second order derivatives.

### *3.4.1. Test case I: Steady subcritical flow in a rectangular channel with a bump*

The same 1m wide, 25m long rectangular frictionless channel as section 3.3.3 is considered to test the reconstruction algorithm for subcritical flow over a bump. The frictionless channel is assumed to have a rectangular cross section. The known free surface profile of the flow is given as discrete values over the domain of calculation as shown in Figure 3.11. It is used as input data for the inverse problem analysis to predict the underlying bed topography.

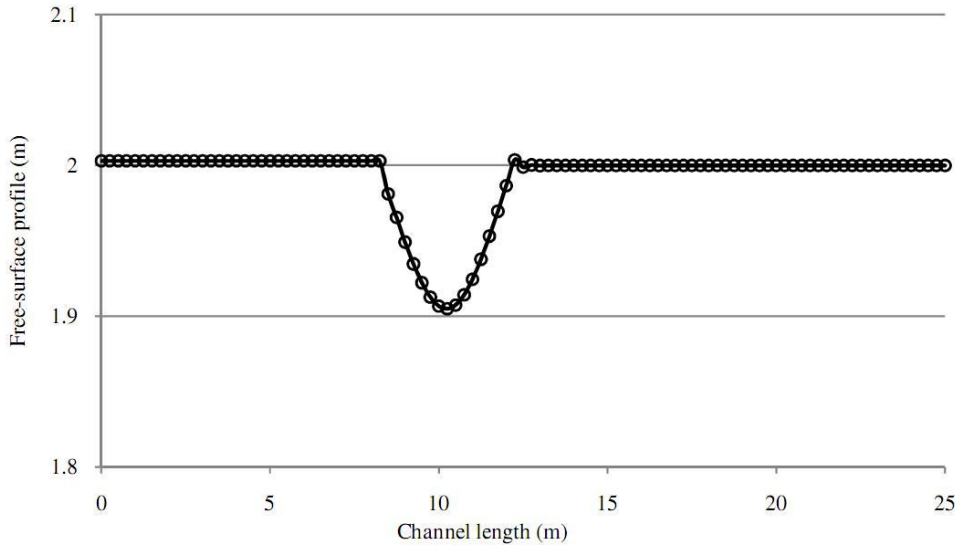


Figure 3. 11: Known subcritical free surface profile to be used for the inverse problem

For this test case, similar boundary conditions as for the forward problem (upstream flow rate $Q = 4.42$ m$^3$/s with the downstream flow depth $h = 2$ m) are imposed for the inverse problem. The spatial and the temporal increments are the same as for the corresponding forward problem. Results are presented in Figures 3.12 and 3.13. This well-studied problem could be used in the future as a benchmark problem for bed reconstruction. The reconstructed bed topography of the inverse problem can be now compared with the respective input bed topography of the forward problem.

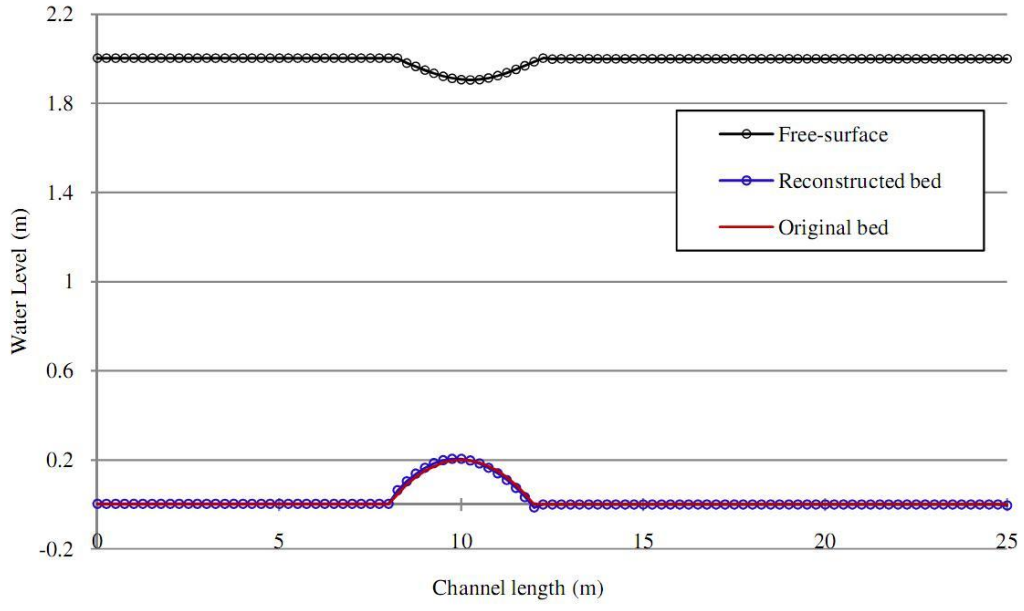

Figure 3.12: Comparison of the reconstructed and the original bed topographies for subcritical flow test case

In Figure 3.12, it can be seen that the reconstructed channel bed topography is in good agreement with the original channel bed topography that was defined for the forward problem. In the following, 5% noise based on the depth of the flow is introduced to the free surface information to account for inaccuracy in the data obtained from field surveys.

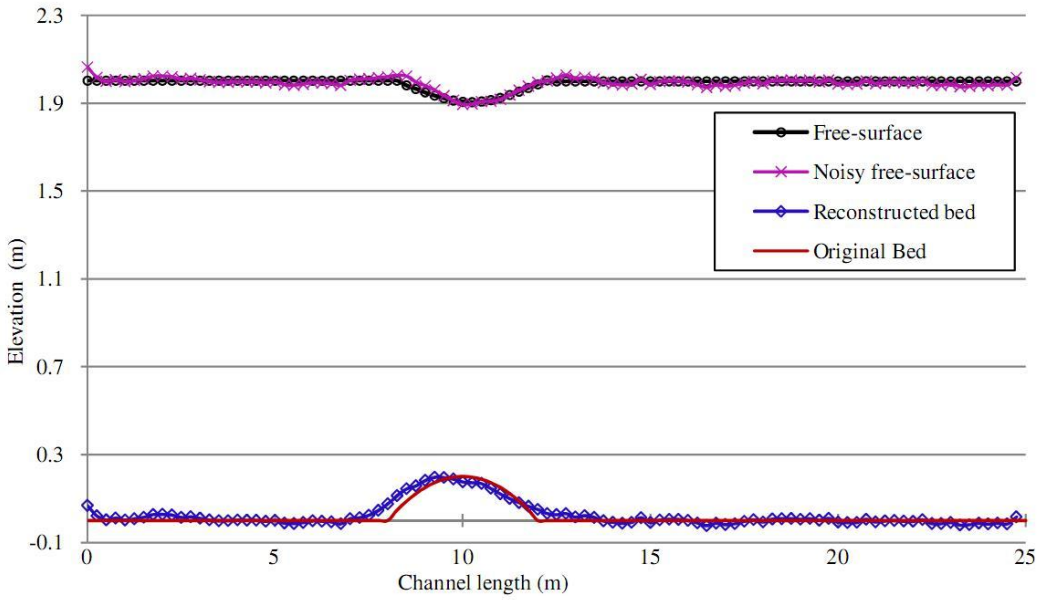


Figure 3.13: Comparison of the reconstructed bed and the original bed (frictionless) using a noisy free surface data for subcritical flow test case

Noise was added to the computed steady free surface profile in order to have data truly representative of experimentally measured data. The resulting profile was then smoothed by using a cubic spline fit. The results show that even with 5% noise added to the free surface data, the channel bed can be reconstructed with a 3.75% maximum difference between the predicted and the original channel bed which is a very encouraging result.

### *3.4.2. Test case II: Steady trans-critical flow in a rectangular channel with a bump*

For this test case, a similar methodology to the subcritical flow case is adopted but the trans-critical nature of the flow makes the inverse problem more challenging. The steady

state free surface profile which was obtained from the forward problem solution is used as input data for the inverse problem. The same boundary conditions as for the forward problem solution are imposed, i.e. the depth at the downstream boundary is set as $h = 0.33\,\text{m}$ and the water inflow condition is specified as $Q = 0.18\ \text{m}^3/\text{s}$.

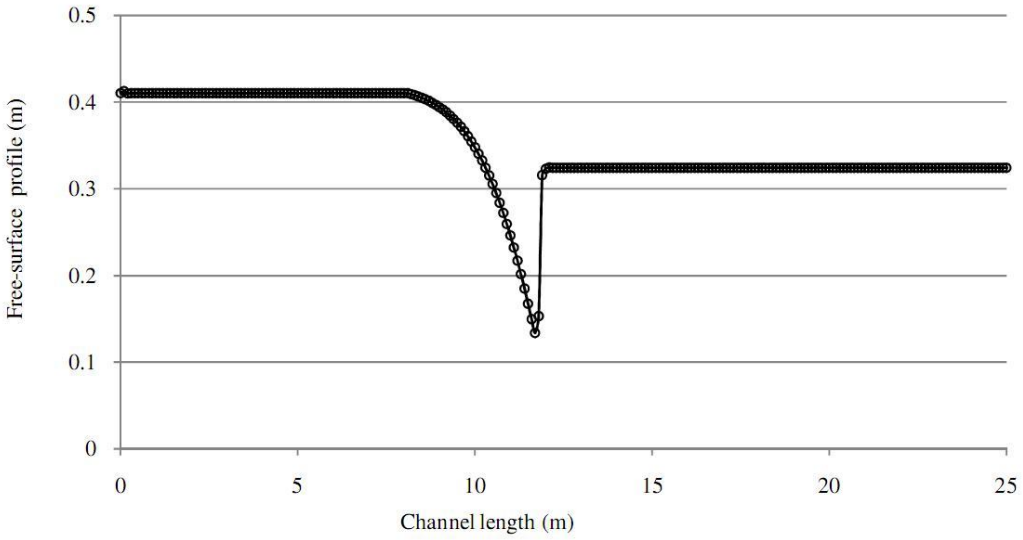


Figure 3.14: Known transcritical free surface profile used for the inverse problem

The time step and spatial increment in the inverse problem analysis are the same as those used for the forward problem. Figure 3.15 depicts the comparison of the reconstructed bed with the original bed topography. It can be seen that the reconstructed channel bed topography is in good agreement with the actual bed topography. The shape and elevation of the underlying bed topography is adequately retrieved.

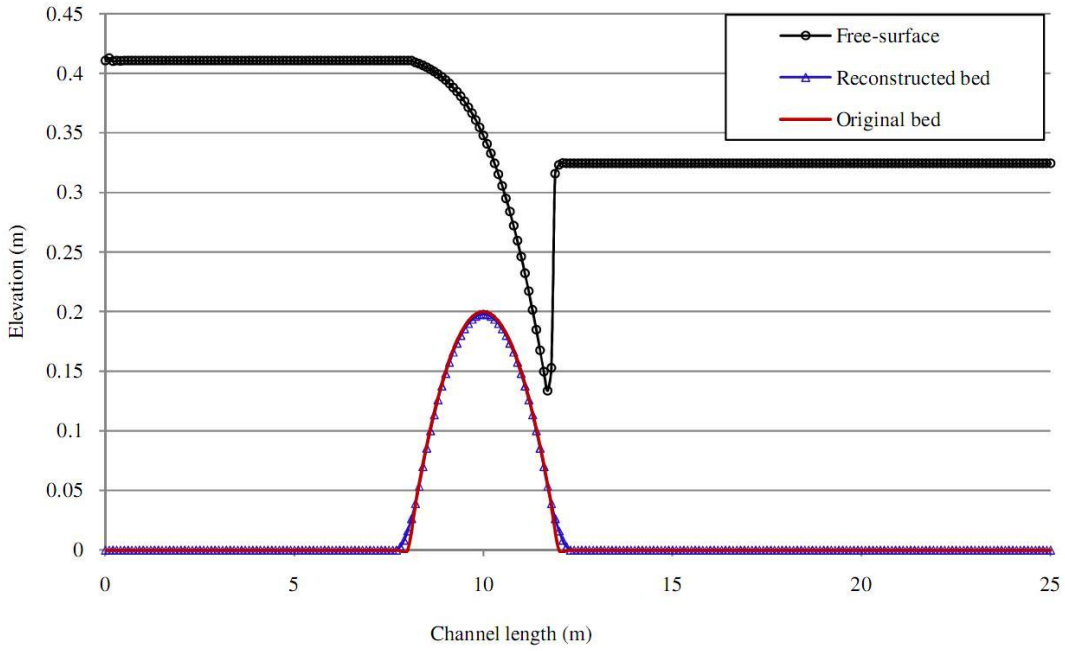


Figure 3.15: Comparison of the reconstructed bed with the original bed topography for the transcritical flow test case

To test the behaviour of the algorithm in the presence of measurement inaccuracy, 5% noise is introduced to the free surface profile. As previously, a cubic spline is fitted to the noisy free surface data for smoothing. Unlike the subcritical flow test case, the maximum difference between the original and reconstructed riverbed is now 7.5%, which shows that the noise in the data has been slightly amplified but is still well within reasonable bounds. The increased amplification is most likely due to the difficulties of the numerical computation to accurately predict the hydrodynamics of the flow at the jump. The noise level in the reconstructed channel bed topography before and after the jump is $\leq 3.75\%$, which is equivalent to the subcritical flow test case. This is an indication that the technique is capable of reconstructing the bed topography from the known free surface profile irrespective of inaccuracies in the free surface profile, although noise amplification is pronounced at the hydraulic jump as shown in Figure 3.16.

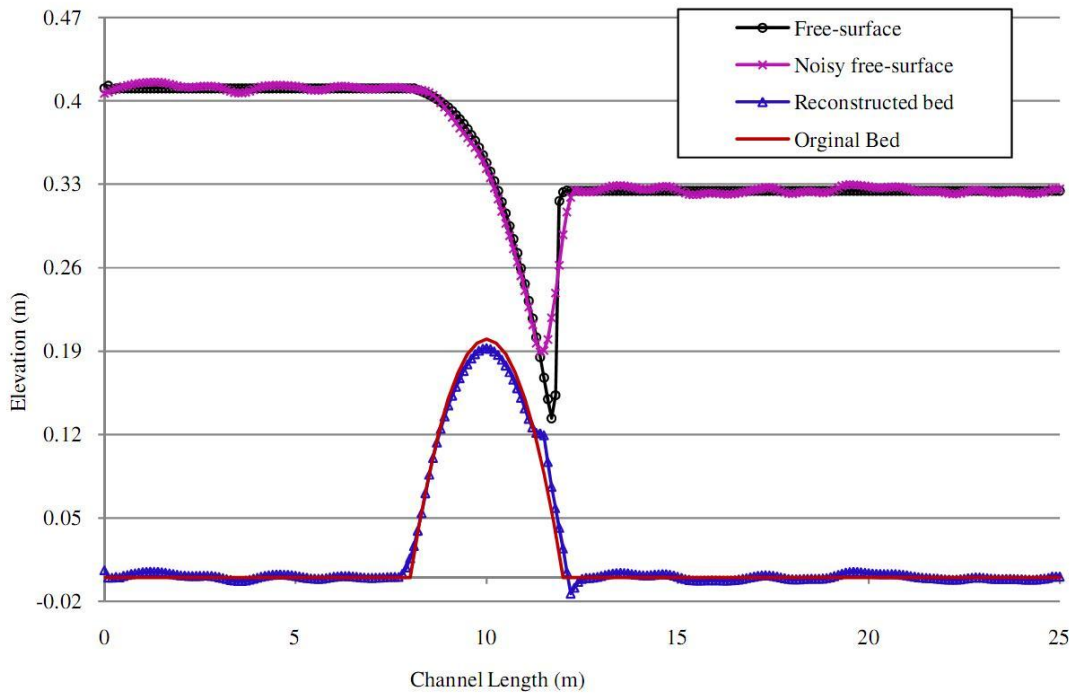


Figure 3.16: Comparison of the original and reconstructed bed topographies from the noisy free surface for the transcritical flow test case

Although results obtained from the computation of similar resolution as the forward problem are presented, this direct numerical approach is capable of reconstructing the channel bed topography from the known free surface profile with different resolution so long as the CFL condition is satisfied.

### *3.4.3. Test case III: Experimental study*

A set of experiments was conducted to measure the free surface data for a given steady flow rate in a horizontal flume at the department of Civil Engineering Department in the University of Canterbury. The flume comprises a rectangular section of channel with 0.56m width which is open at the top. It has clear acrylic walls which are bonded to the bed. A bed form with constant profile along its span is placed and mounted on the flat bed to give an uneven bed profile. Once a steady state flow rate is set, the free surface elevation is measured in the flow direction by a point gauge. The bed topography under

study has the form shown in Figure 1 with a maximum elevation of 62 mm above the horizontal channel.

For given flow conditions, a steady flow rate is set at 25±0.5 litres/second, the depth of the flow at the unaffected upstream position is 144±3 mm; the depth of the flow along the channel is measured hence the free surface elevation can be determined. Figure 3.17 and table 3.1 show the stage of the flow and the measured channel bed topography from the experiment.

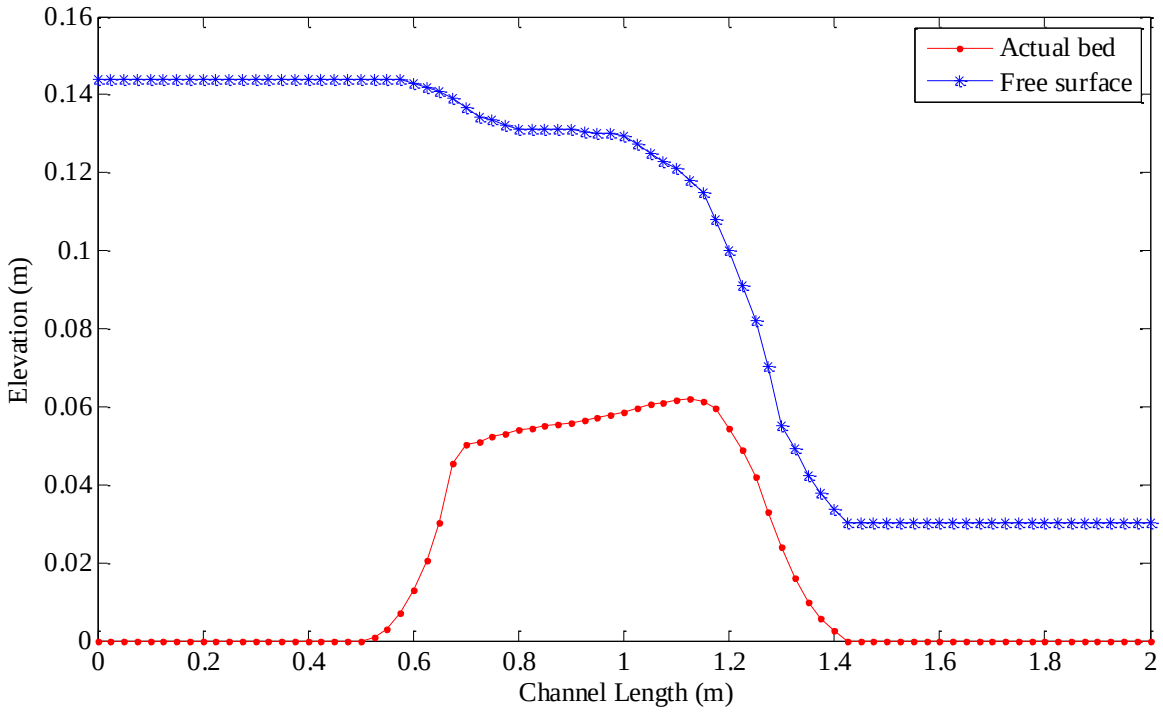


Figure 3.17: Free surface elevation and bed topography (flow is left to right)

| Channel length (m) | Bed level (m) | Stage (m) | Channel length (m) | Bed level (m) | Stage (m) |
|---|---|---|---|---|---|
| 0 | 0 | 0.144 | 1.1 | 0.0646 | 0.121 |
| 0.1 | 0 | 0.144 | 1.2 | 0.056 | 0.1 |
| 0.2 | 0 | 0.144 | 1.3 | 0.021 | 0.055 |
| 0.3 | 0 | 0.144 | 1.4 | 0.0025 | 0.0336 |
| 0.4 | 0 | 0.144 | 1.5 | 0 | 0.0304 |
| 0.5 | 0 | 0.144 | 1.6 | 0 | 0.0304 |
| 0.6 | 0.0128 | 0.143 | 1.7 | 0 | 0.0304 |
| 0.7 | 0.0532 | 0.1366 | 1.8 | 0 | 0.0304 |
| 0.8 | 0.057 | 0.131 | 1.9 | 0 | 0.0304 |
| 0.9 | 0.0584 | 0.131 | 2 | 0 | 0.0304 |
| 1 | 0.0604 | 0.1293 | | | |

Table 3.1 Bed and free surface elevation along the channel

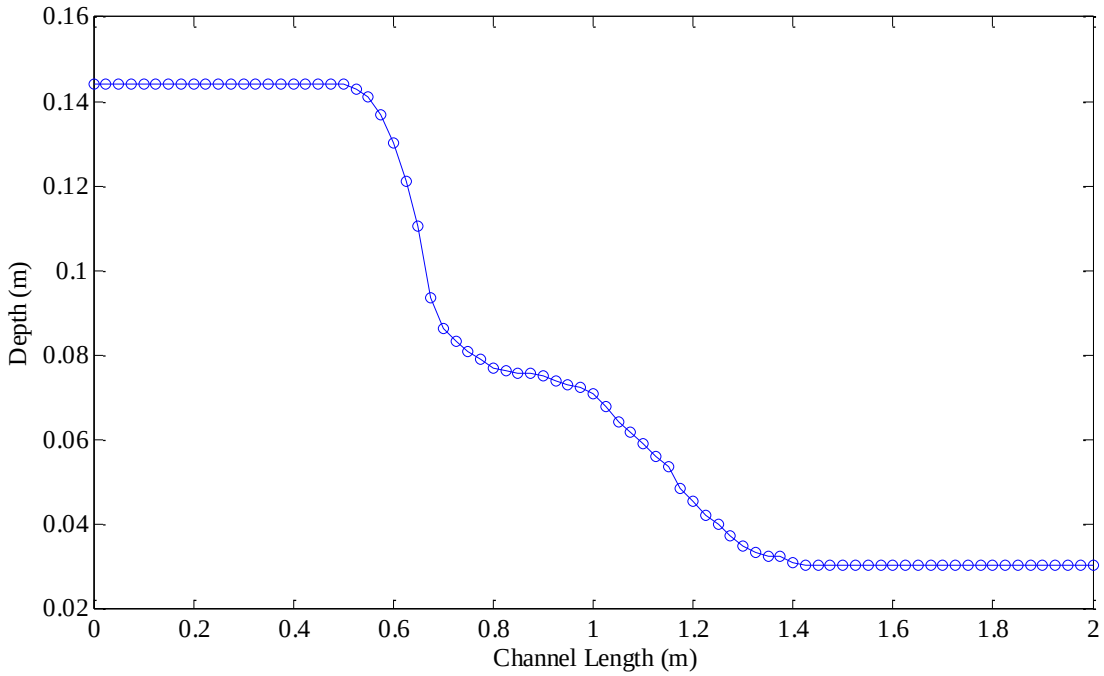


Figure 3.18: Flow depth variation along the channel length

The variation of depth of the flow is shown in Figure 3.18. As can be seen from the above Figures, the presence of the bed form affects the flow conditions. Downstream of the form, the flow has constant depth and it is supercritical in nature while at the upstream, the flow is subcritical. The computed values of Froude number (Fr) ranges from 0.26 to 2.74 at the inlet and outlet of the flow considered for this study.

The known free surface along with the steady flow rate and boundary conditions can be used with the numerical reconstruction algorithm and pseudo-analytical solution methodology to infer the channel bed topography.

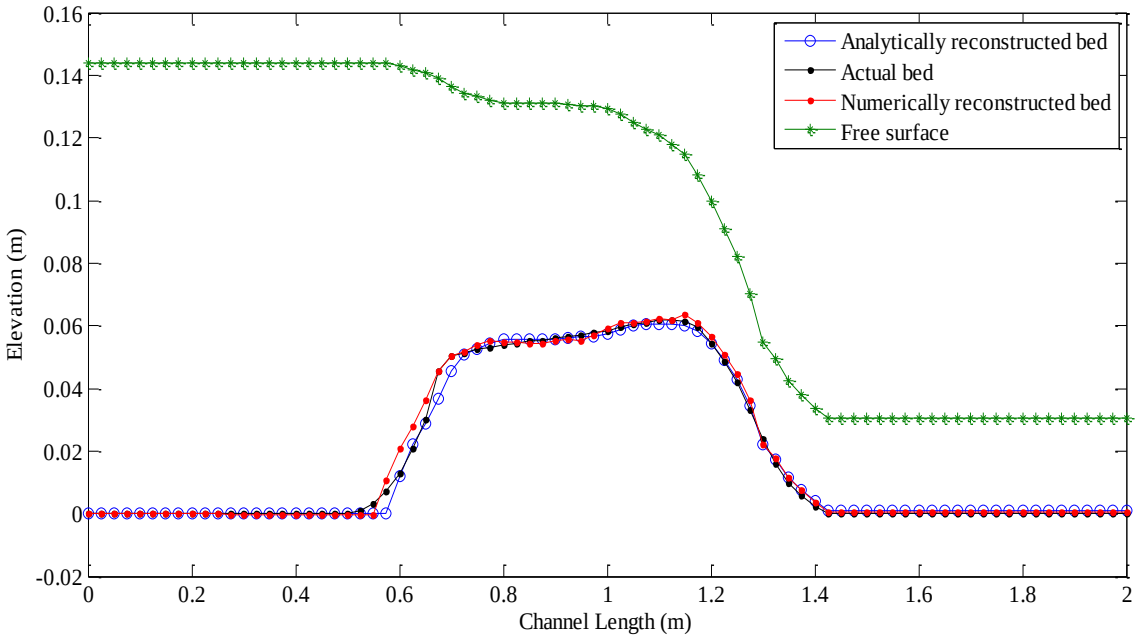


Figure 3.19: Comparison of numerically and pseudo-analytically reconstructed bed with actual bed

As can be seen from Figure 3.19, the numerically and pseudo-analytically reconstructed channel bed topographies and actual bed topography are in good agreement with each other. The slight difference on the left part of the topography arose from steady flow rate variations. The magnitude of the maximum difference in the reconstructed and actual bed topographies is approximately 5%. The uncertainty in the reconstructed bed topography is a consequence of the uncertainty in the steady flow rate measurement.

As can be seen from the above methodology, to infer channel bed topography from the free surface data in shallow water flows, the knowledge of the steady state flow rate, friction coefficient and the flow depth at the boundary depending on the type of the flow are required. In practice the steady flow rate at one particular site can be estimated using techniques such as traditional (*in-situ*) data gathering and remote sensing frameworks, see e.g. [76, 77]. In the traditional framework, measurements of the width of the stream, the flow velocity and the depth of the flow at a particular site are made across the stream. The instantaneous total water discharge is then estimated as the product of these variables. However, the free surface elevation data should be obtained during steady or quasi-steady flows of the river. In the latter, remotely sensed water levels from altimetry or inundation areas from imaging near a gauging station are correlated with the simultaneous ground data (flow area or width) to estimate the total discharge across the stream, see [78] and references therein.

The reconstruction approach, additionally, requires the existence bed topography signature on the free surface. i.e. if there is no free surface variation due to the local change in bed topography, the reconstruction approach ceases to identify the underlying bed topography. For this reason, the one dimensional numerical reconstruction algorithm was tested over ranges of Froude numbers by varying the inlet flow rate and the depth of the flow at the outlet boundary. It was noted that the approach works better for Fr $\geq$0.18. However, further mathematical analysis with more numerical experiments is required to set a generalised statement. The reconstruction approach is limited by the existence the signature of the bed topography on the free surface flows.

In order to test the effect of flow rate uncertainty on the bed reconstruction, the reconstructed riverbed from the true flow rate is compared to the one reconstructed with a flow rate increased by 5%. The difference in the reconstructed riverbeds did not exceed

4.51% confirming once more the robustness of the proposed algorithm which does not amplify measurement errors for 1D steady shallow water flow.

# 4. One-dimensional bathymetry based on the free surface velocity

## Contents

## 4.1. Introduction

The free surface velocity of the flow in open channels varies locally and spatially depending on the type of channel: straight, steep, bends and/or meandering. These variations also exist depending of the state of the flow; uniform, non-uniform, laminar or turbulent. The velocity profile in an open channel flow may also vary depending on the changes in the roughness of the channel, longitudinal bed slope and transverse bed slope, see e.g. [5, 70, 79] Free surface velocity can be measured using different techniques. To mention some, Plant and co-workers [80] used an array of newly developed continuous-wave microwave sensors to measure the free surface velocity and showed that the results of measured free surface velocity agrees well with the near free surface velocities measured by Acoustic Doppler Current Profiler and a current meter. Electromagnetic wave surface velocimetry ($ESV_s$) technique is used in [81] to obtain the water surface velocity measurements from bridges and river banks. Muste et al. [82] used controlled surface waves to measure the free surface velocity of a flowing fluid which gives an instantaneous velocity field over the domain. Large scale particle image velocimetry (PIV) is used by many authors to measure the two-dimensional velocity fields at the free surface of shallow water flows to obtain the fundamental flow properties, see e.g. [83, 84].

Since the idea explored in this chapter is to reconstruct the channel topography from known velocity data, it is necessary first to review the important findings about the velocity distribution in shallow-water flows. The log-law and power-law velocity distributions are the most widely used relationships to describe the vertical profile of velocity in shallow water flows. However, these relationships have their own merits and demerits depending on the flow conditions and regions in the flow. The log-law, for instance, is widely used to approximate the velocity distribution in the turbulent sub-layer region which constitutes 20% of the total depth of the flow. On the contrary, it is asserted

that the power-law could be applied for the bulk of the flow and it has more practical applications in wide open channel flows [85]. In fully developed turbulent open channel flows the velocity distribution can be well approximated by Prandtl's Power-law, [86]. The maximum flow velocity in turbulent flows mostly occurs below the free surface while in the case of laminar flow the maximum velocity occurs at the free surface. For turbulent flows with shallow depth and high velocity, the maximum velocity occurs near the free surface, [23]. In narrow open channels, the free surface velocity is less than the maximum velocity which exists below the free surface at the same position due to the existence of secondary currents which transport low momentum fluids to the centre from the bank and high momentum fluids from the free surface to the bed in the vertical direction, [87-90]. This phenomenon is referred as the dip phenomenon, in this case the log-law and the power law ceases to predict the velocity profile except in the inner turbulent boundary layer region. This is due to the existence of the non-zero vertical velocity in the flow, [23, 87] which occurs in narrow channel turbulent flows with aspect ratio ($b/h < 5$),

According to Plant and co-authors [80], the free surface to mean velocity relationship changes little with the depth or the stage of the flow. Other researchers found that the mean value of the ratio of mean to maximum velocities of flow in a channel section is constant, [90, 91]. Lee and Julien compared laboratory and field measurements of the free surface velocity in open channel flows, [81]. Their results show that the ratio of the cross section averaged velocity to mean free surface velocity can be approximated by a constant value depending on the magnitude of the flow velocity. It is shown that the ratios are approximately 0.88, 0.79, and 0.61 for high flow velocities during flooding, medium flow velocities and low velocities, respectively. Polatel showed that there exists a change in the ratio with changes in depth of the flow and roughness of the channel in open channel flows; for instance, the ratio slightly decreases when roughness increases, [92]. Thus, the

ratio of the two velocities can be assumed to be constant in the flow domain if the changes in the roughness of the channel and the depth of the flow in both directions are acceptably small.

The reconstruction of bed topography from the free surface velocity data follows a similar conceptual idea which is implemented in the previous chapter which is the direct approach. Similar approach is presented in [53] where the the direct solution approach is adopted to infer the substrate topography from the free surface velocity in thin film flows. A numerical technique to infer the channel bed topography from a known free surface velocity field is presented in this chapter. The one-dimensional Saint-Venanat equations are used to derive the ordinary differential equation which allows direct inference of the bed topography from the free surface velocity. Benchmark test cases are used to investigate the validity of the method. These benchmark test cases include subcritical and transcritical flow over a frictionless prismatic channel with a bump and an experimental study.

## 4.2. Simplification of the governing equation and solution methodology

The methodology implemented to infer the channel bed topographic elevation from the free surface velocity is based on the one-dimensional shallow water conservation laws. Thus, the following analysis is based on equations (3.1) and (3.2) simplified for 1D steady flows. Figure 4.1 illustrates the configuration considered here and the adopted notations. It shows that the unevenness of the bed topography creates undulations on the free surface. These undulations depend on the depth of the flow, the slope of the channel bed and the channel friction where the free surface or depth averaged velocity variation exists due to the existence of the uneven bed topography.

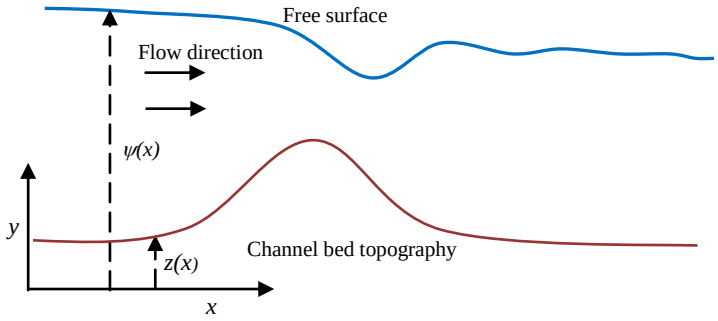

Figure 4. 1: Description of the flow showing the free surface and channel bed elevation

In practice, direct measurement of depth averaged velocity can be difficult; however, the free surface velocity of the flow is more readily measurable. Thus, it is important to use an existing and more efficient relationship between the depth averaged and the free surface velocities. As mentioned in the introduction section, different mathematical models have been used to relate the depth averaged and free surface velocities for open channel flows. By introducing such a relationship into the governing equations, we obtain equations in terms of the free surface velocity instead of the depth averaged velocity.

In previous work, see [25] for example, it is postulated that the depth averaged velocity and the free surface velocity are proportional according to the following relationship.

$$u = \alpha u_s \tag{4. 1}$$

Where $\alpha$ is an empirical proportionality constant assumed independent of $x$ here and $u_s$ is a free surface velocity. For 1D steady flows, the unsteady flow equations are simplified to equations (4.2) and (4.3).

$$hu = q_o \tag{4. 2}$$

where $q_o$ is the steady flow rate (per unit width)

$$\frac{\partial (u^2 h)}{\partial x} + gh\left(\frac{\partial h}{\partial x} + \frac{\partial z}{\partial x}\right) + ghS_f = 0 \tag{4. 3}$$

Where $S_f = \frac{n^2 u\sqrt{(u^2+v^2)}}{h^{4/3}}$

Rearranging equation (4.2) and substituting it in equation (4.3) will give us a governing equation as a function of the steady flow rate and the depth averaged velocity along with the bed topography variable $z(x)$. Accordingly,

$$q_o \frac{\partial u}{\partial x} + g\frac{(q_0)^2}{u}\left(\frac{\partial}{\partial x}\left(\frac{1}{u}\right)\right) + g\frac{q_0}{u}\frac{\partial z}{\partial x} + g\frac{q_0}{u}S_f = 0 \qquad (4.4)$$

Simplifying this equation results in the following one-dimensional 1st order ordinary differential equation for the unknown parameter $z(x)$ in term of the average velocity:

$$\frac{dz}{dx} = -\frac{u}{g}\frac{du}{dx} - q_0\frac{d}{dx}\left(\frac{1}{u}\right) - S_f \qquad (4.5)$$

From the relationship of the depth averaged velocity and the free surface velocity, we can substitute Equation (4.1) in Equation (4.5).

$$\frac{dz}{dx} = -\frac{\alpha^2}{g}u_s\frac{du_s}{dx} - \frac{q_0}{\alpha}\frac{d}{dx}\left(\frac{1}{u_s}\right) - S_f \qquad (4.6)$$

Rearranging equation (4.6) and integrating results in

$$\frac{dz}{dx} = \frac{d}{dx}\left(-\frac{\alpha^2}{2g}u_s{}^2\right) - \frac{d}{dx}\left(\frac{q_0}{\alpha}\frac{1}{u_s}\right) - S_f \qquad (4.7)$$

$$z = -\frac{\alpha^2}{2g}u_s{}^2 - \frac{q_0}{\alpha}\frac{1}{u_s} - \int_{x_0}^{x} S_f\,dx + C_0 \qquad (4.8)$$

where $C_0$ is a constant of integration which can be determined from the boundary conditions.

It is assumed here that the bed elevation is known at the inlet boundary. At $x=0$, $u_s = u_{s0}$ and the value of the constant is $C_0 = z_0 + \frac{\alpha^2}{2g} u_{s0}{}^2 + \frac{q_0}{\alpha}\frac{1}{u_{s0}}$. Substituting this expression back into equation (4.8) results in

$$z = z_0 + \frac{\alpha^2}{2g}\left(u_{s0}{}^2 - u_s{}^2\right) + \frac{q_0}{\alpha}\left(\frac{1}{u_{s0}} - \frac{1}{u_s}\right) - \int_{x_0}^{x_i} S_f\, dx \qquad (4.9)$$

Equation (4.9) relates the free surface velocity $u_s(x)$ to the bed topography elevation $z(x)$ of steady flows when the free surface and depth averaged velocities are related by proportionality constant. Substituting the value of $S_f$ into equation (4.9) will give the explicit expression for the reconstruction algorithm. The final equation will be

$$z_i = z_0 + \frac{\alpha^2}{2g}\left(u_{s0}{}^2 - (u_s)_i{}^2\right) + \frac{q_0}{\alpha}\left(\frac{1}{u_{s0}} - \frac{1}{(u_s)_i}\right) - \int_{x_0}^{x} \frac{n^2\alpha^{7/3} u_{si}{}^{7/3}}{q_0{}^{\frac{1}{3}}} dx \qquad (4.10)$$

The integral in equation (4.10) can be evaluated by trapezoidal rule over discrete data points. The trapezoidal rule is applied for each segment to determine the integral in equation (4.10), meaning from $(i)$ and $(i+1)$ grid points, in order to determine the integral with better accuracy. The values of velocity proportionality constant $\alpha$ and the Manning's friction coefficient $n$ are considered as constants which depend on individual test cases considered here below. The value of the integral to determine $z_i$ will be the difference between the sum of the integral of the segments from the boundary to the $(i^{th})$ grid point and the value of the integral at the boundary. However, the value of the integral does not affect the reconstruction process for the test cases involving frictionless channel topography.

## 4.3. Sensitivity analysis

It is essential to investigate the sensitivity of the solution methodology to perturbations in the known parameters. This perturbation includes changes in the free surface velocity and the velocity ratio $(\alpha)$. A sensitivity analysis is performed for the perturbations in the free surface velocity and the velocity ratio. Rewriting equation (4.9) with a small perturbation in the free surface gives

$$z+\Delta z=-\frac{\alpha^2}{2g}\left((u_s+\Delta u_s)^2\right)-\frac{q_0}{\alpha}\left(\frac{1}{(u_s+\Delta u_s)}\right)-\int_{x_0}^{x}\frac{n^2\alpha^{7/3}(u_s+\Delta u_s)_i^{7/3}}{q_0^{\frac{1}{3}}}dx+C_0 \quad (4.11)$$

Evaluating for $\Delta z$ with the help of Taylor series expansion and neglecting higher order terms the following equation can be obtained.

$$\Delta z=\frac{\alpha^2}{2g}(2u_s\Delta u_s)-\frac{q_0}{\alpha}\left(-\frac{\Delta u_s}{(u_s)^2}\right)-\int_{x_0}^{x}\frac{7}{3}\frac{n^2\alpha^{7/3}}{q_0^{\frac{1}{3}}}(u_s)^{4/3}\Delta u_s dx \quad (4.12)$$

Further simplification for a frictionless channel leads to the following expression for $\Delta z$:

$$\Delta z=-\frac{\alpha^2}{g}(u_s\Delta u_s)+\frac{q_0}{\alpha}\left(\frac{\Delta u_s}{(u_s)^2}\right) \quad (4.13)$$

From this relationship, it can be seen that the perturbation in the reconstructed channel bed is of the same order as the order of perturbation induced on the free surface velocity, i.e. $o(\Delta z)\cong o(\Delta u_s)$, when first order linearization is considered. Additionally, numerical tests have shown that for 10% random noise introduced in the free surface velocity, the resulting noise in the reconstructed bed is lower than 10%. This supports the above argument that noise is not amplified in the reconstruction procedure. Such a noise level is realistic since Muste et al. [84] have shown that the mean velocity can be measured within

3.5% in normal conditions and up to 10% in adverse (less visibility) conditions. Balachandar et al. [93] have also demonstrated that the free surface velocity can be measured to within 2%.

Similar linearization analysis and numerical test cases based on the noise on the velocity ratio shows that, the level of perturbation on the value of the velocity ratio induces an error with comparable order of magnitude as the perturbed value in the reconstruction process. These results show that there will be no noise amplification in the reconstruction algorithm from noisy free surface data of 1D steady shallow water flow.

## 4.4. Numerical test cases of the inverse problem

The following test cases are used to assess the validity of the solution methodology for one dimensional steady flows.

***Test case I**: Idealized subcritical flow over a bump in a frictionless rectangular channel.*

A 1m wide, 25 long channel is considered to test subcritical flow over a bump. The channel bed is assumed to have a rectangular cross section, to be frictionless, and to exhibit a bump. The actual bed form is given by equation (4.14). This test case is a benchmark for investigating the capability of a numerical method for both the forward and inverse problems in 1D steady shallow water flows.

$$z = \begin{cases} 0 & x < 8 \quad \text{and} \quad x > 12 \\ 0.2 - 0.05(x-10)^2 & 8 \le x \le 12 \end{cases} \tag{4.14}$$

Subcritical flow is considered with a flow rate of $Q = 4.42\ \mathrm{m}^3/\mathrm{s}$ and the upstream boundary condition is $z(0) = 0$. The forward problem analysis which consists of

inferring the free surface profile for a given channel topography and the inverse problem analysis are presented in the previous sections. However, the values of the free surface velocity are not directly known for this particular benchmark problem but can be indirectly deduced by using a relationship between the free surface velocity and the depth averaged velocity. For this frictionless channel, the velocity relationship is given by equation (4.1) with a specific value of $\alpha$. However, substituting equation (4.1) into equation (4.10) for $\alpha$, the free surface velocity will be substituted back by the depth averaged velocity. The selection of the value of the velocity ratio $\alpha$ for this test case will not affect the result as it disappears with double substitution in the process, i.e. substituting $u_s$ of Equation (4.10) by $\alpha u_s$ eliminates $\alpha$ in Equation 4.15. Thus for frictionless channel ( $n=0$ ) equation (4.10) can be rewritten as

$$z_i = z_0 + \frac{1}{2g}\left(u_0{}^2 - (u)_i^2\right) + q_0\left(\frac{1}{u_0} - \frac{1}{(u)_i}\right) \qquad (4.15)$$

By solving the direct problem for a bed defined by equation (4.14), one can calculate the river depth and the averaged-velocity from which the free surface velocity can be computed from a known functional relationship between the free-surface and averaged velocity. This “artificial” experimental data can then be used as an input for the inverse problem. For the computation of the reconstructed bed, a spatial grid size of $\Delta x = 0.25\,\mathrm{m}$ is used along with the values of the boundary conditions.

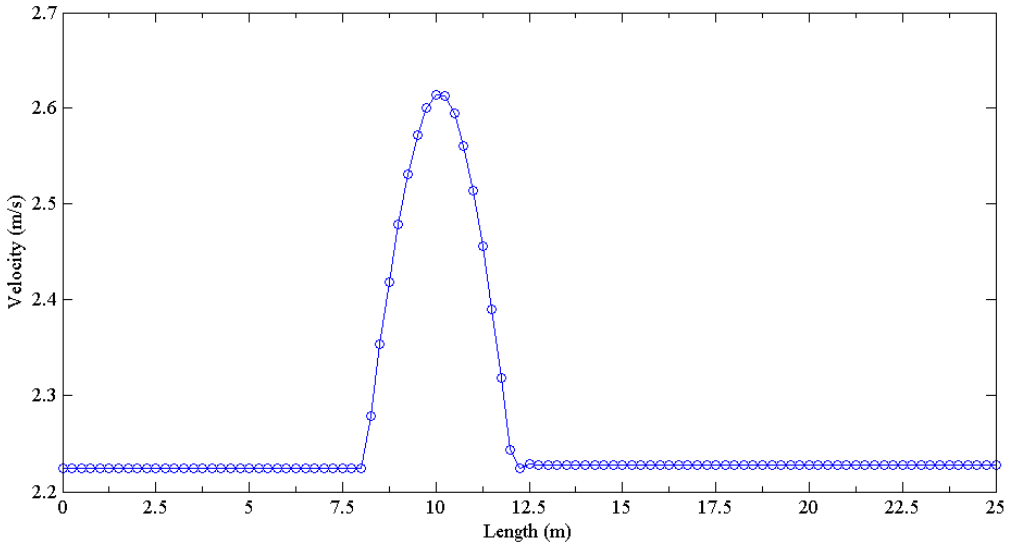


Figure 4.2: Depth averaged velocity distribution for test case I.

In Figure 4.2, the longitudinal profile of depth averaged velocity is given. This velocity is an input variable for the computation of the reconstructed bed.

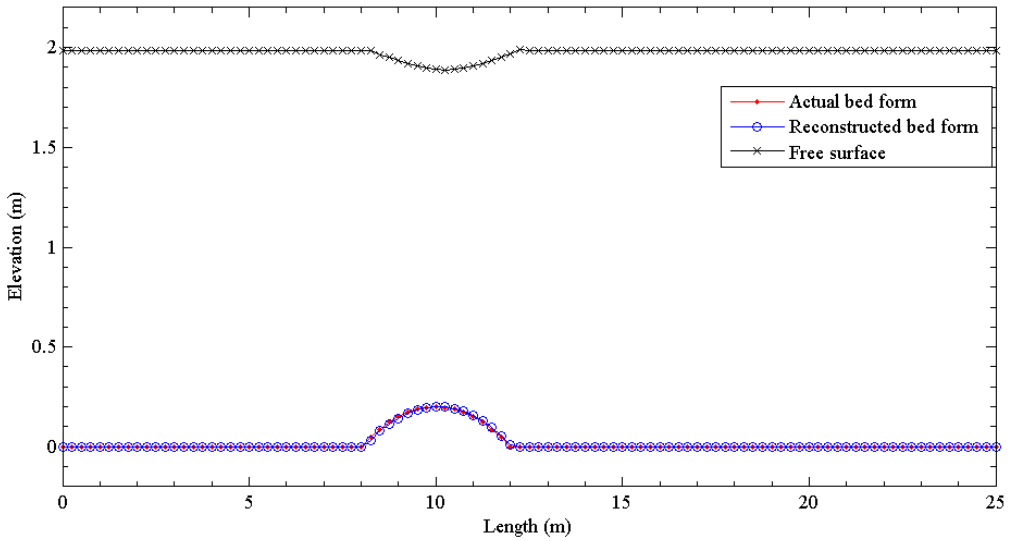


Figure 4.3: Comparison of the reconstructed and the actual bed forms for the subcritical flow case

From Figure 4.3, it can be seen that the reconstructed bed topography matches perfectly with the actual bed topography indicating that the methodology is capable of reconstructing riverbeds in the subcritical flows from the free surface or the depth averaged velocity whichever parameter is obtained from field measurements.

In Figure 4.4, 5% mean flow velocity based noise has been introduced in the free surface data in order to account for possible measurement errors and simulate the effects of errors in the field data. A 5-point moving average smoothing tool "smooth" in MATLAB is implemented in all sections of the analysis to smooth the noisy data.

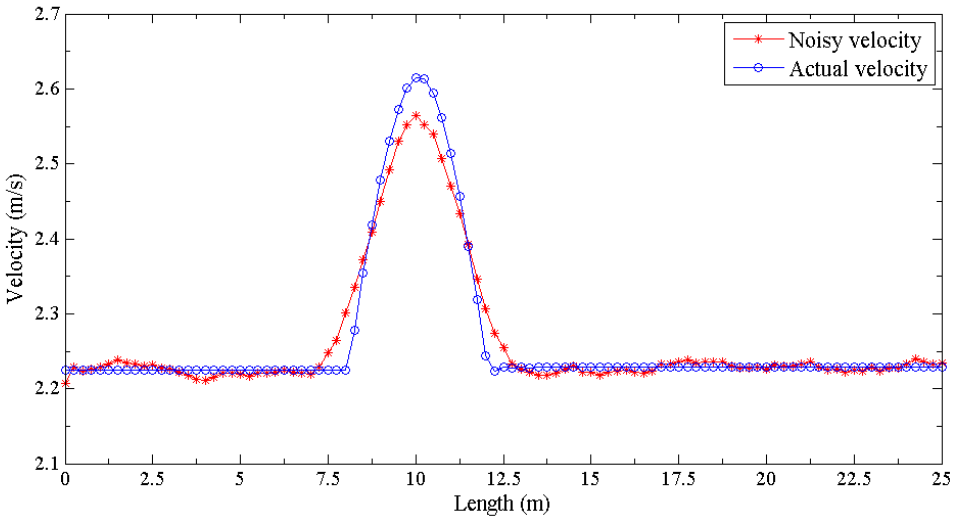


Figure 4.4: Noisy and actual velocity profiles

Figure 4.5 shows the comparison between the reconstructed and the actual bed forms. In this Figure, the relative difference of the reconstructed bed due to the existence of noise is 4.5%. It can be seen that the noise is not amplified in the reconstruction process and the algorithm produced an acceptable result.

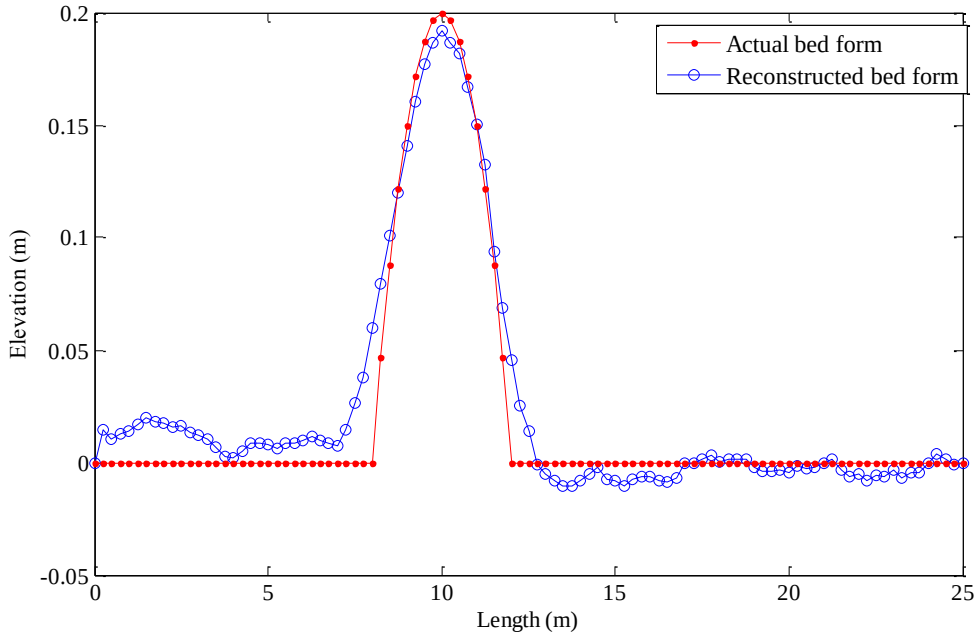


Figure 4.5: Comparison of actual and reconstructed bed forms from noisy free surface data

***Test case II**: Idealized transcritical flow over a bump in a frictionless rectangular channel.*

In this test case, results of chapter 3 for the forward problem are used. The test case is characterised by the same bed topography as test case I of this chapter. The steady flow rate imposed is $Q = 0.18\ \mathrm{m}^3/\mathrm{s}$, the upstream bed is defined as $z(0) = 0$, and the velocity field in the computational domain is shown in Figure 4.6. This test is used to study the performance of the numerical solution methodology towards handling the reconstruction process for transcritical open channel flows. A spatial grid size $\Delta x = 0.25\,\mathrm{m}$ is used. In order to capture the hydraulic jump, the reconstruction process is performed by a space marching approach from both directions of the boundary conditions unlike the subcritical test case.

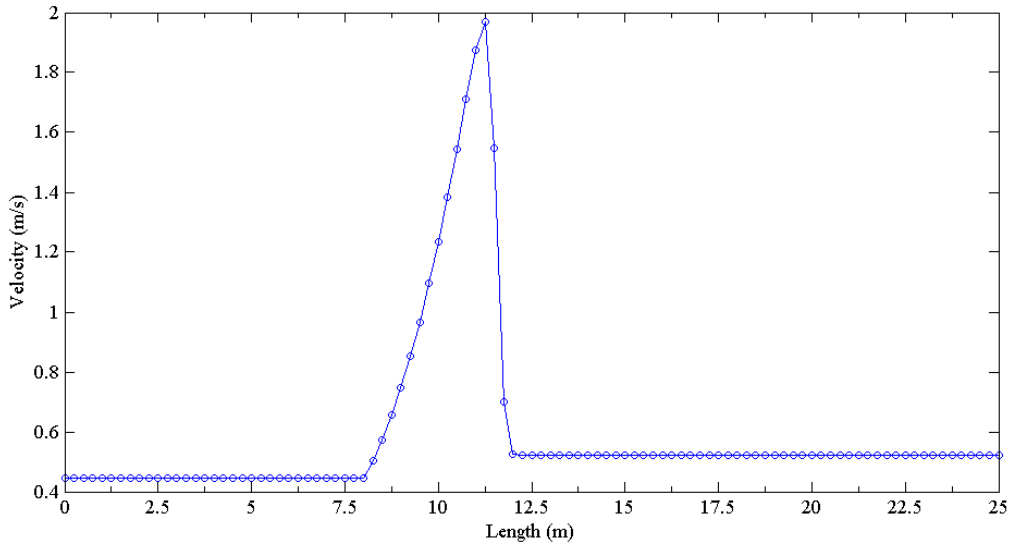


Figure 4.6: Depth averaged velocity profile in the transcritical flow case

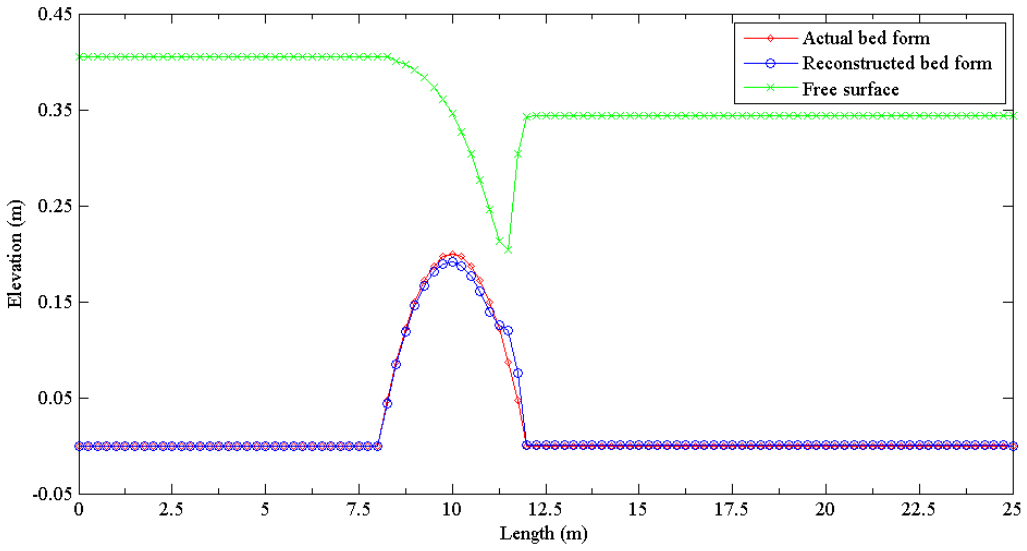


Figure 4.7: Comparison of the actual and the reconstructed bed in the transcritical flow case

As can be seen from Figure 4.7, the channel bed topography is reconstructed and compared with the actual bed form. This is a promising result from the fact that the shape and the size of the bump are reconstructed with acceptable level of discrepancy.

To test the effect of noise on the free surface velocity data, as in the above subcritical flow test case, 5% noise (based on the mean velocity) is introduced in the data. The noisy mean surface velocity is compared with its counterpart in Figure 4.8.

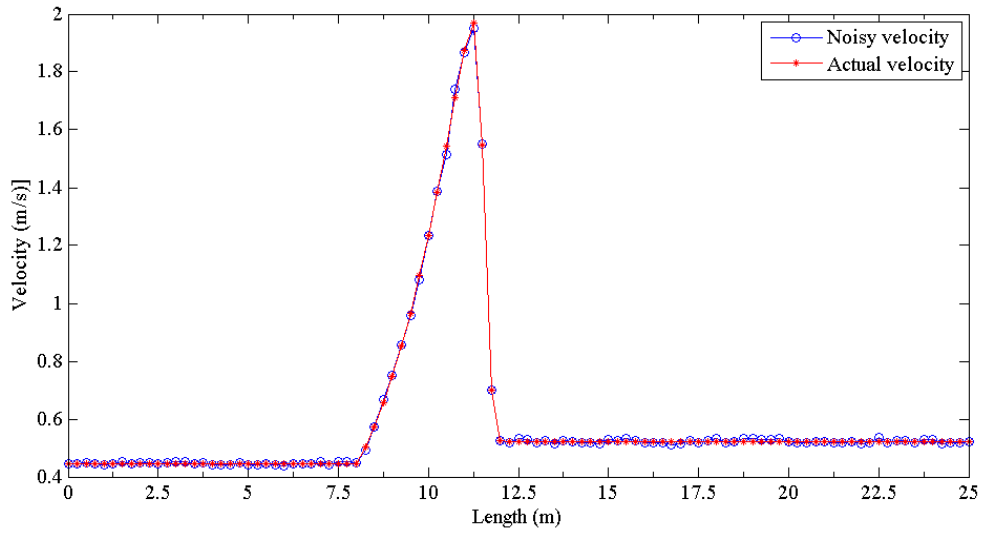


Figure 4.8: Noisy and actual depth averaged velocity profiles

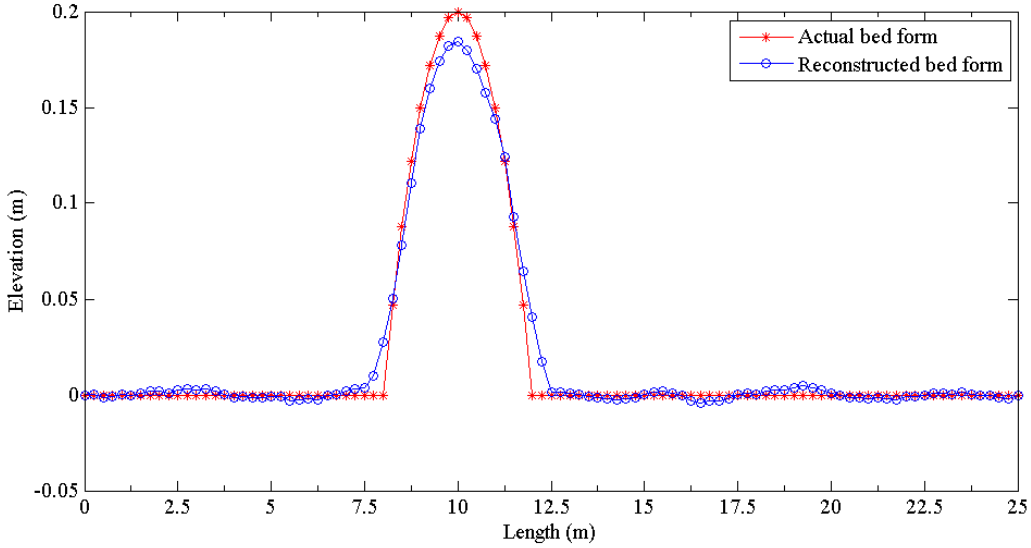


Figure 4.9: Comparison of the actual and the reconstructed bed in the transcritical flow case from noisy data

The comparison of the actual and the reconstructed bed forms from the noisy free surface data, Figure 4.9, shows a good agreement. It can be seen that the bed topography is reconstructed without amplifying the noise. The maximum deviation in the reconstructed bed due to the existence of noise in the free surface velocity is 5.5%. This deviation is comparable with the level of noise introduced in the free surface elevation data.

***Test case III**: flow over a step: experimental study*

This test case, described in section 3.4, is used to assess the capability of the numerical and pseudo-analytical methodology for the reconstruction of the channel bed topography from the free surface elevation. A horizontal flume is used to determine the stage of the flow over a bump which simulates one-dimensional flow with a bump of constant shape along the span. The steady flow rate and depth of the flow at the upstream boundary are 0.025 $m^3$/sec and 144 mm respectively. A Manning's roughness coefficient value of $n = 0.01$ is used. The calculated ranges of Fr are as given in section 3.4. In this test case, the depth averaged velocity is calculated from measurements of the depth of the flow and the free surface elevation data. The computed depth averaged velocity is shown in Figure 4.10. The Froude number (Fr) distribution along the flow is shown in Figure 4.11. This experimental study shows that the flow consititutes regimes of subcritical and supercritical open channel flows.

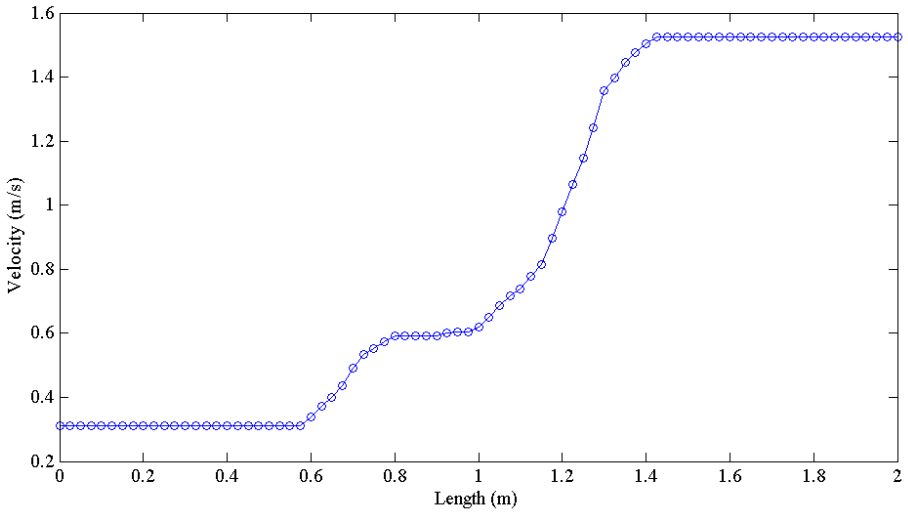


Figure 4.10: Depth averaged velocity along the flow direction

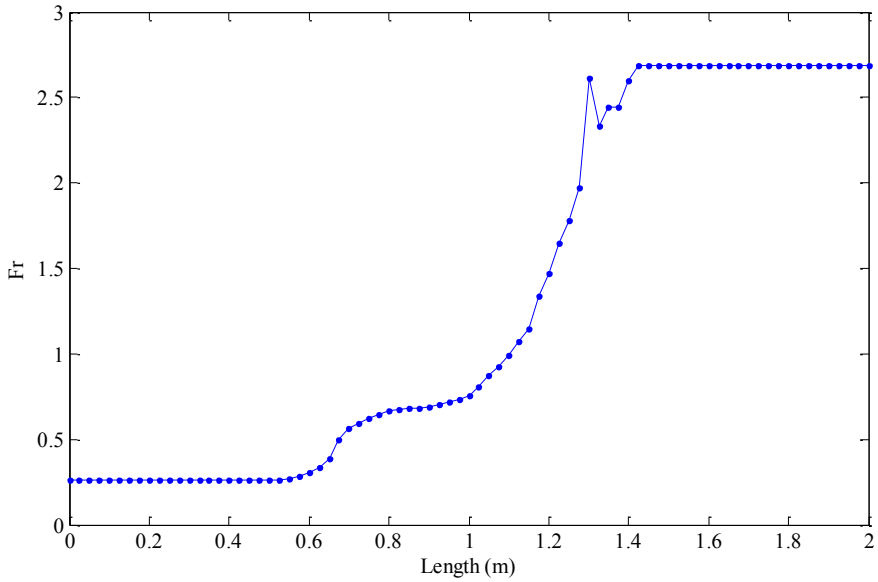


Figure 4. 11: Froude number distribution along the flow

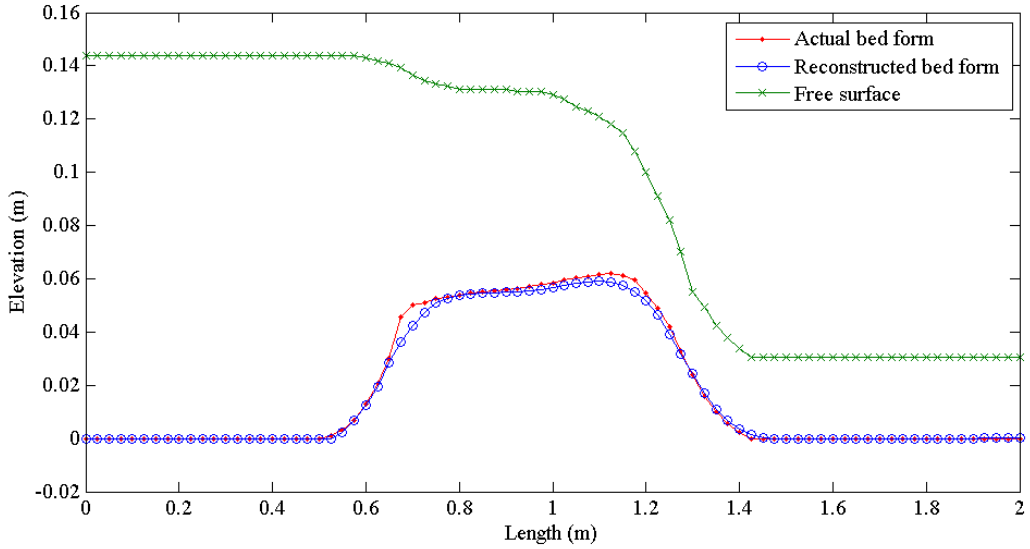


Figure 4.12: Comparison of the reconstructed and the actual bed forms

Using the calculated free surface velocity and measured boundary conditions, the underlying bed topography is numerically evaluated using Equation (4.10). The reconstructed bed from this test case matches well with the actual bed form which was used for the experimental study of the forward problem. The deviation of the results is due to the approximation of the roughness coefficient and the measurement errors in the experiment. It is clearly shown in Figure 4.12 that the actual bed form is reconstructed from the known velocity field which is determined from the experimental data. In order to test the reconstruction capability of the method from a noisy data, 5% noise based on the free surface velocity is introduced.

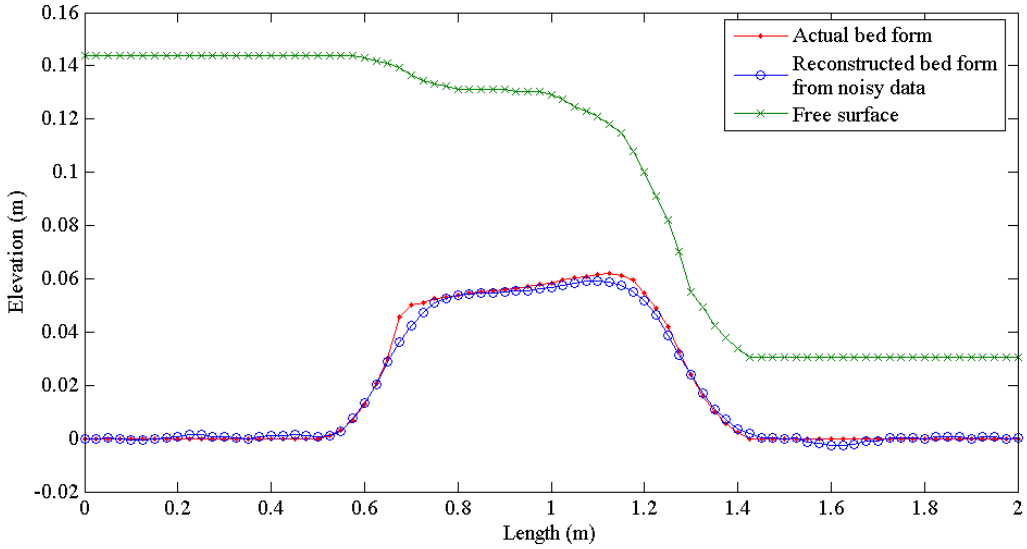


Figure 4.13: Comparison of the reconstructed and the actual bed forms from noisy data

The channel bed topography is well reconstructed from the noisy free surface velocity data as shown in Figure 4.13. The good agreement between the reconstructed and actual bed form indicate the "well-posed" behaviour of the proposed technique.

***Test case IV**: flow over a step in an inclined channel*

This test case uses the twin experiments data presented in [25] for which the free surface velocities were measured for a given bed form. It consists of a 100 m x 16 m rectangular channel with a longitudinal slope of 0.4% and features a bump which spans the whole width, centred at $x = 40$ m with an amplitude of 0.25m and a length of 30m. This bump generates an acceleration of the flow in the region $x \in [25, 60]$. A constant discharge of $8 m^3/s$ is prescribed at the inlet boundary $x = 0$. The boundaries $y = 0$ and $y = 16$ are defined as walls. The value of the Manning friction coefficient is variable along the lateral direction where a value $n = 0.02$ is considered for the central part of the domain, i.e. $|y - 8| \leq 4$ and the value then varies linearly from $n = 0.02$ to a maximum value of $n = 0.04$ at the wall. In [25] , the velocities of several tracked particles are plotted on

the same graph with no reference to their location in the flow domain. Since the flow domain has a variable Manning coefficient, it is impossible to associate one particle velocity profile with one value of the Manning coefficient. It was therefore decided to take two extreme velocity profiles (presumably, a near wall velocity profile and a centreline velocity profile) which envelop all other profiles and use them as input to the inverse problem. For our one-dimensional reconstruction algorithm, roughness coefficient values of $n = 0.02$ to reconstruct the bed topography from the centreline free surface velocity and $n = 0.04$ to reconstruct the bed from the near wall free surface velocity are used. The centreline and near wall free surface velocities in the domain along the length of the channel are shown in Figure 4.14.

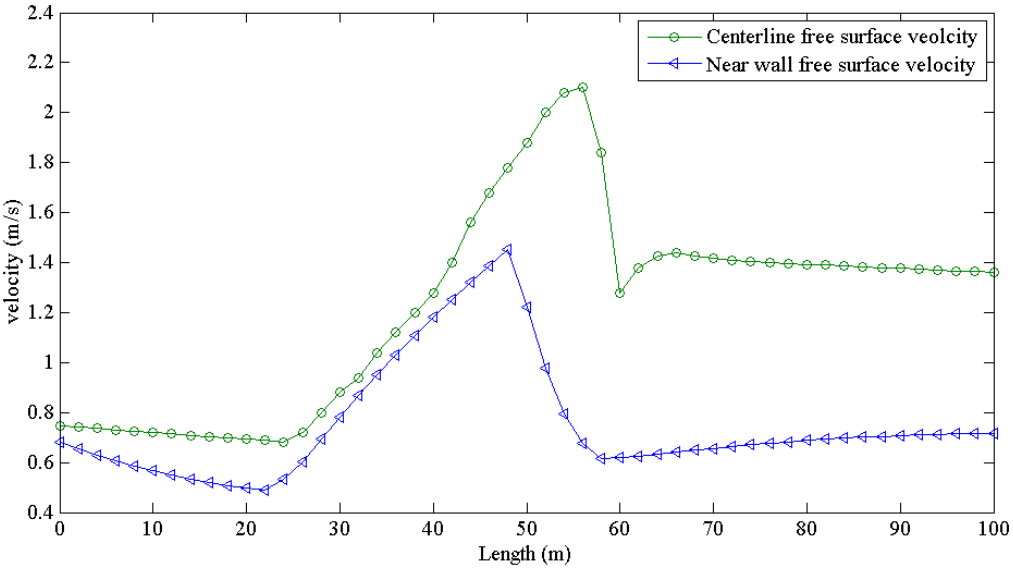


Figure 4.14: Free surface velocity of the flow along the flow direction

The longitudinal profile of velocity given in Figure 13 and a value of $\alpha = 1$ are adapted from reference [25] and are used as input variables for the reconstruction algorithm. The reconstructed bed is compared with the actual bed in Figure 4.15. It can be seen that the maximum deviation between the actual and the reconstructed bed form from the centreline free surface velocity is less than 5% of the depth of the flow. However, when the near-

wall free surface velocity is considered in the reconstruction algorithm, the deviation is as high as 12.5% of the depth of the flow. The main reason for this discrepancy near the wall is due to the fact that the flow experiences higher friction due to the higher values of Manning coefficients. Additionally, the spanwise variation of the Manning coefficient introduces spanwise flow variation by which the two-dimensional flow features clearly cannot be accounted for in our one-dimensional model. Thus in this particular two-dimensional flow case, the near wall velocity fails to represent the average free surface velocity of the flow.

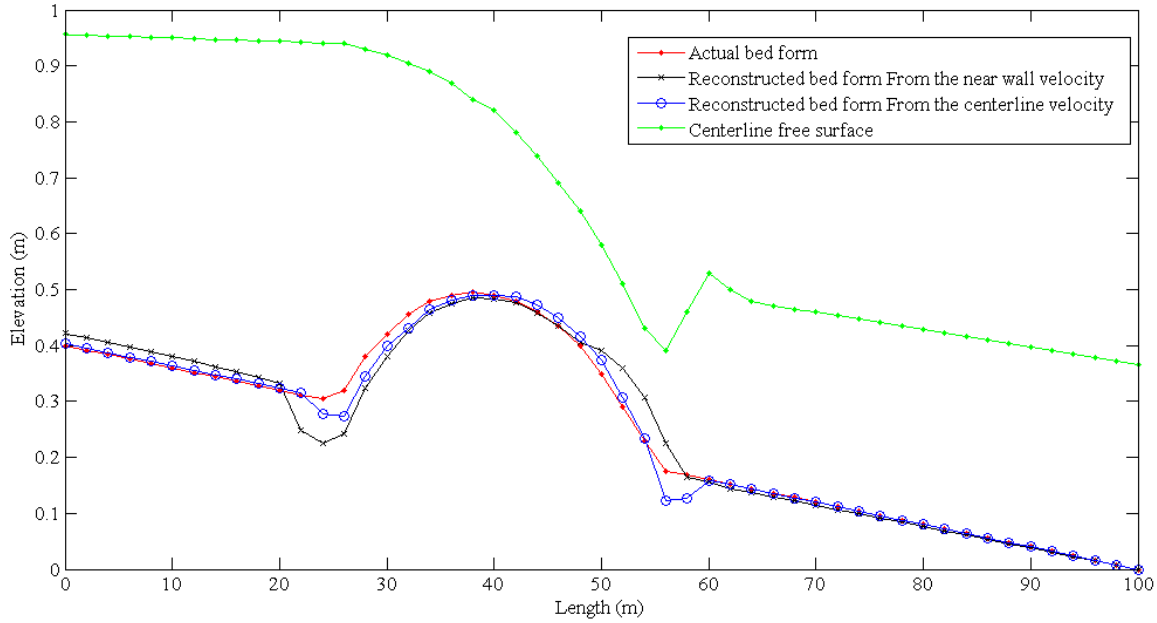


Figure 4.15: Comparison of the reconstructed and the actual bed forms

## 4.5. Summary and conclusion

From the above one-dimensional test cases it can be concluded that the channel bed topography can be reconstructed from known free surface velocity if the steady state flow rate is known along with the flow depth at the boundary and Manning's friction coefficient. It should also be emphasized that the relationship between the free surface velocity and the depth-averaged velocity needs to be known. If it were not, the proposed method is still applicable but with the depth-averaged velocity instead of the free surface

velocity. This is because measuring the free surface velocity is easier than that of the depth averaged velocity.

In the case of subcritical flow the channel bed is reconstructed with minimal error, however the deviation between the reconstructed and the actual bed is comparatively larger when a hydraulic jump exists. Errors increase when the flow is not strictly one-dimensional.

By introducing 5% noise (based on the depth averaged velocity) it is shown that the channel bed topography can be reconstructed with minimal discrepancies confirming that there is no noise amplification in the process.

A new numerical technique is presented to reconstruct the bed topography of a one-dimensional shallow water flow from knowledge of the depth-averaged velocity or free surface velocity. If free surface velocity is to be used, conditions that permit the free surface velocity to be directly related to the depth-averaged flow velocity must be known. Such conditions are described in the literature. It is possible to integrate the 1D steady version of the Saint Venant equations to obtain an integral equation explicitly which gives the bed topography as a function of the depth-averaged or free surface velocity, velocity ratio and Manning's friction coefficient . A simple marching method along with trapezoidal rule is developed to solve this integral equation. One particular advantage of this integral formulation, based on the present experimental studies, is that noise in the input data, i.e. the free surface velocity, will not be amplified by the reconstruction approach. Its applicability is demonstrated on a range of benchmark problems. Two artificial ones for which the free surface velocity is obtained by first solving the direct problem and then used as an input for the inverse problem. Another artificial test case was considered from [25] where all values of the necessary parameters are adopted. The other

benchmark problem is based on experimental data. The good agreement between the reconstructed and actual bed forms even for mildly noisy experimental data indicate the "well-posed" behaviour of the proposed technique. Note that in comparison to reconstruction algorithms based on optimization techniques, this approach is simple to implement, fast, and accurate. Even for the difficult case with an hydraulic jump, the method yielded a reconstructed bed with acceptable accuracy.

# 5. Bathymetry reconstruction based on the zero-inertia shallow water approximation

## Contents

## 5.1. Introduction

Starting from the general form of the Shallow Water Approximation, a whole hierarchy of simplified models has been derived and analyzed in the past in an attempt to simplify calculations yet capture the main flow characteristics. The review of Hunter et al. discusses very well these approximations and their validity window in the context of flood inundation, [94]. The level of approximation is best understood by considering the one-dimensional Saint-Venant equation:

$$\underbrace{\frac{\partial u}{\partial t}}_{(i)} + \underbrace{u\frac{\partial u}{\partial x}}_{(ii)} + g\left(\underbrace{\frac{\partial h}{\partial x}}_{(iii)} + \underbrace{S_f}_{(iv)} - \underbrace{S_0}_{(v)}\right) = 0 \tag{5.1}$$

where, adopting standard hydraulic notations, $u$ denotes the depth-averaged velocity, $h$ the flow depth, $g$ the acceleration of gravity, $S_f$ the friction slope, and $S_0$ the bed slope. The kinematic wave equation arises by retaining terms *(iv)* and *(v)* only. In this case, the friction and bed slope balance each other. The next level of approximation includes term *(iii)* in addition and is referred to as the diffusive wave equation. This approximation basically neglect inertia terms and it will be the focus of this chapter. The addition of term *(i)* leads to the dynamic wave equation.

The hydraulics of steep rivers for which the bed and friction slopes are orders of magnitude greater than the contribution from inertia is a good example where a simplified version of the Shallow Water Approximation can effectively be used, see e.g. [5, 70, 79] The Rhone River, in France, for which the bottom and friction slopes are of order of $10^{-3}$ but its inertial terms are of order $10^{-5}$, [5, 95], can be mentioned as a good illustrative example. Shultiz and his co-workers used the kinematic wave model for distributed hydraulic modeling to evaluate its validity. They confirmed its validity as a predictive tool for artificial rectangular drainage basins and actual ones. Li and co-workers [96]

presented a simple numerical routing procedure to compute open channel and overland flow based on the kinematic wave equation in order to minimize the complexity and instability of complex numerical schemes. Moramarco and his co-workers [97] also investigated the applicability of the kinematic wave approximation for steady flow in prismatic channels by comparing the results of this approximation with those obtained with the full dynamic wave equations solved using a second-order two-step Lax-Wendroff numerical scheme coupled with the characteristic method at the boundaries. The steady flow analysis presented in [97] emphasizes that the kinematic wave solution, despite the influence of the downstream boundary conditions, can be applied for many steady flows without excessive loss of accuracy when compared to the dynamic wave solution. The diffusive wave equation is also used by Horrit to investigate the effect of uncertain topography on the modeling of the flow hydraulics, [54]. In this study, the diffusive wave approximation is used, as the effect of the slope of the depth of the flow is included in the kinematic wave approximation.

The study of the inverse problem, identifying the channel bed topography from other known hydraulic parameters, has diverse applications as mentioned in previous chapters. In Horrit [54], it is shown that the non-linearity of the governing equations and the lack of actual data of model parameters hamper the development hydraulic modeling of environmental processes. Like the previous sections with the one-dimensional bed topography reconstruction, a direct numerical approach is used to infer the channel bed topography from known free surface data for two-dimensional shallow water flows with predominant frictional and gravitational terms.

Section 5.2 presents the simplification process of the governing equations. Section 5.3 presents the analysis of the forward and the inverse problems with results. The concluding remarks of this chapter are presented in section 5.4.

## 5.2. Governing equations and their simplification

In river flow modeling it is extremely important to base the model on appropriate flow equations and their respective initial and boundary conditions. The physical nature of the river and its flood suggest the appropriate equations to be used to model the situation, see e.g. [5]. The majority of studies use shallow water equations to simulate open channel flows where the shallow water approximations are valid.

The two-dimensional shallow water equations representing mass and momentum conservation are considered to deduce the governing equations of the zero inertia shallow water flow. The equations can be written as follows:

$$\frac{\partial h}{\partial t}+\frac{\partial(q_x)}{\partial x}+\frac{\partial(q_y)}{\partial y}=0 \tag{5.2}$$

$$\frac{\partial q_x}{\partial t}+\frac{\partial(q_x u)}{\partial x}+\frac{\partial(q_x v)}{\partial y}=-gh\left(\frac{\partial(\psi)}{\partial x}+\frac{n^2 q_x|q|}{h^{4/3}}\right) \tag{5.3}$$

$$\frac{\partial q_y}{\partial t}+\frac{\partial(q_y u)}{\partial x}+\frac{\partial(q_y v)}{\partial y}=-gh\left(\frac{\partial(\psi)}{\partial y}+\frac{n^2 q_y|q|}{h^{4/3}}\right) \tag{5.4}$$

Where $q_x = uh$ is the discharge in x direction per unit width; $q_y = vh$ is the discharge in $y$- direction per unit width; $h$ is the flow depth; $\psi = z + h$ is the free surface elevation; $z$ is the bed topography; $n$ is the manning roughness coefficient; $g$ is the gravitational acceleration; $u$ and $v$ are the depth averaged velocities in $x$- and $y$- direction, respectively.

Equation (5.2) represents the conservation of mass in the flow. Equations (5.3) and (5.4) represent conservation of momentum in $x$-and $y$-direction respectively where $x$ and $y$ are coordinates in the bed plane. The above equations provide three coupled partial differential equations for the three unknowns $u$ , $v$ and $h$. As mentioned in previous

section, the governing equations are deduced from the Navier-Stokes equations provided some restrictions are fulfilled. Furthermore, if we impose additional restrictions to the shallow water equations based on the flow behaviour and particularity, further simplifications can be made. Cunge and his co-workers [5] address the choice of equations for particular flow situations and show that it is possible to drop some of the terms in the general governing equations. Thus, simpler equations with restricted applicability can be obtained. This kind of approach is possible when the physical insight of the problem is well known. Instead of using the generalized governing equations, which describe the complex phenomenon, it is essential to assess the physical behaviour of the flow and simplify the governing equations accordingly. Examples of such simplifications include: stationary flows, flows over frictionless bed, flows with high advection terms, and flows with prevailing frictional terms, flows with negligible bed slope effect and flows with steep bed slope.

This chapter focuses on two dimensional steady flows with negligible advection terms in the two dimensional shallow water (SW) equations. In other words, open channel flows with paramount frictional and bed slope terms are studied. Solving the general form of the equations can give results with qualitative and quantitative importance but solving the modified governing equations reduces its complexity and the numerical cost of computation with an acceptable level of error. Applying the above mentioned restrictions to the general governing equations results in the modified version of the SW equations as presented below. These governing equations constitute the same continuity equation but a simplified form of the momentum equations.

$$\frac{\partial(hu)}{\partial x}+\frac{\partial(hv)}{\partial y}=0 \tag{5.5}$$

$$\frac{\partial h}{\partial x}+\frac{\partial z}{\partial x}+\frac{n^2 u\sqrt{(u^2+v^2)}}{h^{4/3}}=0 \tag{5.6}$$

$$\frac{\partial h}{\partial y}+\frac{\partial z}{\partial y}+\frac{n^2 v\sqrt{(u^2+v^2)}}{h^{4/3}}=0 \tag{5.7}$$

An interesting feature about these governing equations is that with further simplification and a substitution of $\frac{\partial z}{\partial x}+\frac{\partial h}{\partial x}=\frac{\partial \psi}{\partial x}$ , it can be shown that the ratio of the flow velocities is equivalent to the ratio of the gradients of the free surface profile in the physical domain.

$$\frac{u}{v}=\frac{\partial \psi}{\partial x}\Big/\frac{\partial \psi}{\partial y} \tag{5.8}$$

For a given smooth differentiable free surface profile, the ratio of the gradients at a particular point provides information on the respective ratio of the velocities. It also implies that if the flow velocity in one direction is known along with the free surface data, the other velocity component can be determined with simple algebraic application of equation (5.8). Rearranging the momentum equations gives equations (5.9) and (5.10) where the velocity components can be written as functions of the free surface elevation data, the Manning's friction coefficient and the depth of the flow.

$$u=-\frac{\frac{\partial \psi}{\partial x}}{n\left[\left(\frac{\partial \psi}{\partial x}\right)^2+\left(\frac{\partial \psi}{\partial y}\right)^2\right]^{1/4}}h^{2/3} \tag{5.9}$$

$$v=-\frac{\left(\frac{\partial \psi}{\partial y}\right)}{n\left[\left(\frac{\partial \psi}{\partial x}\right)^2+\left(\frac{\partial \psi}{\partial y}\right)^2\right]^{1/4}}h^{2/3} \tag{5.10}$$

Substituting equations (5.9) and (5.10) in the continuity equation (5.5) gives the simplified form of the governing equation as shown in equation (5.11).

$$\left(\frac{F}{h}\right)\frac{\partial h}{\partial x}+\left(\frac{G}{h}\right)\frac{\partial h}{\partial y}=-\frac{3}{5}\left(\frac{\partial F}{\partial x}+\frac{\partial G}{\partial y}\right) \tag{5.11}$$

Where $F=\dfrac{\dfrac{\partial \psi}{\partial x}}{\left[\left(\dfrac{\partial \psi}{\partial x}\right)^2+\left(\dfrac{\partial \psi}{\partial y}\right)^2\right]^{1/4}}$ and $G=\dfrac{\dfrac{\partial \psi}{\partial y}}{\left[\left(\dfrac{\partial \psi}{\partial x}\right)^2+\left(\dfrac{\partial \psi}{\partial y}\right)^2\right]^{1/4}}$ .

Equation (5.11) relates the free surface profile with the depth of flow for a given boundary condition. From equation (5.11), it can be seen that the roughness coefficient $n$ in the governing equation has disappeared under the present assumption. This is an important result which proves that the bed topography can be uniquely determined from the knowledge of the free surface without the knowledge of the roughness coefficient. The Manning coefficient only appears in the determination of the averaged velocities and discharge in the limits of the given approximation. Note that, for the purpose of this work, the evaluation of the velocities is not necessary and it will therefore not be performed.

Similar analysis using the one-dimensional shallow water flow shows that the reconstruction of the channel bed topography from the free surface elevation data does not require the knowledge of the bed roughness coefficient either. This can be seen in the simplified form of the governing equations for one-dimensional shallow water flow.

$$\frac{dh}{dx}+\frac{dz}{dx}+\frac{n^2 q_o|q_o|}{h^{10/3}}=0 \tag{5.12}$$

where $q_o$ is the steady flow rate per unit width

Equation (5.12) coupled with the continuity equation $(uh = q_0 = constant)$ governs the one-dimensional steady shallow water flows with dominant bed slope and frictional terms. Rewriting equation (5.9) for the one-dimensional flow boundary condition and substituting for $q_0$ in equation (5.12) provides a relationship between the free surface and the depth of the flow which does not include the bed roughness coefficient as given in equation (5.13).

$$\frac{d\psi}{dx} - \frac{C_o}{h^{10/3}} = 0 \tag{5.13}$$

where the constant $C_o = \left.\frac{d\psi}{dx}\right|_0 h_0^{10/3}$ which can be calculated at the boundary.

In equation (5.13), it is clear that the depth of the flow $h$ can be inferred from the free surface elevation data without the knowledge of the roughness coefficient. Thus the bed topography can be reconstructed if the free surface elevation data of the domain and the depth of the flow at a particular location are known. Therefore like the two-dimensional flows, the bed topography reconstruction from the free surface elevation data in one-dimensional shallow water flows with negligible inertia does not require prior information on the channel roughness coefficient.

## 5.3. The forward and inverse problems

Solving the suitable governing equations to predict the free surface evolution from the known bed topography constitutes the forward problem. Equation (5.11) in the context of the forward problem is complex, thus it is only used for the inverse problem analysis.

### *5.3.1. Discretization of the forward problem equations*

For the forward problem, governed by equation (5.5, 5.6, and 5.7), $z(x, y)$ is the known field and $h(x,y)$ the unknown one. Many discretization techniques have been developed to solve the full shallow water equations. The choice of the discretization technique is dependent on particularity of the problem, computational effort, and accuracy requirement of the solution. For the canonical test cases presented below, the MacCormack explicit numerical scheme is implemented, see e.g. [6]. This discretization technique has a predictor and a corrector stage coupled with successive solution methodology. Backward differencing numerical technique is implemented in the predictor stage while forward differencing is used in the corrector stage. The expressions can be written as

Predictor stage

$$\begin{aligned} h^{*}_{i,j} &= h^{k}_{i,j} - \frac{\Delta t}{\Delta x}\left(q_{x}{}^{k}_{i,j} - q_{x}{}^{k}_{i-1,j}\right) - \frac{\Delta t}{\Delta y}\left(q_{y}{}^{k}_{i,j} - q_{y}{}^{k}_{i,j-1}\right) \\ q_{x}{}^{*}_{i,j} &= q_{x}{}^{k}_{i,j} - \frac{1}{2} g \frac{\Delta t}{\Delta x}\left[\left(h^{k}_{i,j}\right)^2 - \left(h^{k}_{i-1,j}\right)^2\right] + g h^{k}_{i,j} \Delta t\left(S_{ox} - S_{fx}\right)_{i,j} \\ q_{y}{}^{*}_{i,j} &= q_{y}{}^{k}_{i,j} - \frac{1}{2} g \frac{\Delta t}{\Delta y}\left[\left(h^{k}_{i,j}\right)^2 - \left(h^{k}_{i,j-1}\right)^2\right] + g h^{k}_{i,j} \Delta t\left(S_{oy} - S_{fy}\right)_{i,j} \end{aligned} \qquad \begin{cases} 2 \le i \le N \\ 2 \le j \le M \end{cases} \tag{5.14}$$

Corrector Stage

$$\begin{aligned} h^{**}_{i,j} &= h^{k}_{i,j} - \frac{\Delta t}{\Delta x}\left(q^{*}_{xi+1,j} - q^{*}_{xi,j}\right) - \frac{\Delta t}{\Delta y}\left(q^{*}_{y\,i,j+1} - q^{*}_{y\,i,j}\right) \\ q_{x}{}^{**}_{i,j} &= q_{x}{}^{k}_{i,j} - \frac{1}{2} g \frac{\Delta t}{\Delta x}\left[\left(h^{*}_{i+1,j}\right)^2 - \left(h^{*}_{i,j}\right)^2\right] + g h^{*}_{i,j} \Delta t\left(S^{*}_{ox} - S^{*}_{fx}\right)_{i,j} \\ q_{y}{}^{**}_{i,j} &= q_{y}{}^{k}_{i,j} - \frac{1}{2} g \frac{\Delta t}{\Delta y}\left[\left(h^{*}_{i,j+1}\right)^2 - \left(h^{*}_{i,j}\right)^2\right] + g h^{*}_{i,j} \Delta t\left(S^{*}_{oy} - S^{*}_{fy}\right)_{i,j} \end{aligned} \qquad \begin{cases} 1 \le i \le N-1 \\ 1 \le j \le M-1 \end{cases} \tag{5.15}$$

Where $N$ and $M$ are the number of grid points in $x$ and $y$ directions, $h^{*}$ and $h^{**}$ are intermediate values for $h$, $q_x{}^{*}$ and $q_x{}^{**}$ are intermediate values for $q_x$, and $q_y{}^{*}$ and $q_y{}^{**}$

are intermediate values for $q_y$ . The new values of the unknown quantities at time $k+1$ is then calculated from the intermediate values which are determined from the predictor and corrector steps

$$h_{i,j}^{k+1} = \frac{1}{2}\left(h_{i,j}^{*} + h_{i,j}^{**}\right), \quad q_{xi,j}^{k+1} = \frac{1}{2}\left(q_{xi,j}^{*} + q_{xi,j}^{**}\right), \text{ and } \quad q_{y_{i,j}}^{k+1} = \frac{1}{2}\left(q_{y_{i,j}}^{*} + q_{y_{i,j}}^{**}\right) \quad (5.16)$$

Reflective boundary conditions are implemented at the walls while Neumann boundary condition is implemented at the outlet. Even though the unsteady equations are used, imposing a constant inflow rate at the inlet boundary provides steady solutions. Uniform water free surface elevation is used as initial condition.

A MATLAB code is written to solve the discretized form of the forward problem equations along with the respective initial and boundary conditions. Once the steady state results are produced to an acceptable level, the solver terminates the computation process.

The following test cases are designed to address the effect of the steepness of the bed form and to assess the effect of a bump on the free surface.

***Test case I: Flow over a constant bump along the span***

A computational domain with 40m length and 40m width is considered to simulate a one-dimensional flow. The topography is invariant in the span-wise direction to generate a flow which is essentially one-dimensional. The bed topography is characterized by a bump at the centre and a uniform slope of -0.005 in the $x$ - direction which is given by the following function.

$$z(x, y) = 0.2\exp\left(\left(x - \frac{x_{\max}}{2}\right)^2 \frac{1}{\delta^2}\right) - 0.005x \quad (5.17)$$

where $x_{max}$ is the length of the computational domain in the longitudinal direction and $\delta = 4$ is a constant parameter which controls the steepness of the topography. A constant flow rate $q_x = 1.2$ m$^2$/s is imposed at inlet boundary. A spatial grid size of 0.5 m in both directions and a temporal grid size of 0.1 seconds are used to comply with the stability criteria of this explicit numerical scheme. A Manning's roughness coefficient $n = 0.02$ is used. The MATLAB code iteratively solves the discretized form of the equations to generate steady solutions.

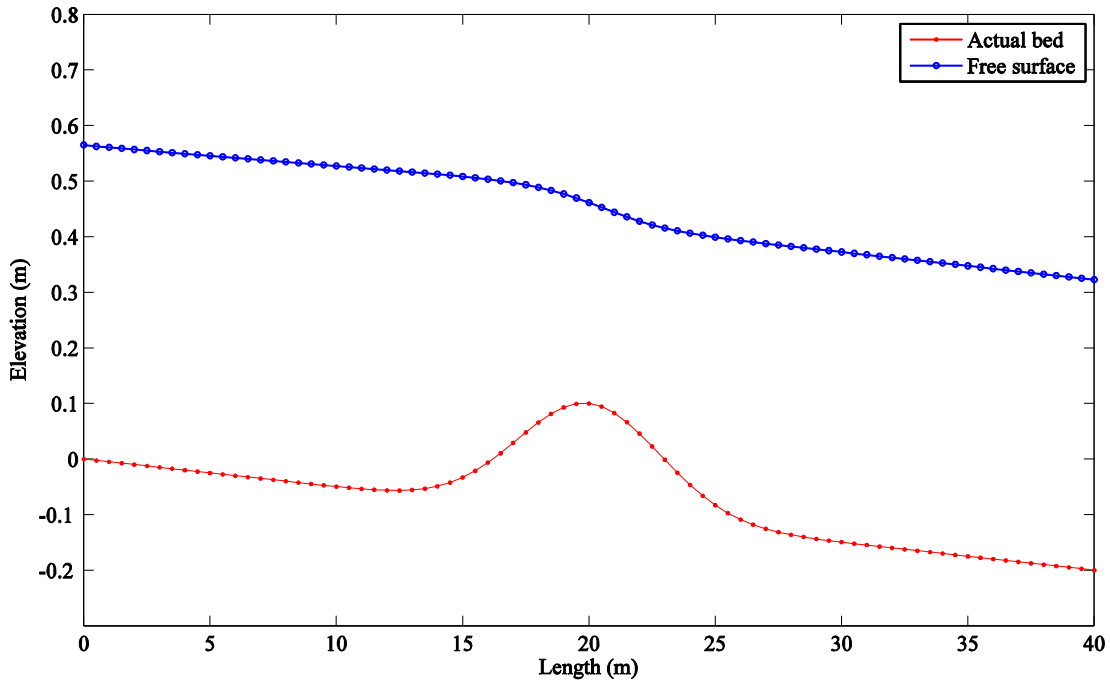


Figure 5.1: Bed topography and free surface elevation

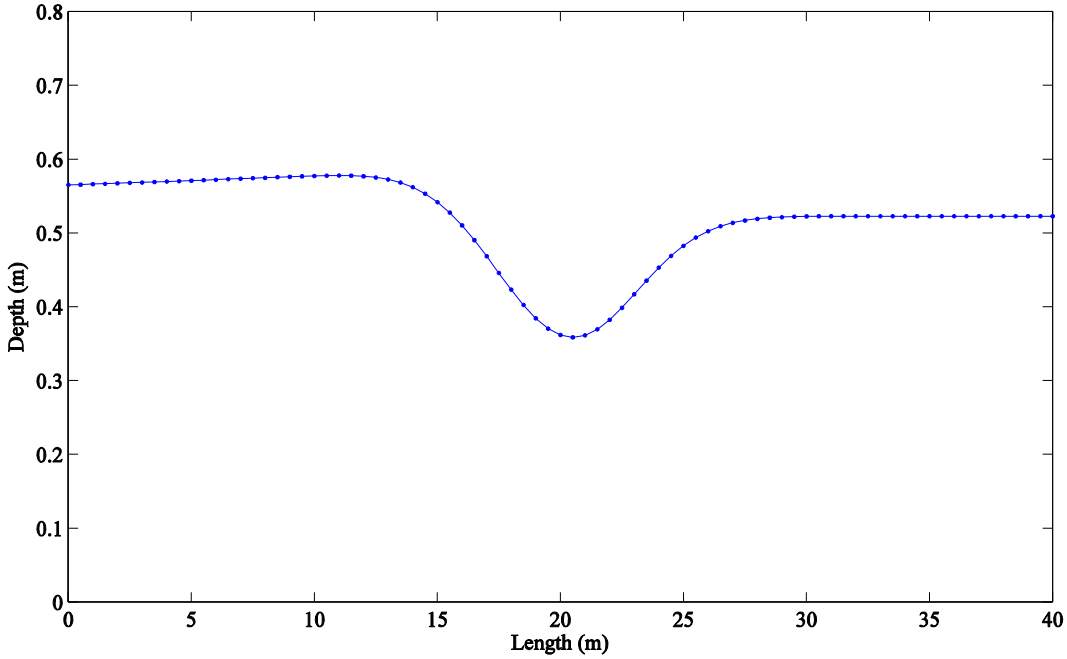


Figure 5.2: Longitudinal depth distribution

Figures 5.1 and 5.2 show the resulting free surface and depth distribution along the $x$-axis, respectively. The steady results show that the existence of the one-dimensional bump creates an undulation on the free surface which results in fluid acceleration upstream and deceleration downstream of the bump. The free surface elevation data will be used in the reconstruction analysis of the inverse problem.

***Test Case II: flow over a localized bump***

In order to investigate a fully two-dimensional flow, topographic variation in both directions is necessary. Thus, a bed topography with a two-dimensional bump is considered for this test case. A computational domain with length 50 m and width 50 m is used to solve the forward problem. The bed topography which is used for the numerical experiment is given by

$$z(x,y) = 0.2\exp\left[\left(\left(x-\frac{x_{\max}}{2}\right)^2\frac{1}{\delta_1{}^2}+\left(y-\frac{y_{\max}}{2}\right)^2\frac{1}{\delta_2{}^2}\right)\right]-0.005x \tag{5.18}$$

Where $x_{\max}$ and $y_{\max}$ are the domain size in the longitudinal and transverse direction; $\delta_1 = 3$ and $\delta_1 = 6$ are constants. The bump is located at the centre of the domain with a pick value of 0.2m and the slope of the bed is -0.005 in the direction of the main flow.

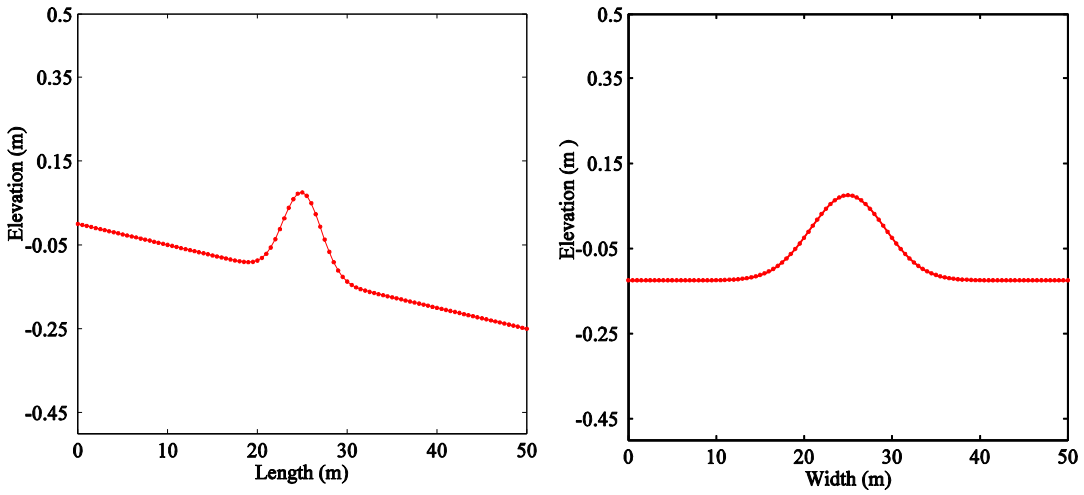


Figure 5.3: Bed form along x-axis (left) and along y axis (right)

Figure 5.3 shows the bed form of the two-dimensional computational domain. The centreline variations of the bed topography along $x$- and $y$- axes are shown on the left and right sides of Figure 5.3, respectively.

A Dirichlet boundary condition with constant flow rate $q_x = 1.2$ m$^2$/s is imposed at the inlet boundary. The same spatial resolution and time steps are used as for the previous benchmark problem. A Manning's roughness coefficient $n = 0.02$ is considered. The MATLAB code solves the discretized forms of the equations until the solution of the problem no longer changes with time producing a steady solution. Figures 5.4 and 5.5 describe the resulting free surface profil and depth variation of the flow respectively.

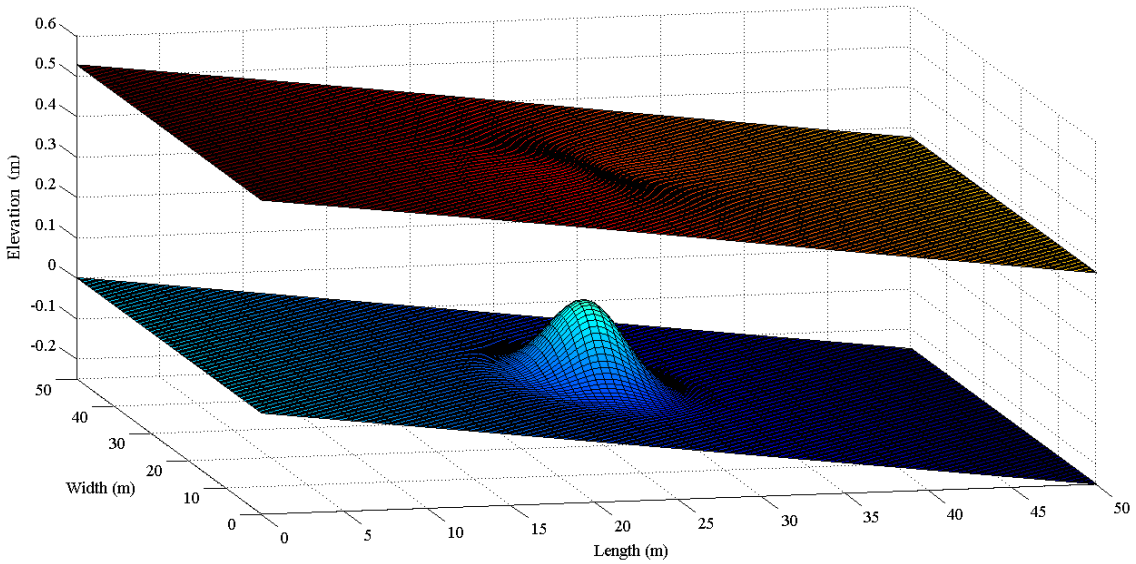


Figure 5.4: Free surface profile resulting from the forward problem

From Figure 5.4, it can be seen that the free surface profile has upstream bump and downstream depression created due to the existence of the two-dimensional bump.

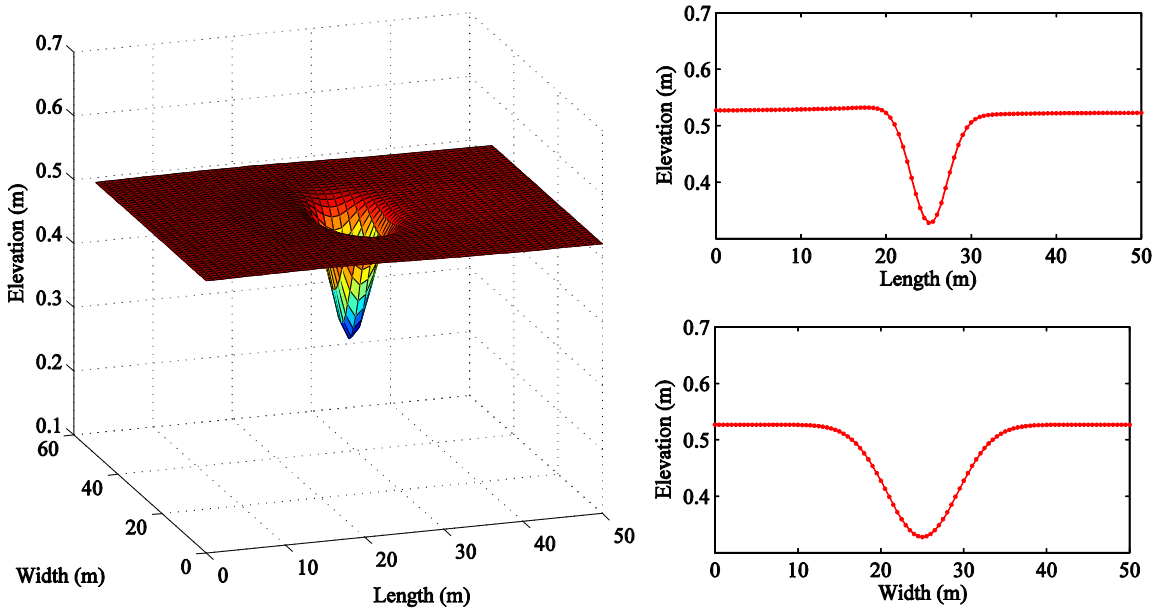


Figure 5.5: Depth of the flow in two dimensions

In Figure 5.5 the depth distribution is shown confirming that the existence of the two-dimensional bump in the bed topography creates two dimensional variations in the flow depth and the free surface profile.

### *5.3.2. The inverse problem*

Equation (5.11), the condensed form of the governing equation, is now considered to solve the inverse problem. The equation which governs the inverse problem is a first order non-linear partial differential equation with variable coefficients.

This equation can be solved using the method of characteristics. Three systems of ordinary differential equations can conveniently represent equation (5.11) and there exists a characteristic curve $C = C\{x(s), y(s), h(s)\}$ which satisfies the ordinary differential equations. Thus, the solution can be integrated along these characteristic curves from the given boundary data. The reduced ordinary differential equations are

$$\frac{dx}{ds} = \frac{F}{h} \tag{5.19}$$

$$\frac{dy}{ds} = \frac{G}{h} \tag{5.20}$$

$$\frac{dh}{ds} = -\frac{3}{5}\left(\frac{\partial F}{\partial x} + \frac{\partial G}{\partial x}\right) \tag{5.21}$$

From equation (5.21), it can be seen that the depth of the flow along the characteristic lines is a function of the second derivatives of the free surface elevation. The values of the independent variables $x$ and $y$ change with the depth of the flow and the respective derivatives of the free surface function along the curve as given by equation (5.19) and (5.20), respectively.

The above systems of ordinary differential equations (ODEs) are solved using simple backward differencing numerical scheme. This method allows us to change these systems of ODEs to a sequence of algebraic updates.

$$x_i = x_{i-1} - \Delta s\left(\frac{F}{h}\right)_{x_{i-1},y_{i-1}} \tag{5.22}$$

$$y_i = y_{i-1} - \Delta s\left(\frac{G}{h}\right)_{x_{i-1},y_{i-1}} \tag{5.23}$$

$$h_i = h_{i-1} + \frac{3}{5}\Delta s\left(\frac{\partial F}{\partial x} + \frac{\partial G}{\partial x}\right)_{x_{i-1},y_{i-1}} \tag{5.24}$$

Where $\Delta s$ is an infinitesimal length along the characteristic curves.

The method of characteristics for the inverse problem adopts an infinitesimal length $\Delta s = 0.5$ m along the characteristic lines. It is large enough to give a grid independent solution. Results of the reconstruction in all test cases are presented below.

Unlike to the definition of inflow rate at the upstream boundary in the forward problem, the inverse problem requires only the depth of the flow at the inlet boundary. Thus the imposed boundary condition in all test cases of the inverse problem are defined as

$$h\big|_{x=0,y} = h_0 \tag{5.25}$$

Where $h_0$ is a measured depth of the flow at the inlet boundary. For a given continuous free surface data $\psi(x,y)$ with continuously differentiable first order derivatives, the depth of the flow can be determined using equation (5.24). The free surface profile obtained from the solution of the forward problem is used in order to check the numerical performance and capability of the algorithm. The test case results show good agreement between the reconstructed and the original bed forms considered in the forward problem. Two illustrative test cases are presented here in order to avoid redundancy and for the

purpose of conciseness. The two test cases presented here are selected because of the fact that test case-I can successfully represent one-dimensional flows, while the features of the other test case are fully two-dimensional.

A MATLAB script is written to solve the discretised form of the characteristic equations (5.22), (5.23) and (5.24). The free surface elevation data obtained from the forward problem analysis is imported along with the given boundary condition to the MATLAB script in order to determine the bed topography. The value of the depth of the flow is determined along the characteristics and it is mapped back to the regular computational domain by interpolation.

The free surface profile resulted from test case-I is imported as two-dimensional grid values to the inverse problem MATLAB code. The depth distribution at the inlet (left boundary) is considered as a known boundary condition. Unlike the forward problem, the inverse problem does not require information about the initial condition and the Manning's roughness coefficient. The results of this inverse problem are shown in the following Figures.

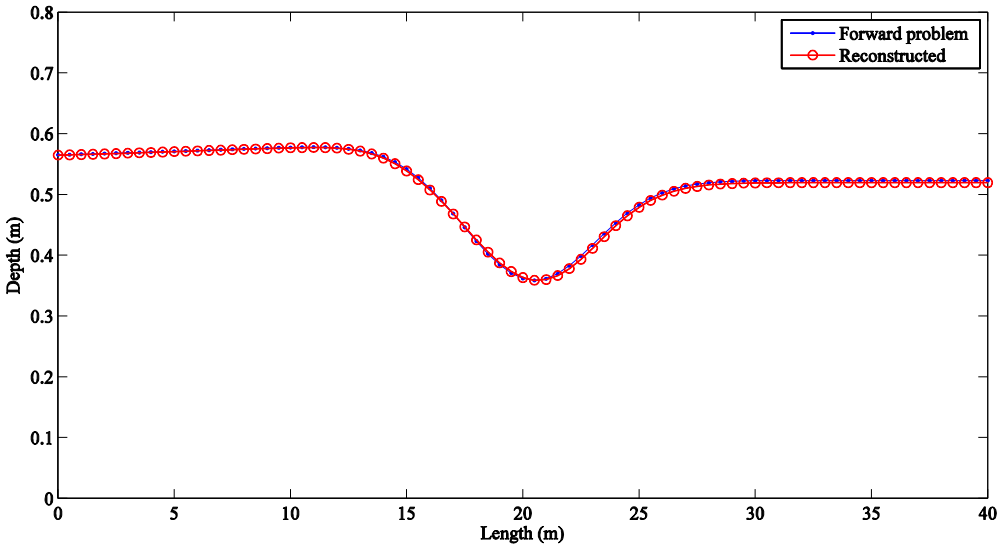


Figure 5.6: Comparison of reconstructed depth with the forward problem depth of the flow.

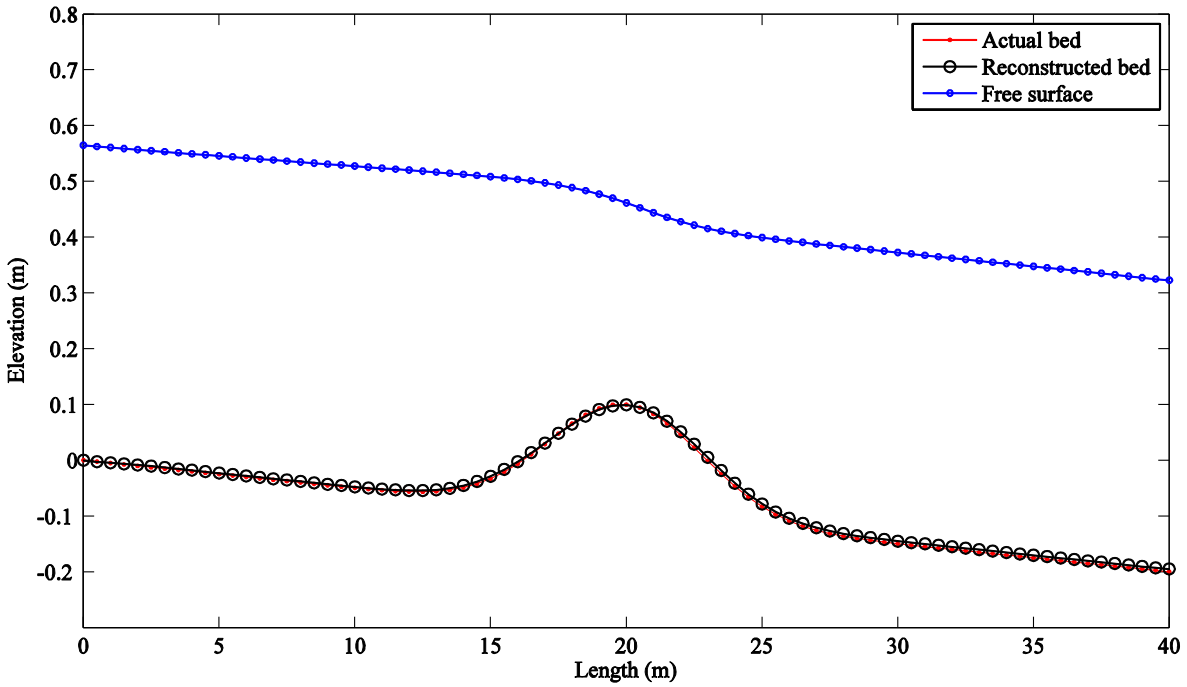


Figure 5.7: Reconstructed bed form

Figure 5.6 shows the comparison of the reconstructed and actual depth distribution while Figure 5.7 shows the comparison of the reconstructed and actual bed forms. From these Figures, it can be seen that there is good agreement between the reconstructed and original fields. The bed form is reconstructed with less than 10 mm of deviation in topographic elevation confirming that the method of characteristics approach to solve the inverse problem provides acceptable results.

In the following the reconstruction results of the two-dimensional test case is presented. The free surface elevation data generated from test case-II is used as input data along with the depth of the flow defined at the inlet boundary.

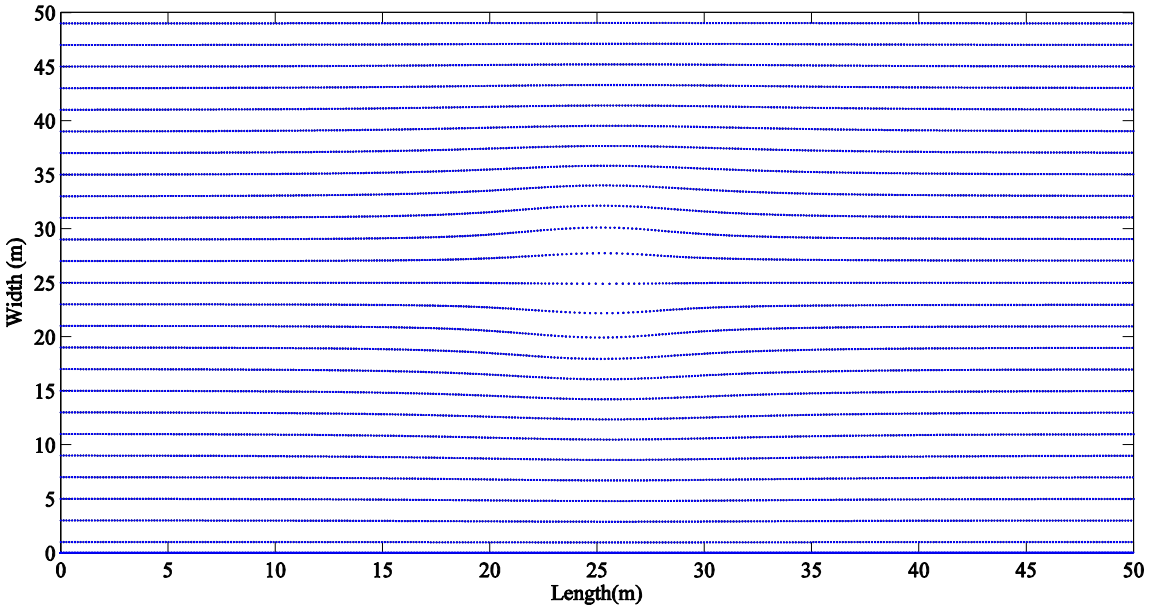


Figure 5.8: Characteristic lines

Figure 5.8 shows the characteristic lines on the computational domain which depicts that the characteristic lines are deflected by the presence of the bump in the channel bed. The characteristics go around the obstacle as intuitively expected.

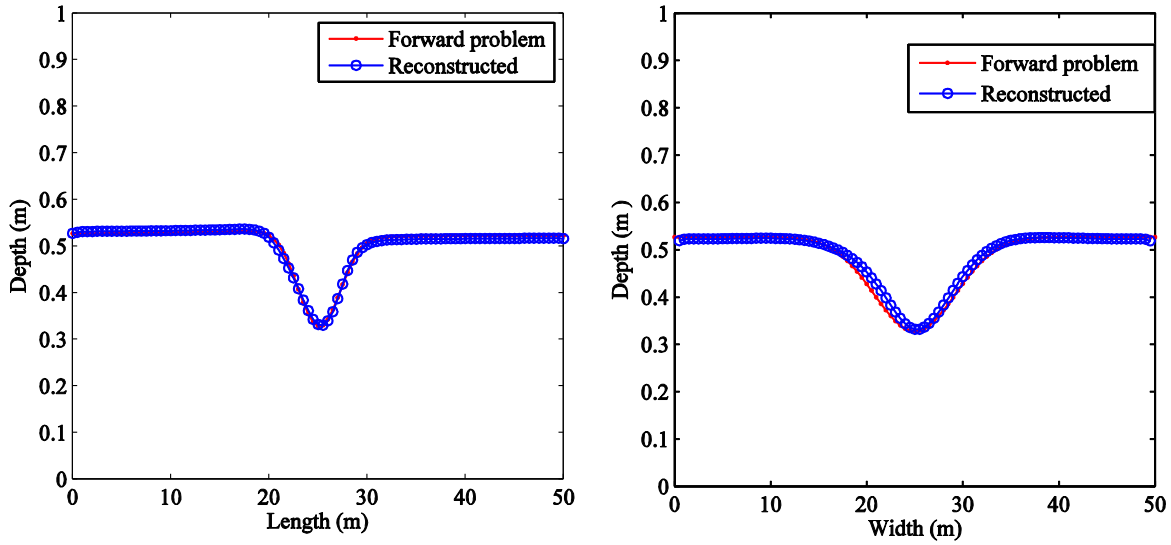


Figure 5.9: Comparison of the reconstructed and the actual depth distribution along the centre lines

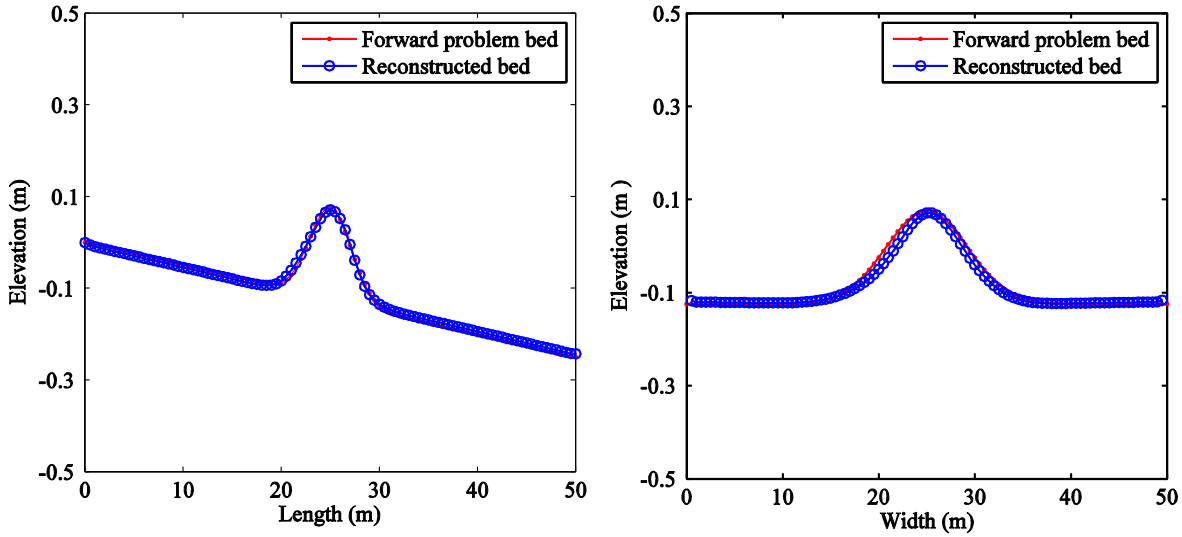


Figure 5.10: Comparison of actual and reconstructed bed profile at the centre (a) along y-axis (b) along x-axis

Comparison of the depth along the centre line of the computational domain is shown in Figure 5.9. The actual and the reconstructed bed topographic elevation comparisons along the centrelines can be seen in Figure 5.10. It can be seen that the reconstructed bed is in good agreement with the actual bed topography.

From the above two test cases, it is seen that the norm of the maximum deviation of the reconstructed bed from the actual bed topography is 0.0158m which is less than 3% of the minimum depth of the flow. The average deviation in the computational domain is below 5% of the maximum the error. The methodology is also tested for the cases where the bed topography constitutes depression instead of bumps and the results confirm good agreement between reconstructed and actual quantities.

The sensitivity of the algorithm to the introduction of noise in the free surface data was also tested. Because the partial differential equation governing the inverse problem (equation (11)) is linear, it can be anticipated that noise in the input free surface data will not be too severely amplified in the reconstructed bed. This is indeed what was observed:

the introduction of random noise amounting to 1% of the "peak to peak" free surface deviation from its undisturbed state resulted in 2% error in the reconstructed bed, 2.5% noise resulted in 3.5% error, 5% resulted in 6.2%, and 10% resulted in 13% error. This confirms that the reconstruction methodology is robust *vis-à-vis* noisy input data.

Thus, it can be concluded that the channel bed topography can be reconstructed from the known free surface data and the known depth of the flow at upstream boundary.

## 5.4. Concluding remarks

A new governing equation which relates the free surface and the bed topography elevation of the shallow water flow in an open channel is presented in the context of diffusive wave equation in the shallow water approximation framework. The governing equation is restricted to rivers or open channel flows with steep bed and paramount channel bed roughness where we can conveniently neglect the advection-convection terms in the momentum equations. The MacCormack solution methodology is adopted to determine the free surface profile for the forward problem analysis. In addition, an algorithm, based on the method of characteristics, is presented to reconstruct the channel bed topography from known free surface elevation data. This approach is easy-to-implement and it has the potential to overcome the shortcomings of traditional optimization based techniques of channel bed reconstruction.

An interesting finding of the analysis is that the knowledge of the channel bed roughness is not required for the reconstruction of the channel bed topography from known free surface elevation data. This is because the Manning's roughness coefficient disappears in the reformulation of the governing equations and appears to be useful to determine the velocity fields. However, the determination of velocity fields is not necessary as the modified governing equation allows a computation of depth of the flow without the simultaneous calculation of the velocity field thereby reducing the computational effort.

For the flow satisfying the given restrictions, it can be concluded that the depth of the flow along the characteristic curves in the computational domain can be determined given the depth at the inlet boundary. From the comparison of the forward and the inverse problem results, it can be concluded that the channel bed topographies in the given test cases can be reconstructed within the maximum error of 3% of the depth of the flow.

# 6. A direct solution approach to the two-dimensional shallow-water inverse problem

## Contents

## 6.1. Introduction

In the previous chapters, either a simplified form of the full two-dimensional shallow water equations or the one-dimensional shallow water equations are used to study the forward and inverse problems. These equations have restrictions imposed on them based on the assumptions made; however, they may not be valid in all situations. For instance, for the simplified form of the two-dimensional shallow water equations, if the gravitational and frictional terms are of the same order as that of the inertial terms, the approach is not applicable. Likewise, in the one-dimensional shallow water flows, if the channel is non-prismatic where the lateral flow variations are comparable to the main flow characteristics, the assumptions ceases to predict the natural phenomena of the flow under study. Thus, the use of full two-dimensional shallow water flow equations is paramount to study shallow water flows. These equations also assume the vertical averaging of hydraulic quantities, but provide reasonably accurate results with considerable simplifications. In fact, these simplifications are the backbone of the inverse problem analysis for using the direct approach used in this thesis.

The need to study the inverse problem based on the two-dimensional shallow water equations has already been justified in previous chapters, however, most practical free surface measurement techniques provide two-dimensional free surface elevation data for which lateral and longitudinal free surface variations are captured. Thus, there is a need of sufficiently and accurately represent three-dimensional bathymetry for the forward problem analysis based on this measured free surface elevation data.

As indicated in the introduction of the thesis, there have been significant developments in experimental techniques to measure river bathymetry and flow depths. However, most experimental techniques to identify the bed topographic elevation are time consuming [9, 12] and expensive [7, 10].

On the other hand, many numerical techniques have been developed to simulate open channel flows. The characteristics of the numerical methods differ depending on the particular problem: methods suitable for studying hydraulic jumps; methods suitable to study dam break problems; methods to study flood plain flows; methods to study steady flows; and methods suitable for high Froude numbers are relevant scenarios worthy of mention.

Comparatively, very little has been studied on the numerical reconstruction of the bed topographic elevation data of open channel flows using full two-dimensional shallow water flows, see e.g. [39, 98]. As mentioned in previous chapters, the direct numerical approach and optimization-based iterative methods are the two main approaches that can be implemented to solve such an inverse problem. The former method is analogous to the approaches implemented in the previous chapters of this thesis.

Section 6.2 introduces the full two-dimensional shallow water equations and the respective discretization technique for the forward problem. Section 6.3 presents a set of forward problem benchmark test cases. Following section 6.3, the inverse problem governing equations and the corresponding discretization technique and the respective inverse problem test cases are presented in section 6.4. In section 6.5, the concluding remarks of this chapter are presented.

## 6.2. Discretization of the governing equations of the forward problem

Considering the two-dimensional shallow water flows a general two-dimensional flow orientation is shown in Figure 6.1.

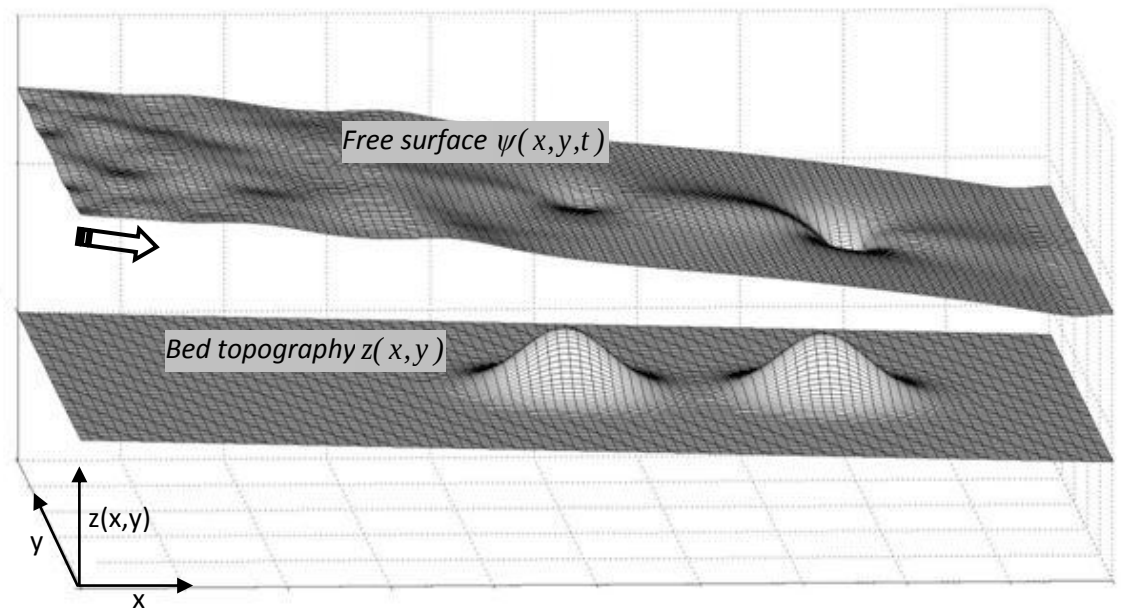


Figure 6. 1: Two-dimensional shallow water flow orientation

Thus, the two-dimensional governing equations which was given can be written in conservative form as

$$H_t + E_x + F_y + S = 0$$

$$H = \begin{pmatrix} h \\ uh \\ vh \end{pmatrix} \quad E = \begin{pmatrix} uh \\ u^2h + \frac{1}{2}gh^2 \\ uvh \end{pmatrix} \quad F = \begin{pmatrix} uh \\ uvh \\ v^2h + \frac{1}{2}gh^2 \end{pmatrix} \quad S = \begin{pmatrix} 0 \\ -gh(S_{ox} - S_{fx}) \\ -gh(S_{oy} - S_{fy}) \end{pmatrix} \tag{6.1}$$

$$S_{fx} = \frac{n^2 u\sqrt{u^2+v^2}}{C_o h^{4/3}} \qquad S_{fy} = \frac{n^2 v\sqrt{u^2+v^2}}{C_o h^{4/3}}$$

$$S_{ox} = -\frac{\partial z}{\partial x} \qquad S_{oy} = -\frac{\partial z}{\partial y}$$

Where $C_o$ is dimensionless constant: $C_o=1$ for SI unit system

The discretization of the governing equations is one of the most important steps in the numerical solution of partial differential equations in engineering and science. Many

discretization techniques have been developed to suit specific problems. In the context of these governing equations, the MacCormack Explicit numerical scheme is implemented for the forward problem, see e.g. [6] and references therein. It has been chosen because it is a standard technique which is reasonably easy-to-implement and yet produces reliable results. This discretization technique has a predictor and a corrector stage coupled with sequential solution methodology. Backward differencing numerical technique is implemented in the predictor stage while forward differencing is used in the corrector stage. The flow variables are known at time step *k* and their values at *k*+1 are to be determined, [6]. Then, for grid point (*i, j*), the approximate equation can be written as

Predictor stage

$$H_{i,j}^{*} = H_{i,j}^{k} - \frac{\Delta t}{\Delta x}\nabla_x E_{i,j}^{k} - \frac{\Delta t}{\Delta y}\nabla_y F_{i,j}^{k} - \Delta t S_{i,j}^{k} \qquad \begin{cases} 2 \le i \le N \\ 2 \le j \le M \end{cases} \tag{6.2}$$

Corrector stage

$$H_{i,j}^{**} = H_{i,j}^{k} - \frac{\Delta t}{\Delta x}\Delta_x E_{i,j}^{*} - \frac{\Delta t}{\Delta y}\Delta_y F_{i,j}^{*} - \Delta t S_{i,j}^{*} \qquad \begin{cases} 1 \le i \le N-1 \\ 1 \le j \le M-1 \end{cases} \tag{6.3}$$

In which $H^{*}$ and $H^{**}$ are intermediate values of $H$. The new values of $H$ at time $k+1$ are obtained from

$$H_{i,j}^{k+1} = \frac{1}{2}\left( H_{i,j}^{*} + H_{i,j}^{**} \right) \tag{6.4}$$

As mentioned above the scheme first uses backward space differencing ($\nabla_x$ and $\nabla_y$) to predict an intermediate solution from the known information at time step $k$. Then the forward differences ($\Delta_x$ and $\Delta_y$) are used in the corrector stage to correct the predicted values. The finite difference operators $(\nabla)$ and $(\Delta)$ are defined as

$$\nabla_x H_{i,j} = H_{i,j} - H_{i-1,j}$$

$$\Delta_x H_{i,j} = H_{i+1,j} - H_{i,j} \tag{6.5}$$

The subscripts in the operators show the direction of differencing. Substituting the flux terms as $U = uh$ and $V = vh$, the final form of the discretized equations can be written as

Predictor stage

$$h^*_{i,j} = h^k_{i,j} - \frac{\Delta t}{\Delta x}\left(U^k_{i,j} - U^k_{i-1,j}\right) - \frac{\Delta t}{\Delta y}\left(V^k_{i,j} - V^k_{i,j-1}\right)$$

$$\begin{aligned} U^*_{i,j} = U^k_{i,j} &- \frac{\Delta t}{\Delta x}\left(U^k_{i,j}u^k_{i,j} - U^k_{i-1,j}u^k_{i-1,j}\right) - \frac{\Delta t}{\Delta y}\left(U^k_{i,j}v^k_{i,j} - U^k_{i,j-1}v^k_{i,j-1}\right) - \frac{1}{2}g\frac{\Delta t}{\Delta x}\left[\left(h^k_{i,j}\right)^2 - \left(h^k_{i-1,j}\right)^2\right] \\ &+ gh^k_{i,j}\Delta t\left(S_{ox} - S_{fx}\right)_{i,j} \end{aligned} \tag{6.6}$$

$$\begin{aligned} V^*_{i,j} = V^k_{i,j} &- \frac{\Delta t}{\Delta x}\left(V^k_{i,j}u^k_{i,j} - V^k_{i-1,j}u^k_{i-1,j}\right) - \frac{\Delta t}{\Delta y}\left(V^k_{i,j}v^k_{i,j} - V^k_{i,j-1}v^k_{i,j-1}\right) - \frac{1}{2}g\frac{\Delta t}{\Delta y}\left[\left(h^k_{i,j}\right)^2 - \left(h^k_{i,j-1}\right)^2\right] \\ &+ gh^k_{i,j}\Delta t\left(S_{oy} - S_{fy}\right)_{i,j} \end{aligned}$$

Corrector Stage

$$h^{**}_{i,j} = h^k_{i,j} - \frac{\Delta t}{\Delta x}\left(U^*_{i+1,j} - U^*_{i,j}\right) - \frac{\Delta t}{\Delta y}\left(V^*_{i,j+1} - V^*_{i,j}\right)$$

$$\begin{aligned} U^{**}_{i,j} = U^k_{i,j} &- \frac{\Delta t}{\Delta x}\left(U^*_{i+1,j}u^*_{i+1,j} - U^*_{i,j}u^*_{i,j}\right) - \frac{\Delta t}{\Delta y}\left(U^*_{i,j+1}v^*_{i,j+1} - U^*_{i,j}v^*_{i,j}\right) - \frac{1}{2}g\frac{\Delta t}{\Delta x}\left[\left(h^*_{i+1,j}\right)^2 - \left(h^*_{i,j}\right)^2\right] \\ &+ gh^*_{i,j}\Delta t\left(S^*_{ox} - S^*_{fx}\right)_{i,j} \end{aligned} \tag{6.7}$$

$$\begin{aligned} V^{**}_{i,j} = V^k_{i,j} &- \frac{\Delta t}{\Delta x}\left(V^*_{i+1,j}u^*_{i+1,j} - V^*_{i,j}u^*_{i,j}\right) - \frac{\Delta t}{\Delta y}\left(V^*_{i,j+1}v^*_{i,j+1} - V^*_{i,j}v^*_{i,j}\right) - \frac{1}{2}g\frac{\Delta t}{\Delta y}\left[\left(h^*_{i,j+1}\right)^2 - \left(h^*_{i,j}\right)^2\right] \\ &+ gh^*_{i,j}\Delta t\left(S^*_{oy} - S^*_{fy}\right)_{i,j} \end{aligned}$$

The new values at time step $k+1$ is then calculated from the intermediate values which are determined from the predictor and corrector steps

$$h_{i,j}^{k+1} = \frac{1}{2}\left(h_{i,j}^{*} + h_{i,j}^{**}\right); \quad U_{i,j}^{k+1} = \frac{1}{2}\left(U_{i,j}^{*} + U_{i,j}^{**}\right); \quad V_{i,j}^{k+1} = \frac{1}{2}\left(V_{i,j}^{*} + V_{i,j}^{**}\right) \tag{6.8}$$

Whereas the primitive variables will be determined from the computed values of $U$ and $V$ in each time step

$$h_{i,j}^{k+1} = h_{i,j}^{k+1}; \qquad u_{i,j}^{k+1} = \frac{U_{i,j}^{k+1}}{h_{i,j}^{k+1}}; \qquad v_{i,j}^{k+1} = \frac{V_{i,j}^{k+1}}{h_{i,j}^{k+1}} \tag{6.9}$$

A reflective wall boundary is implemented at the side walls. This can be implemented by replacing the point on the solid wall by fictitious mirror point in the flow domain while changing the sign of the normal component of velocity.

However, the inlet and the outlet boundary conditions are handled depending the type of the flow. For subcritical flow the depth of the flow at the outlet boundary is defined with the flow rate at the upstream boundary. On the contrary, the depth and the flow rate at the upstream boundary are defined for supercritical flows. On the other side of the defined boundary conditions, it is assumed that the gradient of the parameters along the flow direction is zero. The transverse velocity component at the inlet is also defined as zero.

## 6.3. The forward problem test cases

The governing equations of the forward problem along with their discretization are presented in the above section. The parameters that will be determined from the forward problem are the free surface elevation, the velocity components of the flow, and the depth of the flow. For this purpose some hydraulic parameters are required prior to the computation. These include bed topography elevation, roughness coefficient, flow rate, and the depth of the flow at the boundary depending on the flow regime. In the following, the results of the forward problem test cases are presented and these results will be used as

input data for the validation and assessment of the inverse problem methodology of the two-dimensional analysis.

***Test Case I: one-dimensional steady subcritical flow over a frictionless channel***

This test case is previously given in chapter 3 where a 1 m wide 25 m long channel is considered to test subcritical flow over a bump. The channel bed is assumed to have a rectangular cross section and to be frictionless with a bump. Even if the nature of this test case is one-dimensional, the two-dimensional solution approach should result in identical results if the boundary conditions are correctly implemented. The bed topography is defined by

$$z = \begin{cases} 0 & x < 8 \quad and \; x > 12 \\ 0.2 - 0.05(x-10)^2 & 8 \le x \le 12 \end{cases} \tag{6.10}$$

The depth at downstream boundary condition of the flow is set $h = 2$ m and the water inflow condition $Q = 4.42\,\mathrm{m}^3/\mathrm{s}$ is imposed for the computation of results. This test case is the most common canonical test case used by different authors, see [56, 74, 75] for example, in order to validate their numerical techniques for the convergence of the solution towards steady state and the conservation of discharge along the channel. The Froude numbers for this test case range from 0.496 - 0.635 showing that the flow is subcritical in the entire domain.

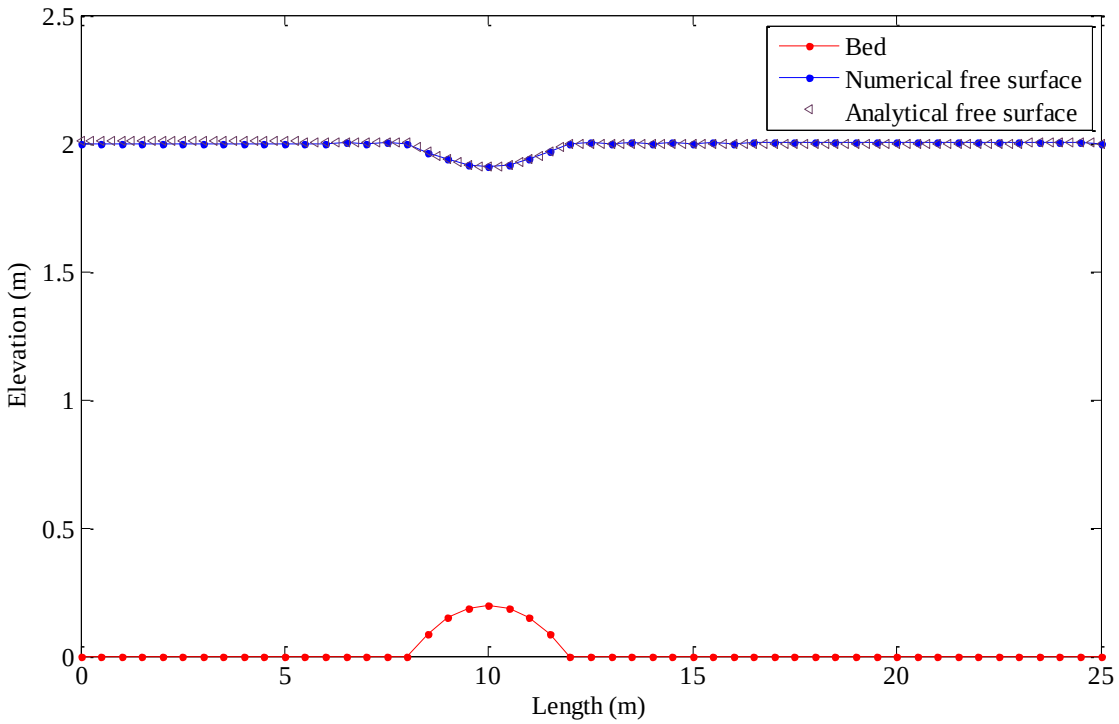


Figure 6. 2: Free surface and bedrock topographies

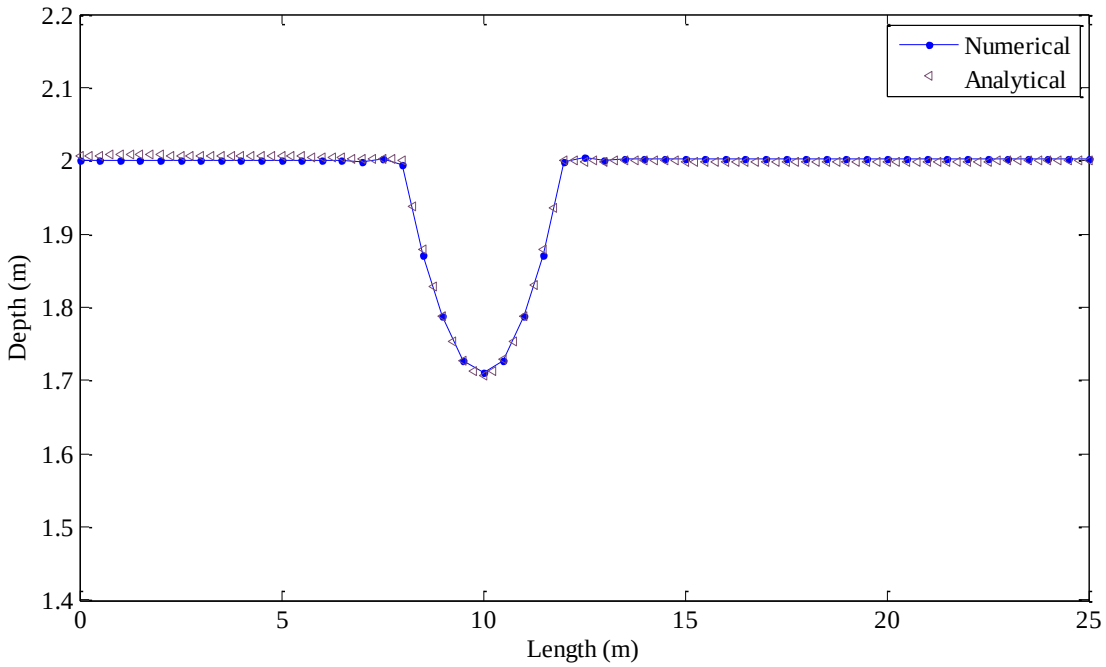


Figure 6. 3: Depth of the flow

The results shown in Figures 6.2 and 6.3 are in good agreement with the results presented in the above references and with the respective pseudo-analytical solution presented in

[99]. As can be seen in Figure 6.2, the existence of the obstacle creates significant change on the free surface profile.

***Test case-II: Three-dimensional flow over a two-dimensional bump***

In this test case, an artificial bed topography with a bump having two-dimensional characteristics is considered to simulate three-dimensional shallow water flows. Thus, the variation of the bed along the longitudinal and the transverse direction is considered in a computational domain of size 100m by 100m. The bed topography is defined by:

$$z = 0.2\,exp\left(-\left(x-\frac{x_{max}}{2}\right)^2\frac{1}{\alpha_1{}^2}-\left(y-\frac{y_{max}}{2}\right)^2\frac{1}{\alpha_2{}^2}\right)-0.001x \tag{6.11}$$

where $x_{\max}$ and $y_{\max}$ are the length scales of the domain in $x$- and $y$- directions. In this test case $x_{max}=y_{max}=100$ m and $\alpha_1=3$, $\alpha_2=6$. A spatial grid size $\Delta x=1$m and the temporal grid size $\Delta t=0.1$s are implemented. The flow rate of 2 $m^3$/s per unit width is defined at the inlet boundary. A Manning's roughness value $n=0.02$ is chosen to account for the effect of friction. A subcritical flow is considered such that at the outlet a depth is 1.0 m is imposed along the transverse direction. A steady solution is generated from the transient governing equation and steady boundary conditions. The Froude numbers for this test case range from 0.56 - 0.92 showing that the flow is subcritical in the entire domain. In the following, plots of the bed elevation along the centre lines and the respective results of the forward problem are presented.

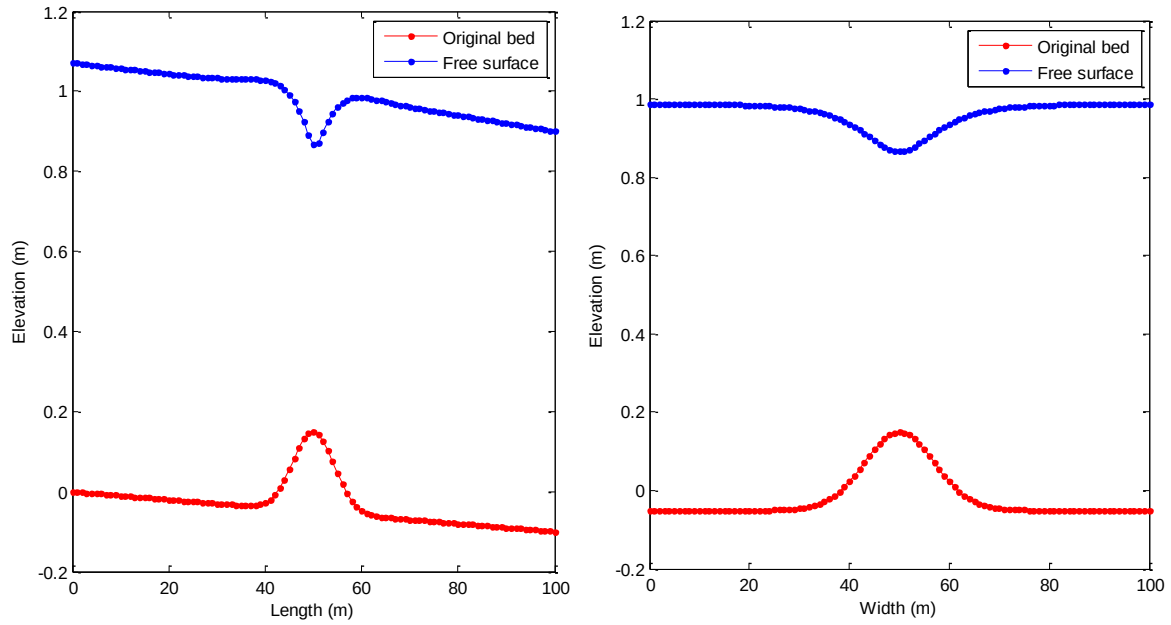


Figure 6. 4: Centreline bed and free surface elevation variation (a) along the length (b) along the transverse direction for test case-II

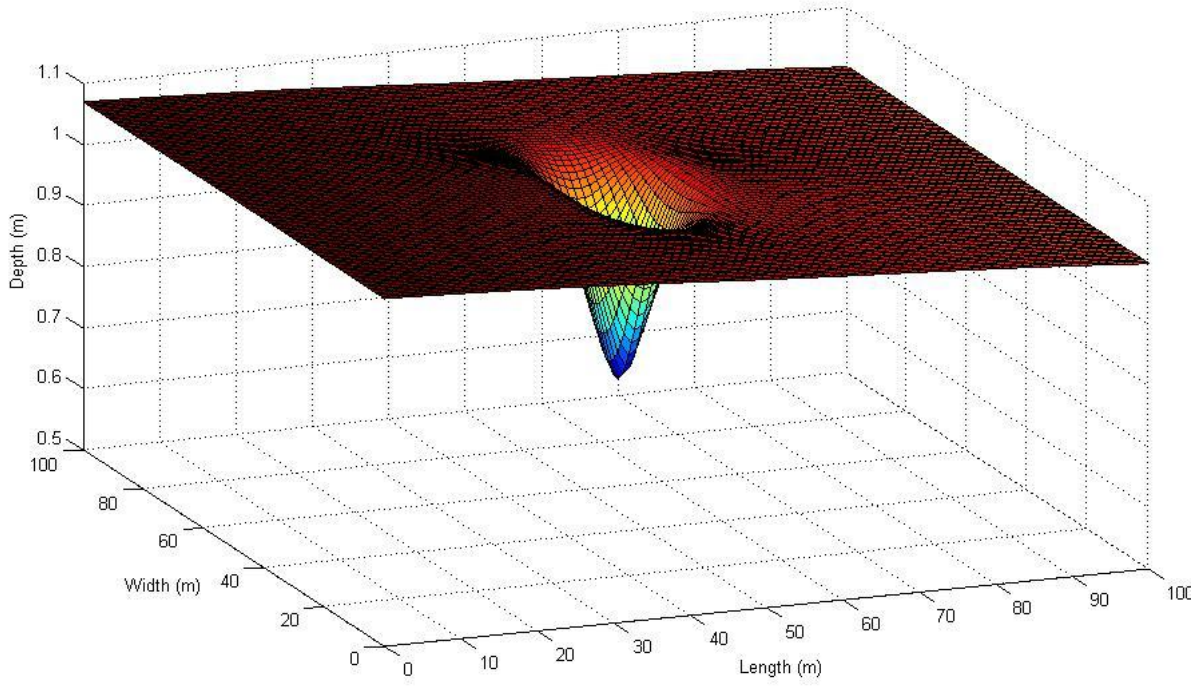


Figure 6. 5: Depth variation for test case-II

From the given bed topographic elevation, steady flow rate, roughness coefficient and boundary conditions, the steady flow is generated. The free surface variation along the centreline is given in Figure 6.4

As can be seen from Figures 6.4 and 6.5, the existence of the bump at the centre of flow domain creates a two-dimensional variation in the free surface elevation. The underlying hypothesis of the inverse problem algorithm is that the shape of this free surface with known boundary conditions contains sufficient information to reconstruct the underlying bedrock. This will be discussed in the detail in the next section. The free surface elevation data of this test case will be used as a known parameter along with other boundary conditions for the inverse problem analysis.

***Test case III: Three-dimensional flow over number of two-dimensional bumps***

In order to investigate the effect of a more complex bedrock topography on the free surface, four bumps are considered in the computational domain. Similar parametric values, grid sizes, and Manning roughness coefficient as for test case II are used. However a flow rate of 4.42m$^3$/s per unit width and flow depth of 2m at the inlet boundary are implemented in this test case. The free surface elevation is generated for the inverse problem analysis by solving numerically equations (6.6), (6.7), (6.8) and (6.9). The bedrock topography is given by

$$z = 0.2\exp\left(-\left(x-\frac{x_{\max}}{2}\right)^2\frac{1}{\alpha_1^{\,2}}-\left(y-\frac{y_{\max}}{2}\right)^2\frac{1}{\alpha_2^{\,2}}\right)+0.2\exp\left(-\left(x-\frac{x_{\max}}{2}\right)^2\frac{1}{\alpha_1^{\,2}}-\left(y-\frac{y_{\max}}{2}\right)^2\frac{1}{\alpha_2^{\,2}}\right)+$$
$$0.2\exp\left(-\left(x-\frac{x_{\max}}{2}\right)^2\frac{1}{\alpha_1^{\,2}}-\left(y-\frac{y_{\max}}{2}\right)^2\frac{1}{\alpha_2^{\,2}}\right)+0.2\exp\left(-\left(x-\frac{x_{\max}}{2}\right)^2\frac{1}{\alpha_1^{\,2}}-\left(y-\frac{y_{\max}}{2}\right)^2\frac{1}{\alpha_2^{\,2}}\right)-0.001x \quad (6.12)$$

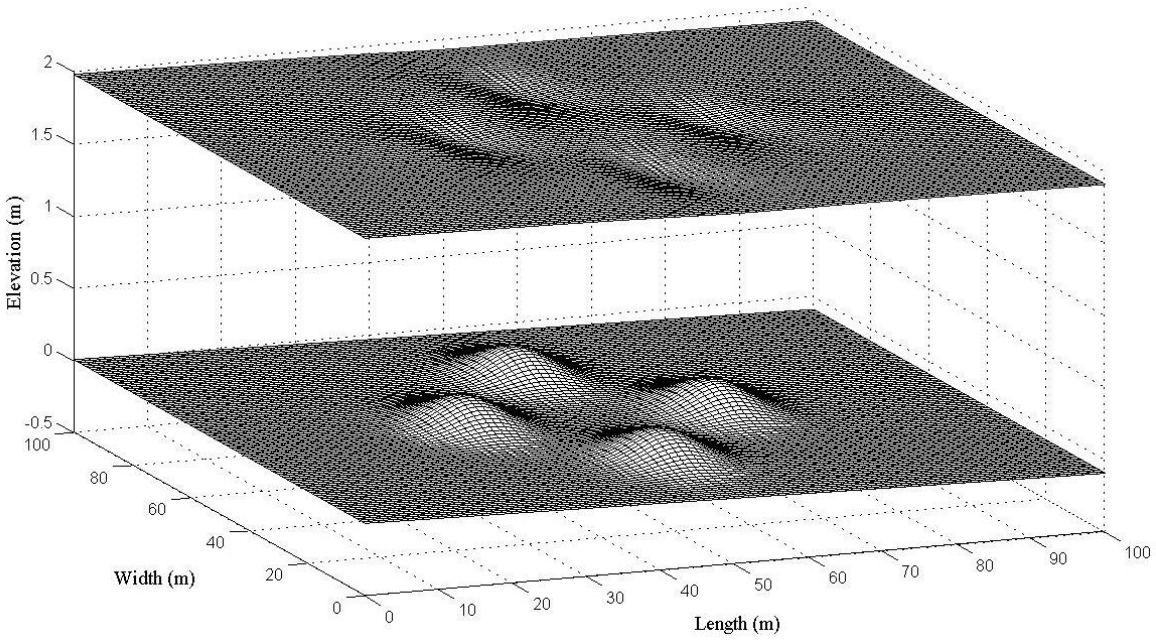


Figure 6. 6: Water level on an inclined bed with four bumps

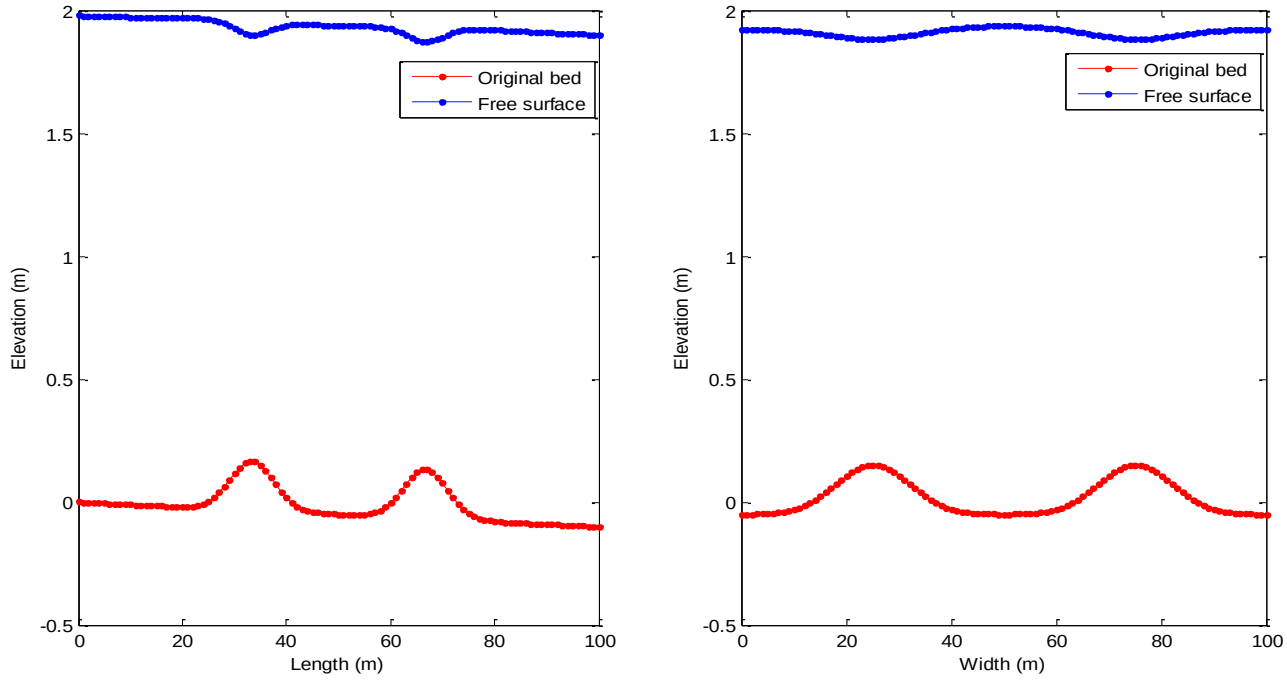


Figure 6. 7: Bed and free surface along the centreline (left) longitudinal (right) transverse variation

From Figures 6.6 and 6.7, it can be seen that each bump introduced on the bed has its own effect on the free surface. The undulations on the free surface are the manifestations of the bump on the bed and these free surface undulations, if accurately captured, can provide sufficient information of the bed and other parameters. The Froude numbers for this test

case range from 0.49 - 0.6 showing that the flow is subcritical in the entire domain. The free surface generated in this test case will be used as input data for the respective inverse problem test cases.

## 6.4. The inverse problem analysis

The shallow water equations will be rearranged and used for the inverse problem analysis. However, there is a difference in the known and unknown parameters. For the inverse problem the free surface elevation data, Manning's roughness coefficient, steady flow rate, and depth of the flow at the boundary are the required parameters. The governing equation of the inverse problem can be rewritten after substituting a free surface function by $\psi(x,y) = z(x,y) + h(x,y)$ as in the previous cases.

$$H_t + E_x + F_y + S = 0$$

$$H = \begin{pmatrix} h \\ uh \\ vh \end{pmatrix} \quad E = \begin{pmatrix} uh \\ u^2h \\ uvh \end{pmatrix} \quad F = \begin{pmatrix} vh \\ uvh \\ v^2h \end{pmatrix} \quad S = \begin{pmatrix} 0 \\ -gh(S_{\psi x} - S_{fx}) \\ -gh(S_{\psi y} - S_{fy}) \end{pmatrix} \tag{6.13}$$

$$S_{fx} = \frac{n^2 u\sqrt{u^2+v^2}}{C_o h^{4/3}} \qquad S_{fy} = \frac{n^2 v\sqrt{u^2+v^2}}{C_o h^{4/3}}$$

$$S_{\psi x} = -\frac{\partial \psi}{\partial x} \qquad S_{\psi y} = -\frac{\partial \psi}{\partial y}$$

The discretization of the inverse problem governing equations differs from the forward problem in such a way that only backward differencing explicit numerical scheme is implemented. This approach has a stability restriction but is easy-to-implement and fast to provide a solution.

$$
\begin{aligned}
h_{i,j} &= h_{i,j}^{k} - \frac{\Delta t}{\Delta x}\left(U_{i,j}^{k} - U_{i-1,j}^{k}\right) - \frac{\Delta t}{\Delta y}\left(V_{i,j}^{k} - V_{i,j-1}^{k}\right) \\
U_{i,j} &= U_{i,j}^{k} - \frac{\Delta t}{\Delta x}\left(U_{i,j}^{k}u_{i,j}^{k} - U_{i-1,j}^{k}u_{i-1,j}^{k}\right) - \frac{\Delta t}{\Delta y}\left(U_{i,j}^{k}v_{i,j}^{k} - U_{i,j-1}^{k}v_{i,j-1}^{k}\right) + gh_{i,j}^{k}\Delta t\left(S_{\psi x} - S_{fx}\right)_{i,j} \\
V_{i,j} &= V_{i,j}^{k} - \frac{\Delta t}{\Delta x}\left(V_{i,j}^{k}u_{i,j}^{k} - V_{i-1,j}^{k}u_{i-1,j}^{k}\right) - \frac{\Delta t}{\Delta y}\left(V_{i,j}^{k}v_{i,j}^{k} - V_{i,j-1}^{k}v_{i,j-1}^{k}\right) + gh_{i,j}^{k}\Delta t\left(S_{\psi y} - S_{fy}\right)_{i,j}
\end{aligned}
\tag{6.14}
$$

The boundary condition is implemented in a similar way as that of the forward problem. The new values of parameters $h, U, V, S_{\psi x}$ and $S_{\psi y}$ at time step $k+1$ are calculated from the previous time step values. The depth of the flow and the flow velocities are solved simultaneously and iteratively using Equation (6.14).

In this analysis, the expression used to find the new values of $h$ $U$ and $V$ differ from the forward problem approach. This is because, in the inverse problem, unlike for the forward problem analysis, no information is transferred from the downstream to the upstream direction making the backward difference approach a suitable choice. As the backward differencing scheme is implemented, the definition of the outlet boundary condition does not affect the solution of the problem in the upwind direction as there is no upstream wave propagation. Thus, inlet boundary condition is implemented irrespective of the flow regime. The primitive variables $(u,v)$ will be determined from the computed values of $U$ and $V$ at each time step. Once the values of $(h,u,v)$ are determined the bed topography elevation is evaluated by a simple subtraction for the depth of the flow from the free surface elevation function.

$$
z_{i,j}^{k+1} = \psi_{i,j}^{k+1} - h_{i,j}^{k+1} \tag{6.15}
$$

The results of the inverse problem are then counterchecked against the forward problem results in order to identify the capability of the algorithm in reconstructing the bed topographic elevation. Thus, similar test cases will be considered for the numerical experiment of the algorithm.

***Test case-I: Steady one-dimensional subcritical flow over a bump in a frictionless channel.***

The free surface elevation data obtained from the forward problem and the respective boundary and initial conditions along with the steady inflow rate are used as an input parameter for the inverse problem analysis. Unlike the depth at the downstream boundary in the case of the forward problem, the inverse problem requires boundary conditions at the inlet boundary. A depth at the upstream boundary $h = 2$ m and the water inflow rate $Q = 4.42\ \mathrm{m}^3/\mathrm{s}$ are imposed. A time step of 0.05 s and spatial grid size of 0.5 m are used in the computation.

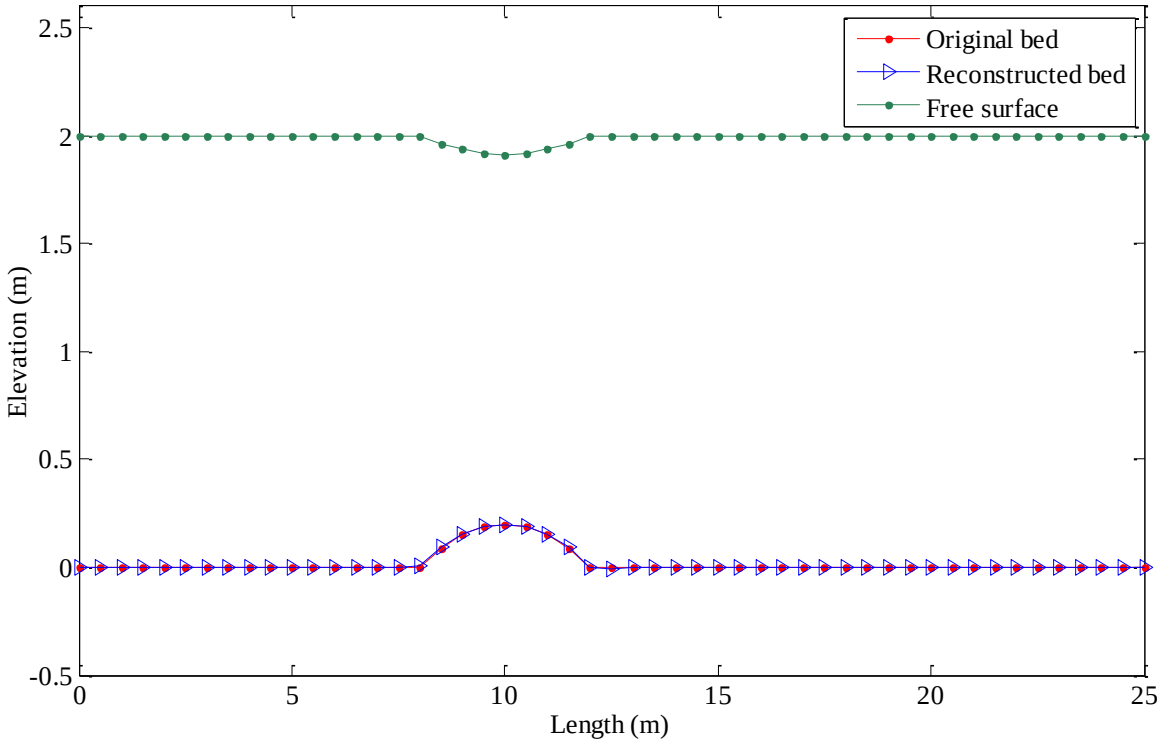


Figure 6.8: Reconstructed bed: subcritical test case

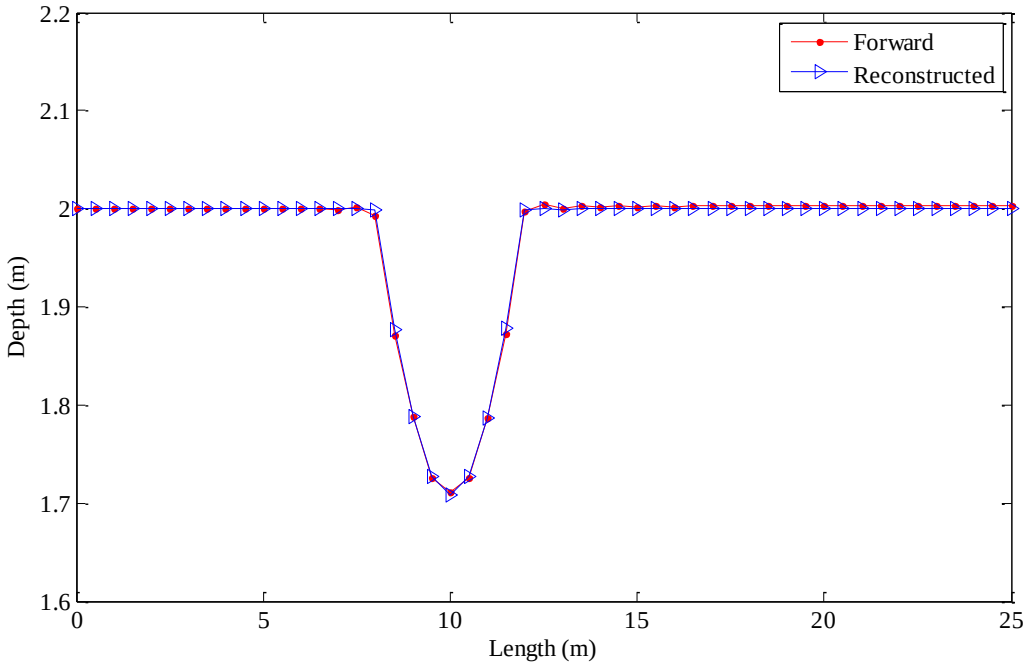


Figure 6.9: Comparison of the reconstructed and forward problem depth variation for the case of subcritical flow

Figure 6.8 shows the comparison of the reconstructed and actual bed forms. In Figure 6.9 the reconstructed and actual depth of the flow are compared. The results show that there is good agreement between the reconstructed and actual riverbed topography. The bed topography reconstruction in this particular test case agrees well with the results presented in the one-dimensional reconstruction analysis which validates the two-dimensional approach. This confirms that the algorithm can be used for bed topography reconstructions of open channel flows of one-dimensional nature.

***Test case-II: Steady two-dimensional flows over a bump in a rectangular channel.***

This test case is used to test the algorithm for its capability to reconstruct an unknown bed topographic elevation from known free surface elevation data which was generated in the forward test case-II. In the respective forward test case, the effect of bed slope, friction coefficient and local bed deflection were implemented to generate the free surface profile

which is now used as input parameter. Along with the free surface profile, depth and steady flow rate at the inlet boundary are required. For the inverse problem analysis, a spatial grid size $\Delta x = 1\text{m}$ and the time step $\Delta t = 0.05\text{s}$ are implemented. A flow rate of $2\text{m}^3/\text{s}$ per unit width and the depth at the upstream boundary are identical to the ones used for the forward problem. A Manning's roughness value $n = 0.02$ is used as in the case of the forward problem. A total computation time of 100 seconds (on an Intel® Core™2 Duo processor) was sufficient to generate steady reconstructed parameters.

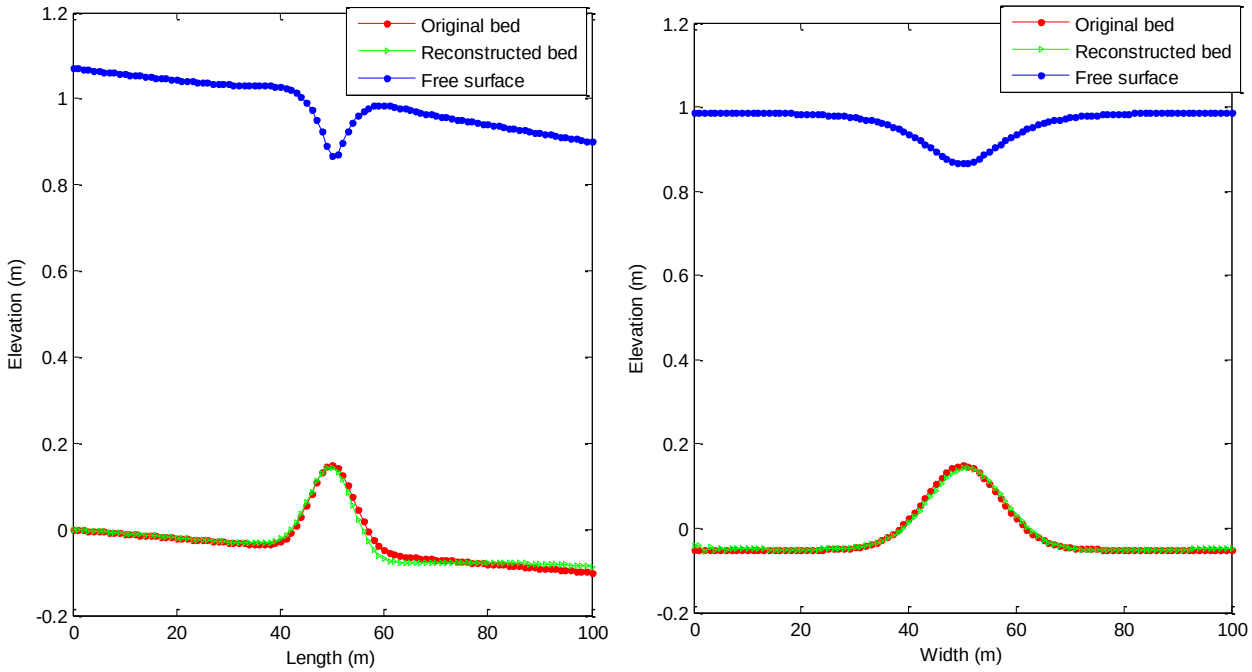


Figure 6.10: Comparison of original and reconstructed bed forms

As can be seen from Figure 6.10, the bed form is successfully reconstructed with very good agreement with the actual bed used in the forward problem. The bump is well captured along with the bed slope showing that the methodology used can use the signal from the free surface to successfully identify its source. Quantitatively, the bed topography is reconstructed with 3% maximum deviation. The sensitivity of the algorithm to the introduction of noise in the free surface data was also tested on ranges of noise magnitude with respect to the signal on the free surface. Noise magnitudes ranging from

1- 5 % of the “peak-to-peak” free surface deviations are considered. In Figure 6.11, the reconstructed bed topography from a 1% noise is shown and it is evident that the noise is not amplified in the reconstructed bed.

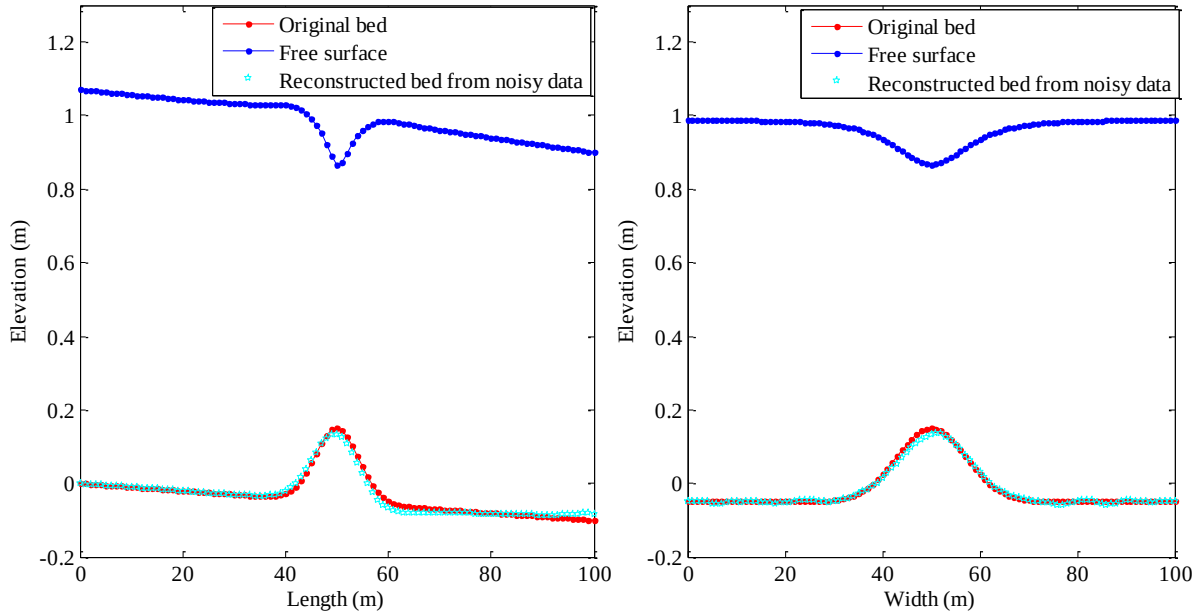


Figure 6.11: Reconstructed bed form from noisy free surface data

***Test case-III: The reconstruction of bed topography used in test case-III of the forward problem.***

Like the above inverse problem test cases, the free surface topographic data from the forward problem analysis is used as input parameter to reconstruct the corresponding bed topographic elevation. Additionally, a flow rate of 4.42m$^3$/s per unit width and flow depth of 2m at the upstream boundary are imported from the corresponding forward problem. The reconstructed bed along with the free surface profile is shown in Figure 6.12.

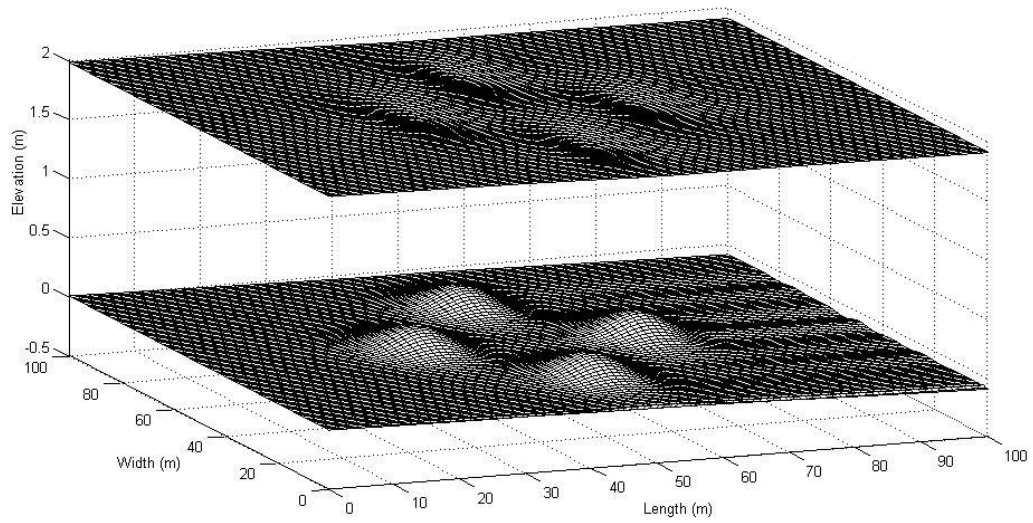


Figure 6.12: Reconstructed bed topographic elevation

As can be seen from Figure 6.12, the four bumps in the original bump are successfully reconstructed. However, there is an apparent but small difference, downstream of the bumps, between the reconstructed and original beds. The comparison of the bed topography along the centreline is presented in Figure 6.13.

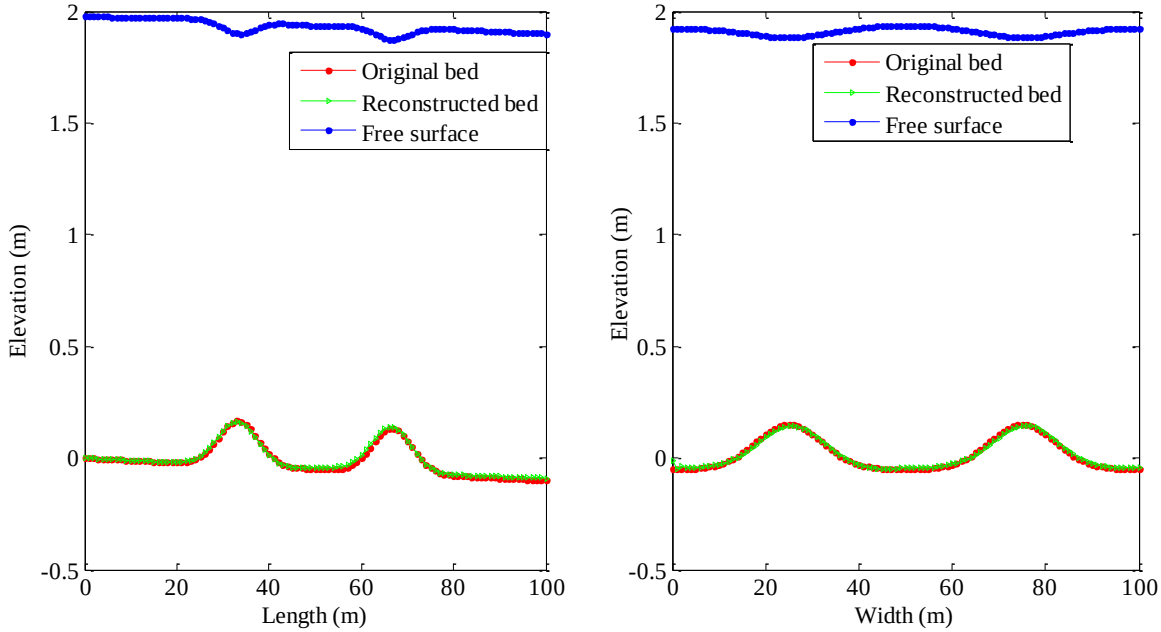


Figure 6.13: Comparison of the reconstructed and original bed forms

As can be seen in Figure 6.13, the reconstructed and original bed forms are in good agreement with each other. The difference between the original and the reconstructed bed lies below 0.5%.

Like test case II, the reconstruction algorithm is tested for its applicability to infer the channel bed topography from noisy free surface elevation data. The magnitude of the noise introduced is 1% of the signal of the free surface variation and the results (Figure 6.14) show that the bed topography is reconstructed without amplification of the noise in the reconstructed bed elevation.

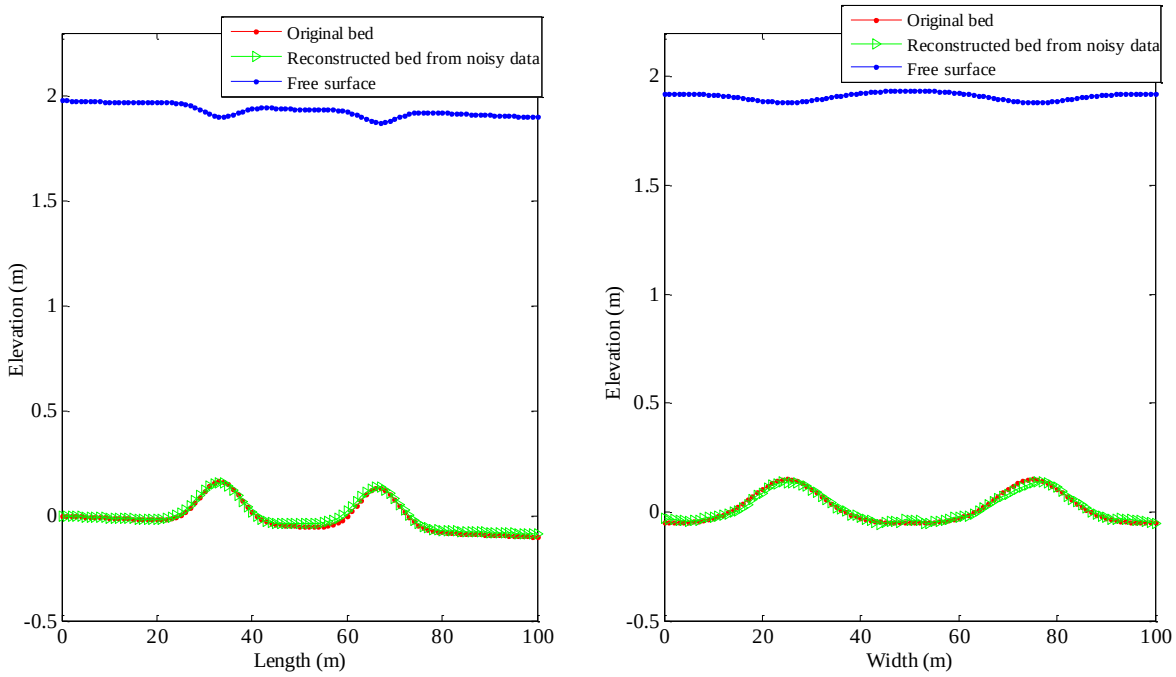


Figure 6.14: Comparison of the original and reconstructed bed forms from noisy free surface data

In practice it is difficult to get a smooth free surface elevation from field measurements which often include noise. Thus, to identify the capability of the algorithm to handle noisy input data, 1, 2.5, and 5% noise levels are introduced in the free surface data of all of the above test cases. The noise is based on the signal on the free surface. A Savitzky-Golay smoothing filter is used in MATLAB to smooth the 2D noisy free surface data before the computation. The reconstruction of the bed topography from the noisy data revealed that

the level of discrepancy in the reconstructed bedrock elevation is in the range of 1%, 5%, and 9.5%, respectively. Sample results based on 1% noise on both test cases are shown in Figures 6.11 and 6.14.

The algorithm used for the inverse reconstruction of the bed topography from the free surface elevation data is fast and easy to implement. It has the ability to reconstruct the bed from noisy free surface data with the help of smoothing techniques. The methodology requires the values of the steady flow rate, depth of the flow at inlet boundary, and the roughness coefficient in addition to the free surface elevation data. The flow in all test cases is subcritical as it is shown by the calculated ranges of the Froude number. Similar analysis indicated that the proposed approach is not suitable for transcritical and supercritical flows because hydraulic jumps and surges are not accommodated by the solution approach, thus it requires further developments to perform bed topography reconstruction in the cases of such flows .

The presented methodology works well for steady flows. The effect of a flux change in the flow will have local effect on the free surface which will send a wrong signal to the algorithm in the reconstruction process. The scope of this study is therefore limited to 2D steady shallow open channel flows of subcritical nature.

## 6.5. Summary and concluding remarks

The study of open channel flow modelling based on two-dimensional flows calls for input parameters like bed topography (bathymetry) and roughness coefficient in order to accurately predict the hydrodynamics of the three-dimensional shallow water flow. A methodology based on an explicit finite difference scheme is used to reconstruct the bed elevation from the free surface data. The methodology requires a steady flow rate, knowledge of the roughness coefficient and the depth of the flow at the inlet boundary.

The algorithm is tested on a set of benchmark test cases and encouraging results are found. The bed topography is well reconstructed with a deviation of 3% or less relative error from the known free surface elevation data. The numerical methodology is easy-to-implement and fast to produce a solution but has a CFL restriction because of its explicit nature. This approach is suitable for steady open channel flows for which the shallow water approximation holds where the signal due to the existence of the underlying bed topography is captured by the free surface measurement technique.

In practice, the measured free surface contains noise. The presented methodology is found to be capable of reconstructing the channel bed topography from noisy free surface elevation data. When tested on a set of noisy numerical data, the methodology was found to introduce no noise amplification in all test cases considered here for validation purposes.

# PART - II

# GLACIER BEDROCK RECONSTRUCTION

# 7. Glaciers and the Shallow Ice Approximation

## Contents

## 7.1. Introduction

Systematic long term monitoring and data recording of glaciers is very important for a number of reasons, [27, 100]. These include: (*i*) to map glaciers and better understand climate interactions; (*ii*) to assess and monitor glacier induced water resources, sea level rise, and small and large scale natural hazards; and (*iii*) to monitor glaciers for tourism and recreational purposes due to the growing public interest, [101]. Glacier monitoring may involve the determination of parameters to identify different characteristics of a particular glacier. These include:

1. Determination of surface mass balance, length variations, and volume changes to directly or indirectly investigate glacier response in the context of climate change.
2. Determination of the speed of the flow to provide important data for glacier flow modelling.
3. Determination glacier characteristics to provide an inventory of basic data (delineation and surface area) for a particular point in time thus providing an important foundation for numerous glaciological, hydrological, climatological and geomorphological investigations
4. Determination of englacial temperature for the evaluation of thermal changes in glaciers at high elevations.

However, the task of determining all the aforementioned components is not an easy task and there are various associated challenges. Most of the measurement techniques are demanding in terms of logistics and instruments, laborious, and time consuming. The details of these measurement techniques are not included here for the purpose of

conciseness and scope of the thesis. However, it is important to mention the relevance of glaciers and their response to climate changes.

Because glaciers are highly sensitive to the earth surface energy changes, they can provide one of the clearest climate change signals if appropriately measured and monitored, [100]. These signals provide information of past climate changes varying from years to millennia. There are significant numbers of environmental factors affecting the characteristics of the climate change signals. For instance, the effect of climate change on these ice bodies may consist of: (*i*) changes in the accumulation/ablation rates, (*ii*) changes to the energy flux from atmosphere through the surface into the glacier, and (*iii*) changes to geothermal heat flux to alter the conditions at the base of the glacier or the combination of all, [13]. While the sunshine duration, wind effects, temperature, and precipitation levels [101] are also key factors which affect directly or indirectly the above features.

Modelling of glaciers and ice sheets has a wide range of application such as for dating ice cores, studying the role of large ice masses on climate change [27], studying the effect of climate change and the dynamics of the flow in case of mountain glaciers. Each specific modelling or study has a predefined objective. For instance, the modelling of mountain glaciers may have an objective of studying their response towards climate change because mountain glaciers react quickly to local climate changes which is manifested by their flow dynamics and geometry change. Thus, the information from these changes can be used to indicate climate variability, [100]. Suitable numerical modelling of these ice bodies provides important information to capture the complexity of the flow dynamics and allow the possibility to identify the corresponding climate change responses. These responses involve several processes and interactions of different parameters specific to the glacier

and the surrounding environment. To perform numerical modelling, these parameters are defined in mathematical relationships which properly represent the flow dynamics.

Many glacier flow mathematical models are available to numerically simulate glacier flows, however, the selection of an appropriate model may depend on the nature of the glacier, the parameters involved and the complexity of the problem. Among existing models the SIA, Higher-Order Approximations, and the Full Stokes models are some to mention (with increasing complexity). The SIA and Higher-Order Approximation models are derived from the Stokes equation under some restrictions and thus have limited applications. The details of the derivation the Shallow Ice approximation model from the Stokes equation are given in section 7.3.

## 7.2. The Full Stokes equations

The Stokes equation is believed to be the closest approximation to represent the dynamics of the ice flow. In the following, the derivation of the full stokes equation is presented.

Considering a Cartesian coordinate $(O,x,y,z)$ system, the parameters defining the free surface and the bedrock elevations are expressed in this coordinate system. The free surface elevation is defined as $S = S(x,y,z,t)$ and the respective bedrock elevation is $z_b = z_b(x,y,z)$ as depicted in Figure 7.1

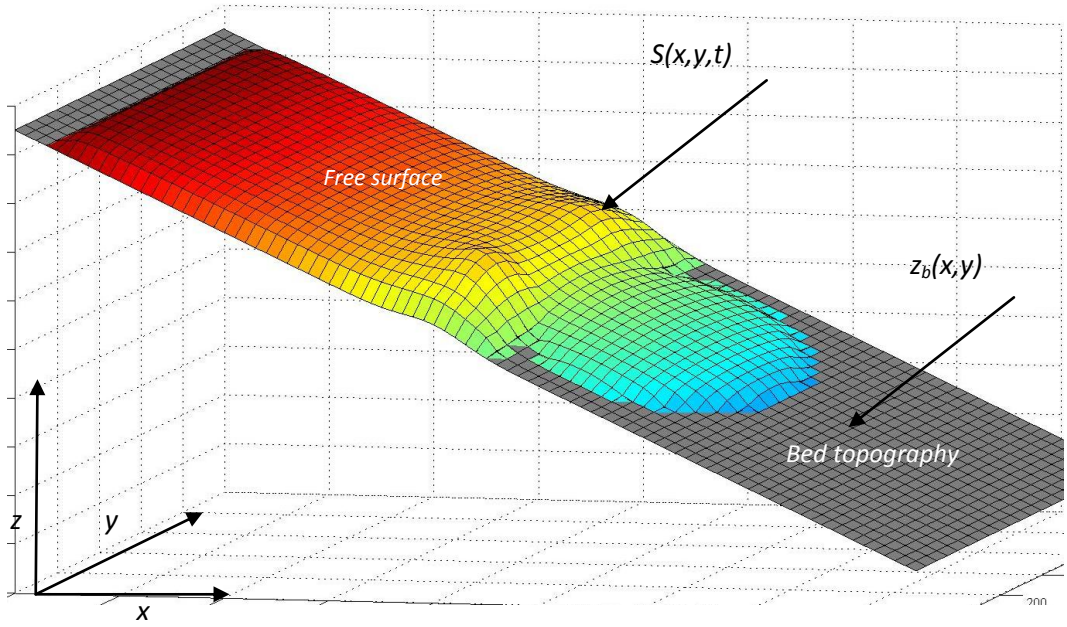


Figure 7. 1. Orientation of glacier flow

Starting from the general form of the conservation laws and assuming that the ice is an incompressible fluid, the conservation of mass and momentum equations (neglecting the inertia terms) can be written as

$$\nabla \cdot \mathbf{U} = 0, \tag{7. 1}$$

$$\nabla \cdot \tau + \rho g = 0, \tag{7. 2}$$

where $\mathbf{U}$ is the velocity vector, $\tau$ is the stress tensor, $\rho$ is ice density, $g$ is the acceleration due to gravity.

The stress tensor $\tau$ in equation (7.2) involves the deviatoric part $\tau'$ and the isotropic pressure $p$ according to:

$$\tau_{ij} = \tau'_{ij} + p\delta_{ij}, \tag{7. 3}$$

where the term $\delta_{ij} = \begin{cases} 0, & if \ i \neq j \\ 1, & if \ i = j \end{cases}$ is the Kronecker delta.

The stress and strain rate are related by

$$\tau_{ij} = 2\eta\dot{\varepsilon}_{ij}, \tag{7. 4}$$

where $\eta$ is the effective viscosity of the ice.

The strain-rate components $\dot{\varepsilon}_{ij}$ are defined from the velocity components as

$$\dot{\varepsilon}_{ij} = \frac{1}{2}\left(\frac{\partial u_i}{\partial j} + \frac{\partial u_j}{\partial i}\right), \quad i, j = x, y, z \tag{7. 5}$$

The constitutive relation that links the deviatoric stresses to the strain rate $\dot{\varepsilon}_{ij}$ is a power law which is referred to as the Glen's flow law. This relationship is given in equation (7.6).

$$\dot{\varepsilon}_{ij} = A(T)\tau_*^{n-1}\tau'_{ij} \quad , \quad \tau_*^2 = \frac{1}{2}\tau'_{ij}\,\tau'_{ij} \tag{7. 6}$$

where the term $A(T)$ is the Glen's law parameter which depends on the temperature and specifies the ice rheology.

The force balance in the three dimensions will result the Stokes Equations

$$\begin{aligned} &\frac{\partial \tau_{xx}}{\partial x} + \frac{\partial \tau_{xy}}{\partial y} + \frac{\partial \tau_{xz}}{\partial z} = 0 \\ &\frac{\partial \tau_{xy}}{\partial x} + \frac{\partial \tau_{yy}}{\partial y} + \frac{\partial \tau_{yz}}{\partial z} = 0 \\ &\frac{\partial \tau_{xz}}{\partial x} + \frac{\partial \tau_{yz}}{\partial y} + \frac{\partial \tau_{zz}}{\partial z} = \rho g \end{aligned} \tag{7. 7}$$

The downward flow of the glaciers is mainly due to the effect of gravity, however, in temperate glaciers (where the glacier bed is not dry) the basal sliding also contributes to the ice motion,[27]. In line with these equations, the boundary conditions are important to solve the problem under the actual constraints. The free surface which is the interface

between ice and air is considered as a stress-free surface where the kinematic equation/condition can be imposed for all points on the free surface.

$$\frac{\partial S}{\partial t} + u\frac{\partial S}{\partial x} + v\frac{\partial S}{\partial y} - w = a \tag{7. 8}$$

where $a$ is the ablation/accumulation rate on the glacier surface

The combination of equations (7.1 - 7.8) are known as the Stokes equations governing glacier flows which constitutes five unknowns (three terms of the velocity vector, one for isotropic pressure and another for the free surface elevation) and five partial differential equations.

Glacier flow models use either the full Stokes equations or its simplified versions based on different approximations. For instance, the SIA and the Higher-Order approximations are the simplified version of the full Stokes equation by employing restrictions and approximations. Higher-Order approximation equations are derived from the full Stokes equation after imposing two restrictions, see e.g.[102] . The first assumption constitutes imposing a hydrostatic pressure assumption/restriction on the z-momentum equation. The second assumption is by considering the horizontal gradients of the vertical velocity to be small compared to the vertical gradients of horizontal velocities. These restrictions simplify the Stokes equation into two coupled linear equations with two unknowns (the two horizontal velocities) called the Higher Order approximations which was reported by Pattyn in 2003 and the details can be found in [102]. On the other hand, imposing another sets of restrictions on the Stokes equations, result in other sets of governing equations, (SIA) for example), which is covered in detain in section 7.3.

Many respective solution methodologies, depending on the model equations, have been developed to simulate glacier flows. Full Stokes equations, for instance, can be solved by

using the finite element code Elmer, [103]. However, for this study, the SIA equations are used for the reconstruction of the glacier bedrock elevation, thus a detailed description of the solution methodology for the full Stokes and the Higher-Order approximation is not presented in this thesis.

## 7.3. The derivation of SIA equations

The shallow ice approximation was first introduced by Kolumban Hutter in 1983, [13]. The derivation of shallow ice approximation is explicitly given in [104]. To start with the derivation process, a vertical integration of the mass conservation equation (7.1) from the ice bottom to the free surface under the kinematic boundary condition equation (7.8) leads to:

$$\frac{\partial H}{\partial t} = a - \nabla_{\perp} \cdot q_{\perp} \tag{7. 9}$$

Equation (7.9) expresses the rate of change of the flow thickness $H$ as the difference between the ablation/accumulation rate $a$ and the horizontal divergence of the flux. This horizontal flux $q$ is obtained by vertical integration of the velocity over the ice thickness.

$$q_{\perp} = \int_{z_b}^{S} u_{\perp} \, dz \tag{7. 10}$$

In the formulation of the SIA equations, to express the shallowness, a key assumption is that the depth of the ice body is much smaller than the other length scales. This ratio, called the aspect ratio, can also be expressed by the characteristic velocities in the respective horizontal and vertical directions. However, this relationship only works well with land based ice sheets not for ice shelves, [19, 104, 105].

Let $\xi = H / L$ be the aspect ratio which expresses the shallowness of the ice sheet or glacier and it will serve as the main scaling parameter for the problem. It can also be noted that the smallness of $\xi$ compared to 1 is a prerequisite for the applicability of the Shallow

Ice approximation as it is based on a perturbation expansion under the form of series of powers of $\xi$, [104, 105].

In the derivation of the shallow ice equations, the non-dimensional forms of the variables are presented as follows.

$$\begin{aligned}
&(u,v) = [U_L](\tilde{u},\tilde{v});\ w = [U_H]\tilde{w},\\
&(x,y) = [L](\tilde{x},\tilde{y});\ z = [H]\tilde{z},\\
&(\tau'_{xz},\tau'_{yz},p) = \xi\rho g[H](\tilde{\tau}'_{xz},\tilde{\tau}'_{yz},\tilde{p}),\\
&(\tau'_{xx},\tau'_{yy},\tau'_{zz},\tau'_{xy}) = \xi^2\rho g[H](\tilde{\tau}'_{xx},\tilde{\tau}'_{yy},\tilde{\tau}'_{zz},\tilde{\tau}'_{xy}).
\end{aligned} \tag{7.11}$$

The choice of the scale parameters should then be consistent to comply with the above scale variables. For instance, the velocity terms are chosen such that the ratio $U_H/U_L$ is equal to the aspect ratio $\xi$. This is because the flow exhibits similar shallowness in the velocity field such that the ratio of typical vertical to horizontal velocities is of the same order as the aspect ratio. Similarly the deviatoric stress tensor terms are scaled in their relative importance. Implementing the above scaling, the scaled form of the Stokes equations can be given by

$$\begin{aligned}
&\xi^2\frac{\partial\tilde{\tau}'_{xx}}{\partial\tilde{x}} + \frac{\partial\tilde{p}}{\partial\tilde{x}} + \frac{\partial\tilde{\tau}'_{xy}}{\partial\tilde{y}} + \frac{\partial\tilde{\tau}'_{xz}}{\partial\tilde{z}} = 0,\\
&\xi^2\frac{\partial\tilde{\tau}'_{xy}}{\partial\tilde{x}} + \xi^2\frac{\partial\tilde{\tau}'_{yy}}{\partial\tilde{y}} + \frac{\partial\tilde{p}}{\partial\tilde{y}} + \frac{\partial\tilde{\tau}'_{yz}}{\partial\tilde{z}} = 0,\\
&\xi^2\frac{\partial\tilde{\tau}'_{xz}}{\partial\tilde{x}} + \xi^2\frac{\partial\tilde{\tau}'_{yz}}{\partial\tilde{y}} + \frac{\partial\tilde{\tau}'_{zz}}{\partial\tilde{z}} + \frac{\partial\tilde{p}}{\partial\tilde{z}} = 1.
\end{aligned} \tag{7.12}$$

For the second invariant of the deviatoric stress tensor, $\tau_* = \xi\rho g[H]\tilde{\tau}_*$ can be assumed and from the above expressions, the non-dimensional expression is given

$$\tilde{\tau}_* = \sqrt{\tilde{\tau}'^2_{xz} + \tilde{\tau}'^2_{yz} + \frac{1}{2}\xi^2(\tilde{\tau}'^2_{xx} + \tilde{\tau}'^2_{yy} + \tilde{\tau}'^2_{zz} + 2\tilde{\tau}'^2_{xy})} \tag{7.13}$$

For the two required strain rates, assuming that $\dot{\varepsilon}_{xz} = [U_L]/[H]\tilde{\dot{\varepsilon}}_{xz}$ and $\dot{\varepsilon}_{yz} = [U_L]/[H]\tilde{\dot{\varepsilon}}_{yz}$, the respective non-dimensional expressions of strain rate and stresses can be expressed as

$$\begin{aligned}
&\tilde{\dot{\varepsilon}}_{xz} = \frac{1}{2}\left(\frac{\partial \tilde{u}}{\partial \tilde{z}} + \xi^2 \frac{\partial \tilde{w}}{\partial \tilde{x}}\right),\ \tilde{\dot{\varepsilon}}_{yz} = \frac{1}{2}\left(\frac{\partial \tilde{v}}{\partial \tilde{z}} + \xi^2 \frac{\partial \tilde{w}}{\partial \tilde{y}}\right) \\
&\tilde{\tau}_{xz} = \eta\left(\frac{\partial \tilde{u}}{\partial \tilde{z}} + \xi^2 \frac{\partial \tilde{w}}{\partial \tilde{x}}\right),\ \tilde{\tau}_{yz} = \eta\left(\frac{\partial \tilde{v}}{\partial \tilde{z}} + \xi^2 \frac{\partial \tilde{w}}{\partial \tilde{y}}\right)
\end{aligned} \tag{7. 14}$$

To obtain the SIA equations, one can assume a small value of $\xi$ and neglect the terms involving $\xi^2$ or perform a perturbation expansion analysis to obtain identical equations. This can be done by assuming the aspect ratio $\xi$ as a small perturbation quantity such that the field variables of the above equations can be expanded under the form of power series of $\xi$. The perturbation expansion for any scalar $G$ can be written as $G = \sum_{p=0}^{\infty} G_{(p)} \xi^p$ in which the different $G_{(p)}$ terms are the terms of the $p^{th}$ power of $\xi$. It can be seen that the smaller the value of $\xi$, the most accurate the expansion. Thus, the Stokes equations can be rewritten after replacing all the variables by their respective power series. When the zeroth order of this power expansion is considered it leads to the SIA equations. The zeroth order system of equations is thus obtained by equating all terms of $G_{(0)}$ of the zeroth power of $\xi$ in the expanded equations. The scaled form of the Stokes equations thus gives

$$\begin{aligned}
&\frac{\partial \tilde{p}_{(0)}}{\partial \tilde{x}} + \frac{\partial \tilde{\tau}'_{xz(0)}}{\partial \tilde{z}} = 0, \\
&\frac{\partial \tilde{p}_{(0)}}{\partial \tilde{y}} + \frac{\partial \tilde{\tau}'_{yz(0)}}{\partial \tilde{z}} = 0, \\
&\frac{\partial \tilde{p}_{(0)}}{\partial \tilde{z}} - 1 = 0
\end{aligned} \tag{7. 15}$$

and for the $\tau_*$ and the required strain rate expressions:

$$\tilde{\tau}^2_{*(0)} = \tilde{\tau}'^2_{xz(0)} + \tilde{\tau}'^2_{yz(0)}; \quad \tilde{\dot{\varepsilon}}_{xz(0)} = \frac{1}{2}\left(\frac{\partial \tilde{u}_{(0)}}{\partial \tilde{z}}\right); \quad \tilde{\dot{\varepsilon}}_{yz(0)} = \frac{1}{2}\left(\frac{\partial \tilde{v}_{(0)}}{\partial \tilde{z}}\right) \tag{7. 16}$$

Where the subscript $(0)$ refers to the zeroth order term of each variable and these equations correspond to the scaled equations with a small value of $\xi$. For the study of bedrock reconstruction, the zeroth order SIA equations are employed, thus higher order equations are beyond the scope of this study and are not presented here.

The solutions of equation (7.15) are

$$\tau_{xz} = \rho g(z - S)\frac{\partial S}{\partial x}, \quad \tau_{yz} = \rho g(z - S)\frac{\partial S}{\partial y}, \quad p(z) = \rho g(z - S). \tag{7. 17}$$

and after accounting for the expressions of $\tau_*$ and the strain rates, the substitution of equation (7.16) leads to

$$\frac{\partial u_\perp}{\partial z} = -2A(\rho g)^3 (S - z)^3 \left|\nabla_\perp S\right|^2 \nabla_\perp S, \tag{7. 18}$$

Integrating the horizontal velocities from the bedrock to the free surface allows the expression of the velocity vector as a function of the free surface gradient and ice thickness. There resulting relationships is

$$u_\perp = \frac{1}{2} A(\rho g)^3 \left|\nabla_\perp S\right|^2 H^4 \nabla_\perp S, \tag{7. 19}$$

where $u_\perp = (u, v)$, $\nabla_\perp S = (\partial S/\partial x, \partial S/\partial y)$ and $\left|\nabla_\perp S\right|^2 = (\partial S/\partial x)^2 + (\partial S/\partial y)^2$. From the above relations it can be seen that the velocity is proportional to the ice thickness to the fourth power order.

Integrating the horizontal velocities from the ice bottom to the upper free surface according to equation (7.10) gives the horizontal flux as

$$q_\perp = \frac{2A(\rho g)^3}{5} \left|\nabla_\perp S\right|^2 H^5 \nabla_\perp S, \tag{7. 20}$$

Substituting equation (7.20) into equation (7.9) will result the zeroth order SIA equations.

$$\frac{\partial H}{\partial t}=\frac{\partial S}{\partial t}=a+\frac{2A(\rho g)^3}{5}\left[\frac{\partial}{\partial x}\left(D\frac{\partial S}{\partial x}\right)+\frac{\partial}{\partial y}\left(D\frac{\partial S}{\partial y}\right)\right],\ \text{with}\quad D=H^5|\nabla S|^2 . \qquad (7.\ 21)$$

Where $A$ is the Glen's law parameter, $S$ is the free surface elevation, $H$ is the depth of the flow and $a$ is the ablation accumulation rate which is variable in time and space.

Equation (7.21) constitutes the SIA equations. However, if the bottom sliding of a particular glacier has a significant effect on the flow dynamics, an additional term can be introduced to capture this effect. This is valid for the wet bed glaciers. Thus the general SIA equation, [13, 27, 106], is written as

$$\begin{aligned}&\frac{\partial H}{\partial t}=\frac{\partial S}{\partial t}=a+\frac{2(\rho g)^3}{5}\left[\frac{\partial}{\partial x}\left(D\frac{\partial S}{\partial x}\right)+\frac{\partial}{\partial y}\left(D\frac{\partial S}{\partial y}\right)\right],\\&D=H^3|\nabla S|^2\left(AH^2+\frac{5\beta A_s}{2}\right)\end{aligned} \qquad (7.\ 22)$$

Where $A_s$ a sliding rate factor, $\beta$ is a coeffeicnt to account sliding of dry and wet bed glaciers. $\beta=1$ will be assigned if the glacier has a wet bedrock while for dry bed glaciers $\beta=0$ will be assigned.

Equation (7.22) is a 2nd order partial differential equation which will be used for the reconstruction algorithm to reconstruct the bedrock topographic elevation from the known free surface data in the subsequent chapter.

# 8. One-dimensional glacier bedrock reconstruction from known free surface data: a direct approach

## Contents

## 8.1. Introduction

Glacier flow dynamics incorporate dependent and independent variables to express the flow in a mathematical form. From the glacier flow equations and physical interpretation of the flow, it can be seen that some glacier parameters depend to each other. For instance, a specific free surface profile or glacier flow velocity distribution is the manifestation of a particular bed topography and climatic condition. Typically, in glacier flow modelling, the free surface position is computed for a given bedrock shape. This problem constitutes the forward problem. The corresponding inverse problem is the identification of unknown glacier parameters from measured glacier data such as finding the glacier bedrock topography from the free surface velocity or free surface elevation as mentioned in the previous chapters. In [17] and references therein, it is shown that a volume-area scaling relation can be used to estimate the volume of glaciers and in-turn infer the ice thickness distribution using ice flow models. Thus, the inverse problem can be solved by incorporating these ice flow models, such as the SIA, Higher-Order approximation, and Full Stokes model (FS), with the known free surface data to estimate the unknown glacier flow parameters, see e.g. [17, 35] . Recent developments have demonstrated the limitations of SIA applicability while the higher order and FS models have wide range of applicability [19]. However, the ease of coding and the requirement of low computational cost make the SIA model a popular choice in glacier modelling, see e.g. [29-31]. To solve SIA-based governing equation, different numerical approaches have been proposed: explicit finite difference scheme [29], semi implicit scheme [32], alternating-direction-implicit (ADI) method [33], or finite volume scheme [34]. In relation to the inverse problem, Farinotti et al. [17] presented a method based on mass turnover and principle of ice flow mechanics to infer the ice volume and ice thickness distribution of Alpine glaciers from a known surface topography. They reported that the ice thickness can be

reproduced with an average deviation of 25% from the measured ones. Additionally see e.g. [17, 35-37] for more on inverse problems in glacier flows.

The one –dimensional inverse problem model presented here requires prior knowledge of free surface elevation and ablation/accumulation data of the glacier in order to infer its bedrock. Satellite and aerial based remote sensing techniques combined with DEMs provide glacier free surface elevation. The mass balance components (ablation and accumulation) can also be measured using a geodetic method by repeated glacier surveys with the help of airborne and radar based techniques [21, 107]. The model presented here uses the SIA equation to directly infer the glacier bedrock from the known free surface elevation and ablation/accumulation rates. Similar techniques on the different context have been applied to thin film flows to reconstruct the substrate topography [50-52, 108] from measurable quantities. Similar approaches as Part I, direct numerical and pseudo-analytical are exploited to tackle this inverse problem where the governing equation is directly solved for the unknown parameter (bedrock elevation data) of the inverse problem.

In this part of the study, analytical and numerical techniques to identify the bedrock topography of glaciers from a known free surface elevation given the ablation/accumulation distribution are presented. Section 8.2 presents the governing equations followed by the analysis of the forward problem using the explicit finite difference scheme in section 8.3. In section 8.4, the analytical and numerical reconstruction techniques with the results and the corresponding discussions of the benchmark test cases are presented. Lastly the concluding remarks of this chapter are presented in section 8.5.

## 8.2. Governing equations and the forward problem

The dynamics of glacier flow is a complex phenomenon because it depends on rapidly changing climatic conditions and non-climatic parameters. Bedrock topography, temperature distribution, and ablation/ accumulation distribution are some important parameters as mentioned before. The SIA equation (7.22) rewritten for one-dimensional glacier flow is used in the following.

Consider a glacier flow in one dimension as shown in Figure 1.

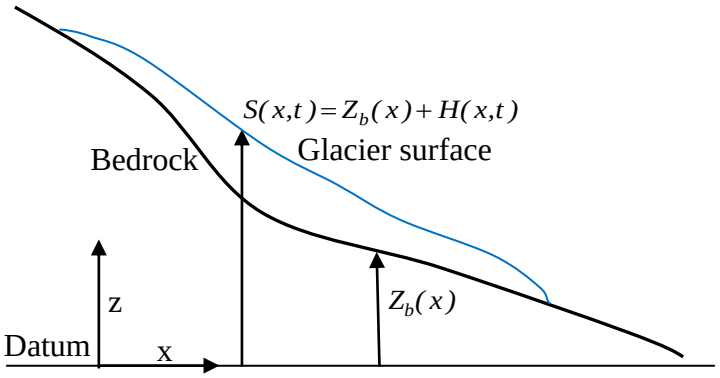


Figure 8.1: Sketch and notations of the problem considered

The SIA equation in one dimension can be written as

$$\frac{\partial H}{\partial t} = a + \frac{2(\rho g)^3}{5}\frac{\partial}{\partial x}\left(D\frac{\partial S}{\partial x}\right) \tag{8.1}$$

where $D = H^3|\nabla S|^2\left(AH^2 + \frac{5\beta A_s}{2}\right)$, and $S = Z_b + H$

The diffusion coefficient $D$ depends on the existence of sliding $\beta = 1$ or not $\beta = 0$.

Typical values of the constants incorporated in this study are summarized in Table 8.1.

| **Parameter** | **Values** |
|---|---|
| Glen's Law Parameter, $A$ | 4.1x 10-17 $pas^{-3}$ $a^{-1}$ |
| Density, $\rho$ | 880kg/$m^3$ |
| Acceleration due to gravity, g | 9.81m/$s^2$ |
| Sliding coefficient, $A_s$ | 5x 10-14 $m^8$ $N^{-3}$ $a^{-1}$ |

Table 8.1: Typical values of constants used in the calculations, [30]

For the one-dimensional glacier flow modelling it is assumed that, the effect of the flow in the transverse direction is negligible.

To solve the forward problem, equation (8.1) is discretized explicitly in time. The spatial discretization is based on a central finite difference scheme. A staggered grid in space is used to allow the computation of $D$ at grid points that are offset from those where the ice surface (S) is defined. Thus, the terms in equation (8.1) are discretized as follows and all the terms are calculated at the same old time step.

$$\frac{\partial}{\partial x}\left(D\frac{\partial S}{\partial x}\right)=\frac{\left(D\frac{\partial S}{\partial x}\right)_{i+\frac{1}{2}}-\left(D\frac{\partial S}{\partial x}\right)_{i-\frac{1}{2}}}{\Delta x}$$

$$\left(D\frac{\partial S}{\partial x}\right)_{i+\frac{1}{2}}=\left(\frac{D_{i+1}+D_i}{2}\right)\left(\frac{S_{i+1}-S_i}{\Delta x}\right);\quad \left(D\frac{\partial S}{\partial x}\right)_{i-\frac{1}{2}}=\left(\frac{D_i+D_{i-1}}{2}\right)\left(\frac{S_i-S_{i-1}}{\Delta x}\right) \qquad (8.2)$$

$$D_i=H_i^3\left|\frac{S_{i+1}-S_{i-1}}{2\Delta x}\right|^2\left(AH_i{}^2+\frac{5\beta A_s}{2}\right)$$

Here, $\Delta x$ is the spatial increment.

Therefore, the final discretized equation will be

$$H_i^{n+1}=H_i^n+\Delta t a_i+\frac{\Delta t}{2\Delta x}\frac{2(\rho g)^3}{5}\left\{\left(D_{i+1}^n+D_i^n\right)\left(\frac{S_{i+1}^n-S_i^n}{\Delta x}\right)-\left(D_i^n+D_{i-1}^n\right)\left(\frac{S_i^n-S_{i-1}^n}{\Delta x}\right)\right\} \qquad (8.3)$$

This discretized equation along with the initial and boundary conditions is solved iteratively using a MATLAB script until a steady state result is obtained. The steady state represents the balance between the accumulation above the equilibrium line and the ablation below the equilibrium line due to continuous flow of ice from the accumulation to the ablation zones. The value of the depth at the current time step is estimated from the

old time step values which are incorporated in the right hand side of this equation. Equation (8.3) along with a given bedrock topographic elevation $z$ will be used to determine the glacier surface elevation. During each time stem $S_i = Z_{bi} + H_i$ will be used to update the surface elevation values.

There are two forms of initial conditions which can be considered for glacier flow modelling: a zero ice thickness and a known ice thickness distribution in the computational domain. However, if the glacier eventually reaches a steady condition, the initial condition ceases to affect the final results. Therefore, since only steady glaciers considered here, a zero ice thickness is considered as an initial condition for canonical test cases. The boundary conditions are defined in such a way that the glacier thickness at the land-ice interface including the snout is zero. However, for symmetrical glaciers zero flux boundary condition can be implemented at the symmetry plane. In this work, a zero glacier thickness at the far ends of the computational domain is implemented. The depth is explicitly forced to remain positive by setting the depth to a zero value if a negative value occurs. This is standard practice in solving the SIA, see e.g. [106].

The forward problem approach is tested against a benchmark test case given in [30] and on realistic glaciers: Glacier de Saint-Sorlin and Gries glacier presented by Le Meur & Vincent [106] and Piccasso et al. [109], respectively. In addition to these test cases idealized test cases are formulated for a glacier flow over an inclined bed involving a bump and depression for future reference of testing the inverse problem solution procedure. In test cases I and II given below, the effect of sliding is neglected and thus the value of $A_s$ is considered as zero.

***Test case I: Glacier evolution on an inclined flat bed***

In this test case, a flat bed with constant slope but with a variable accumulation/ablation rate is considered in order to investigate its role on the evolution of the glacier. The spatially varying bedrock geometry is given by

$$z_b(x) = \alpha(x_l - x), \tag{8.4}$$

Where $\alpha$ is the bedrock slope, $x_l = 4300$m is the maximum length in x-direction, and bedrock topographic elevation $z_b(x = x_l) = 0$.

The ablation/accumulation rate varies spatially along the length of the computational domain. It is given by

$$a(x) = \begin{cases} a_0\left(1 - \dfrac{300 - x}{100}\right) & if\ x \le 300 \\ a_0\left(\dfrac{2200 - x}{1900}\right) & if\ x \ge 300 \end{cases} \tag{8.5}$$

where $a_0$ is the maximum value of the accumulation/ablation rate in meters of water equivalent column per annum (m w.e. $a^{-1}$).

The first part of this test case consists in assessing the effect of the bed slope for a constant value of $a_0 = 0.5$. Tests are carried out for values of $\alpha$ ranging from 0.1 and 0.5 with interval of 0.1 and the results are shown in Figure 8.2. The resolution of the computational mesh is $\Delta x = 50$ m and $\Delta t = 0.1$ years. As shown in Figure 8.2 the glacier thickness decreases with the bed slope meaning that the steeper the slope the thinner the glacier as expected.

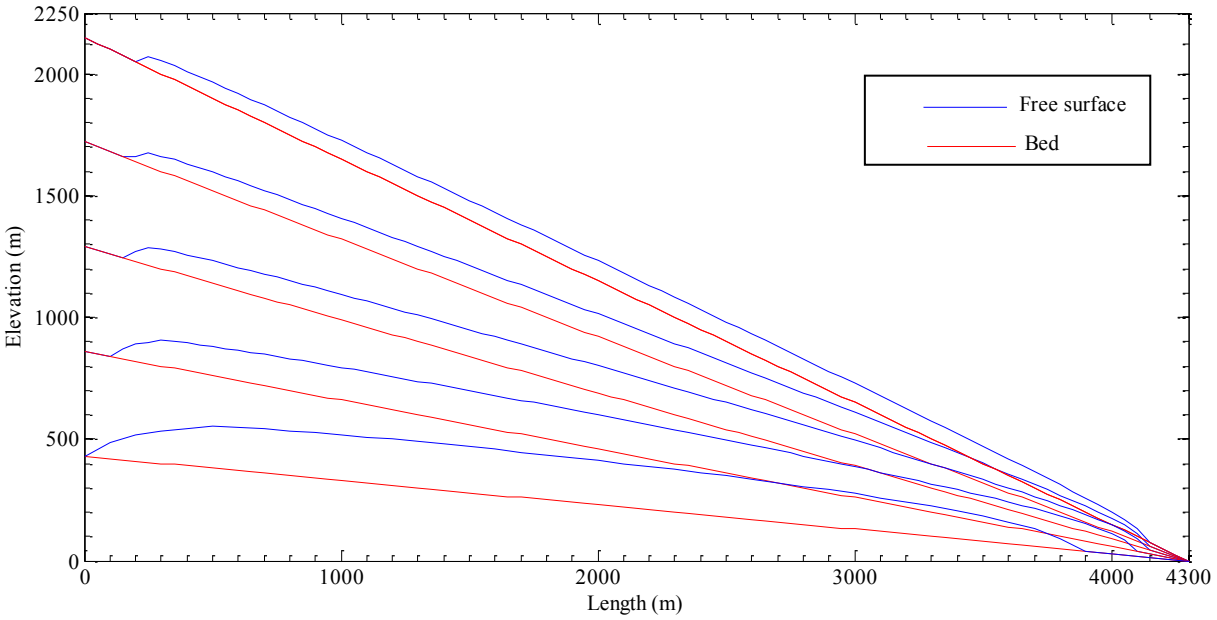


Figure 8.2: Glacier evolutions on a flat bed of different slope for a given accumulation/ablation distribution [m w.e.a$^{-1}$]

On the other hand, a test with a variable value of $a_0$ = 0.5, 1.0, and 2.0 on a fixed slope bed of $\alpha$ = 0.4 is conducted. Likewise, there is a direct relationship between the accumulation variable $a_0$ and the glacier thickness. As expected, larger values of $a_0$ result in a thicker glacier as shown in Figure 8.3.

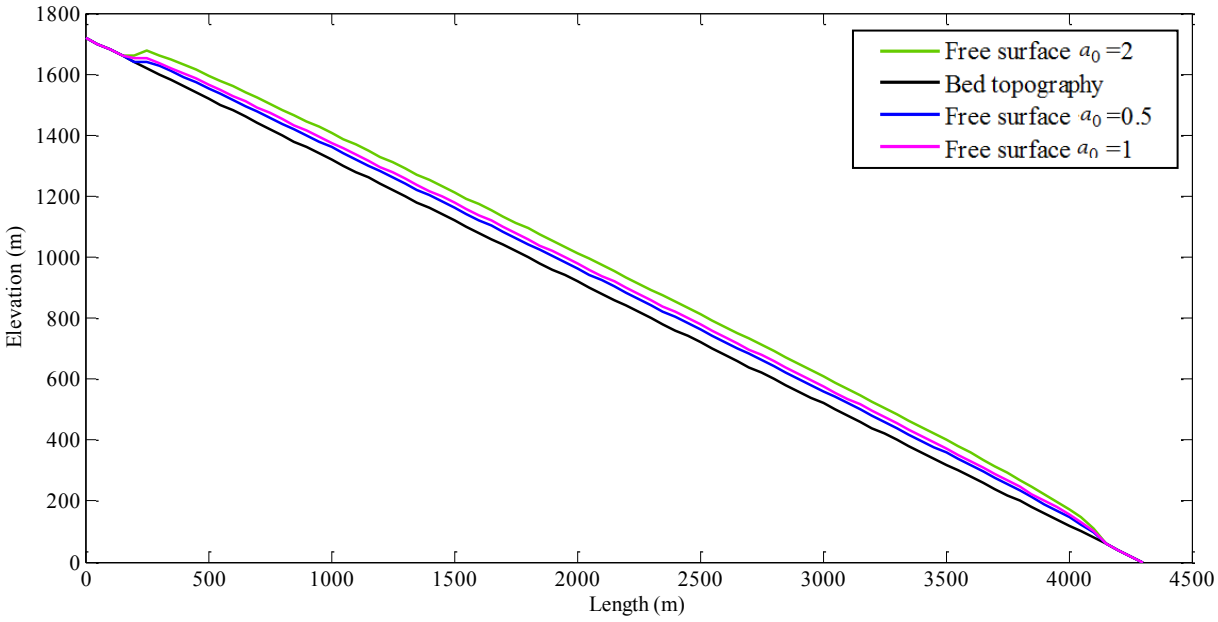


Figure 8.3: Glacier evolution on an inclined bedrock for variable $a_0$

These results are in a good visual agreement with the results reported in [30]. Thus the algorithm is capable of modelling the evolution of the glacier for a known bedrock elevation and flow parameters in the cases of variable slope bedrock and ablation/accumulation rate.

***Test case II: Glacier evolution on an inclined bed with a bump/depression***

To further investigate the effect of topographical features on the evolution of glaciers, a bump and a depression are introduced in the flat bedrock profile. The free surface profile obtained for this "idealized" test case will be used in the next section to establish the validity of the bedrock reconstruction algorithms. We consider the bump and depression cases separately as described below.

a. Theoretically, the left hand side of the bump hinders the glacier flow as it introduces positive slope and the right hand side facilitates glacier flow towards the downstream direction as it constitutes a steepened bed in the downward

direction. The introduced bump is a differentiable function of $x$ to allow an unambiguous evaluation of the gradients. The bed topography function is defined as

$$z_b(x) = z_0 - \alpha x + \gamma \exp\left(-\frac{(x-2000)^2}{\delta^2}\right) \tag{8.6}$$

where $z_0$ = 1720, $\alpha$ = 0.4, $\gamma$=100 $\delta$ = 200 are constants. The value of $\gamma$ and $\delta$ indicates the extent of the bump height and the bump width respectively.

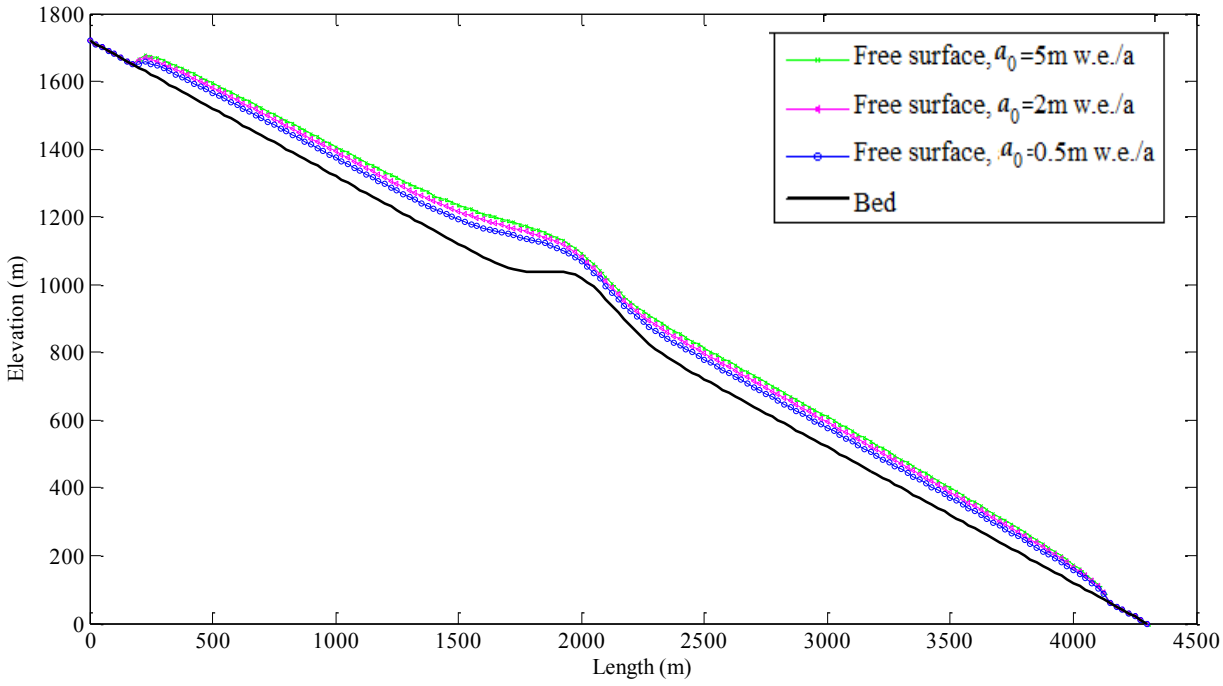


Figure 8.4: Glacier evolution with variable $a_0$ on an inclined bed with a bump

As can be seen in Figure 8.4, the existence of the bump affects the upstream and downstream free surface elevation. It can also clearly be seen from the depth distribution function that the maximum depth is upstream of the centre of the bump while a depression is visible downstream of the bump, see Figure 8.5.

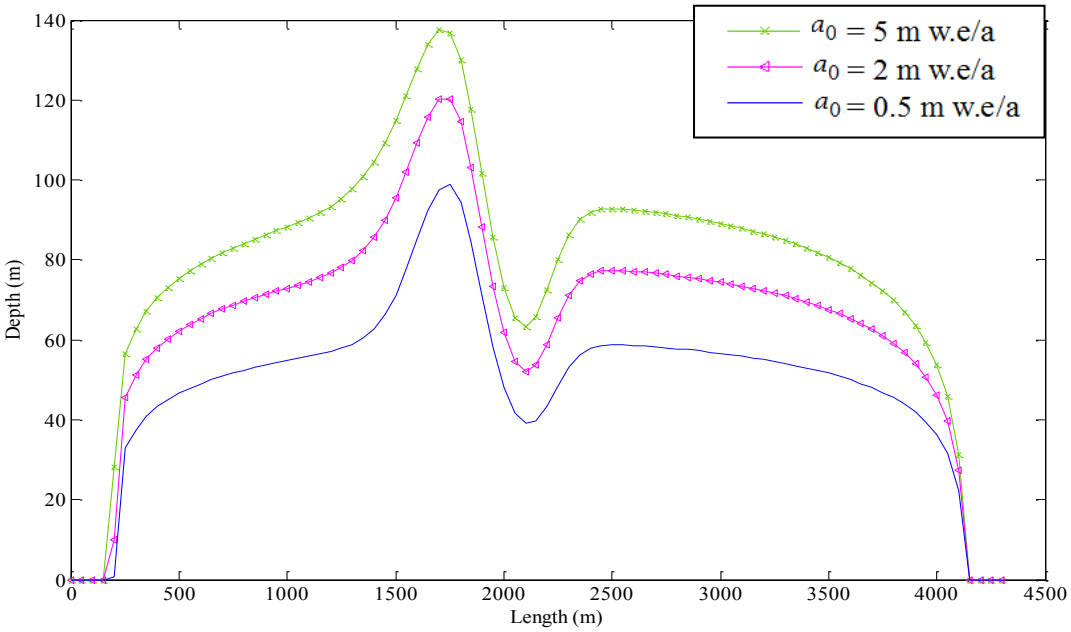


Figure 8.5: Glacier depth distribution in the case of a bump on an inclined bedrock

b. Unlike the bump case, there is a sharp downward gradient upstream of the depression which creates a thinner glacier. The effect can be easily seen on the glacier surface profile in Figure 8.7. The bed profile considered for the numerical calculation is given by equation (8.7) with similar constants to those in the bump test case.

$$z_b(x) = z_0 - \alpha x - \gamma \exp\left(-\frac{(x-2000)^2}{\delta^2}\right). \tag{8.7}$$

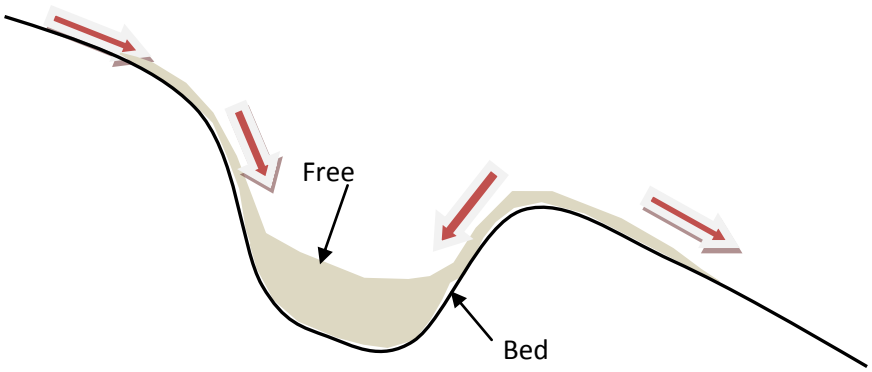


Figure 8.6: Directions of ice movement in the immediate vicinity of a depression

In the depression, more ice accumulates creating larger glacier thickness because of the fact that the sides of the trough create bed bounds which push the glacier towards the centre of the hump. Figure 8.6 shows the glacier flow directions.

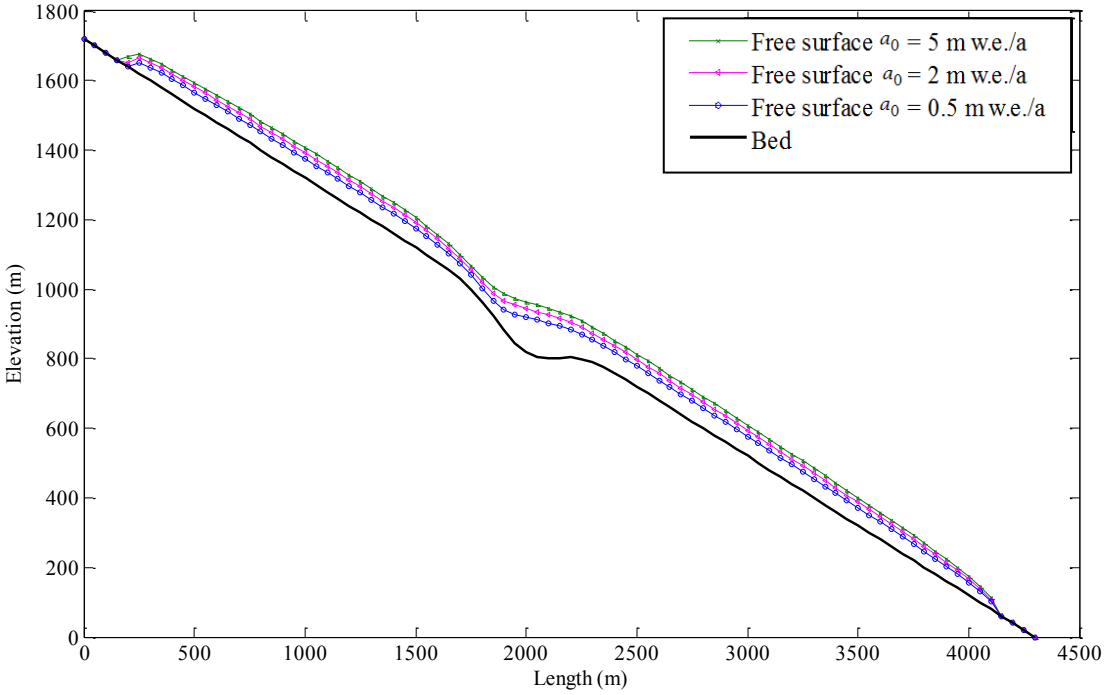


Figure 8.7: Glacier evolution with variable $a_0$ on an inclined bed with a depression

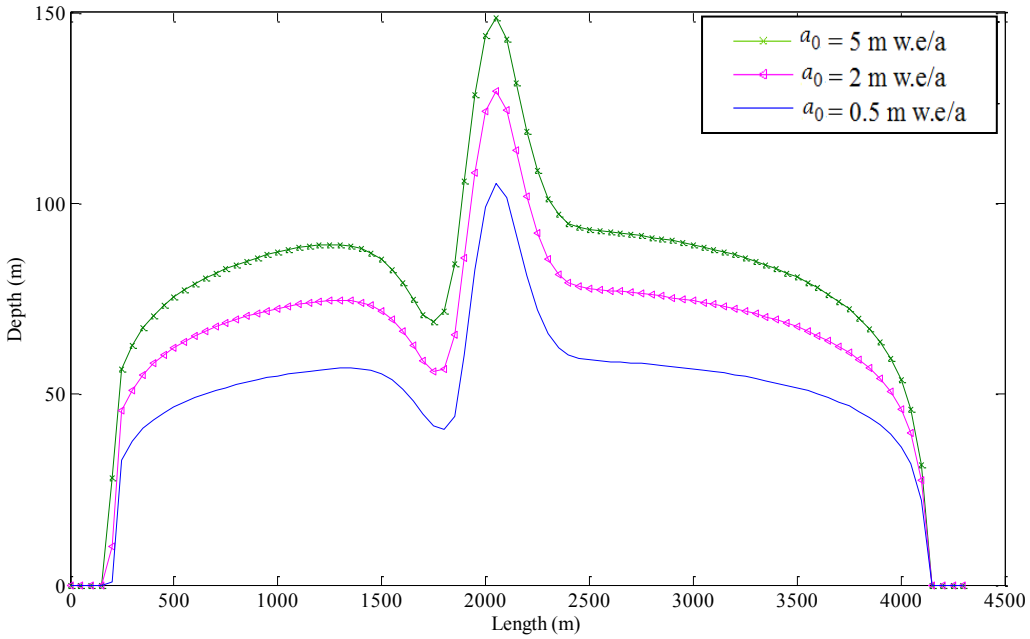


Figure 8.8: Glacier depth distributions in the case of a depression on an inclined bedrock

As can be seen in Figure 8.7 and 8.8, the maximum depth is in the immediate vicinity of the centre of the depression, a result consistent with the directions of the glacier flow shown in Figure 8.6. This result shows that the steeper the gradient the thinner the glacier. As mentioned in an earlier section, the depth of the flow not only depends on the slope of the bed but also on the ablation/accumulation distribution.

The existence of the bump or depression in the bedrock topography affects the local glacier surface profile. This effect is pronounced in the immediate vicinity of the downstream and upstream part of the local change of the bed profile. It is thus expected that this "signature" can be used to be able to reconstruct the bedrock.

***Test case III: Longitudinal profile glacier de Saint-Sorlin, France***

The glacier de Saint-Sorlin is a crique type small glacier ($3km^2$) situated in the Grandes Rousses range in the French Alps at an altitude ranging from 3300m to 2500m, [106]. It has a typical small aspect ratio which makes it suitable for the applicability of the SIA equations. Mass balance data from direct glaciological measurements is available for the period of 1957-99. The seasonal and annually averaged ablation/accumulation distribution along the flow line is reported by Vincent and others [110]. Detailed description of the glacier can be found in the aforementioned references [106] and [110].

In this test case, unlike the above test cases, a sliding factor $A_s = 15 \times 10^{-14} N^{-3} a^{-1}$ is introduced to account for sliding on the glacier evolution. The seasonal distribution of ablation/accumulation rate is reported in [106] and [110]. However, the annually averaged distribution of the mass balance with additional extrapolation is used for the numerical calculation. The average ablation/accumulation distribution is approximated in equation (8.8) after fitting a polynomial function.

$$a(x) = \begin{cases} 2.6\times10^{-10}x^3 - 1.1\times10^{-6}x^2 + 1.1\times10^{-4}x + 1.2434 & \text{if } x \le 2550 \\ -1.8787 - 1.10\times10^{-3}(x - 2550) & \text{otherwise} \end{cases} \quad (8.8)$$

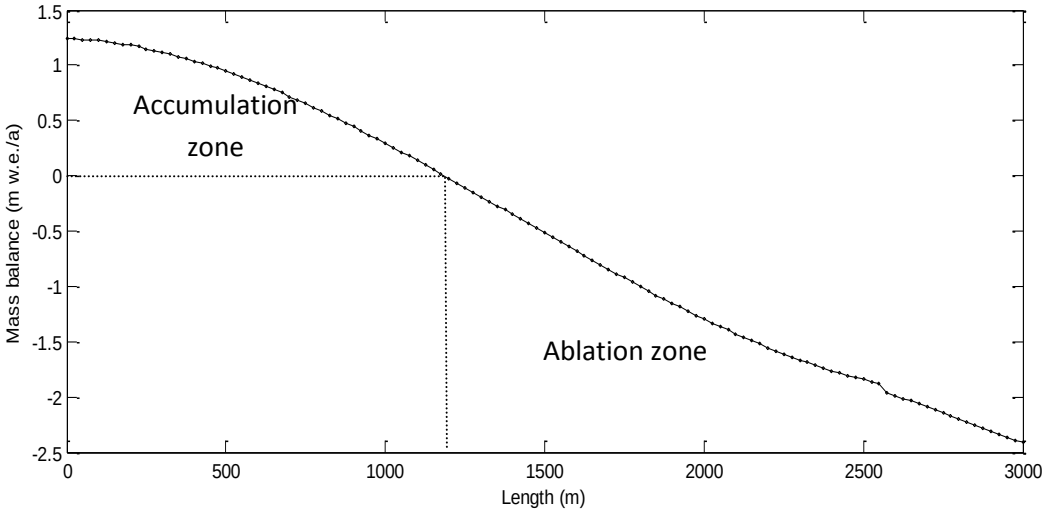


Figure 8.9: Annually averaged ablation/accumulation distribution

The modelling results shown in the Figure 8.10 are with 10 cm, 20 cm, 30 cm and 50 cm w.e.$a^{-1}$ accumulation on top of the ablation/accumulation distribution given by equation (8.8). The results are in a good visual agreement with the results presented in [106].

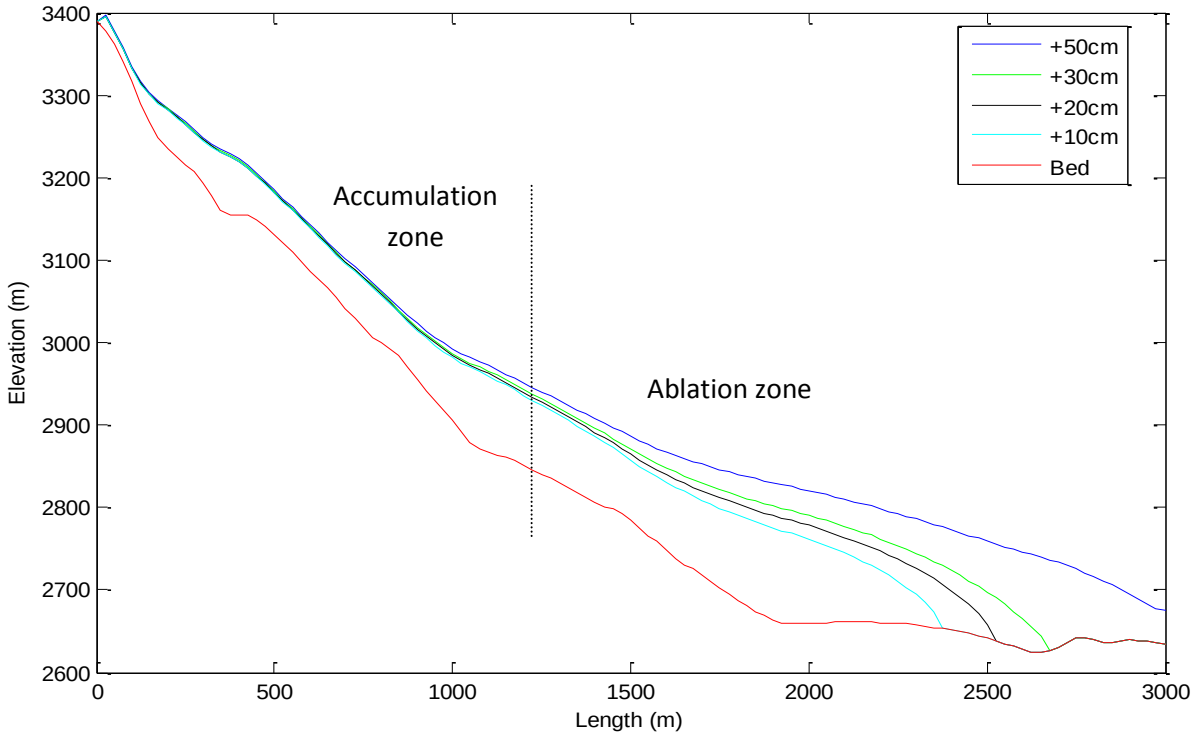


Figure 8.10: Glacier de Saint Sorlin bedrock and free surface

As can be seen in Figure 8.10, the glacier thickness increases with an increase in the accumulation of ice on the surface of the glacier and more ice accumulates on the flatter part of the bed. An interesting feature which can be seen in Figure 8.10, is that on the downstream side of the glacier, the ablation is balanced by glacier flow from upstream. In addition to the flow due to deformation, sliding contributes to maintain a thicker glacier front towards the ablation zone.

***Test case IV: Numerical simulation of Gries glacier, Switzerland***

The Gries glacier is a temperate valley glacier situated in the Lepontine Alps in the canton of Valais in Switzerland [101]. Mass balance measurements started in 1961 and topographic maps exist for various years. The glacier bedrock and free surface topographic elevation for the year 1961 and 1991 are reported in [109]. This test case is

important in order to assess the capability of the numerical technique to model unsteady glacier flows.

Measured ablation/accumulation distribution as a function of time is available for the periods of calculation which can be found in [111]. In the following the 1961 glacier is considered as the initial condition along with known ablation/accumulation rates to predict the 1991 and 2021 glacier shapes numerically. The comparison of the results is shown in Figure 8.11.

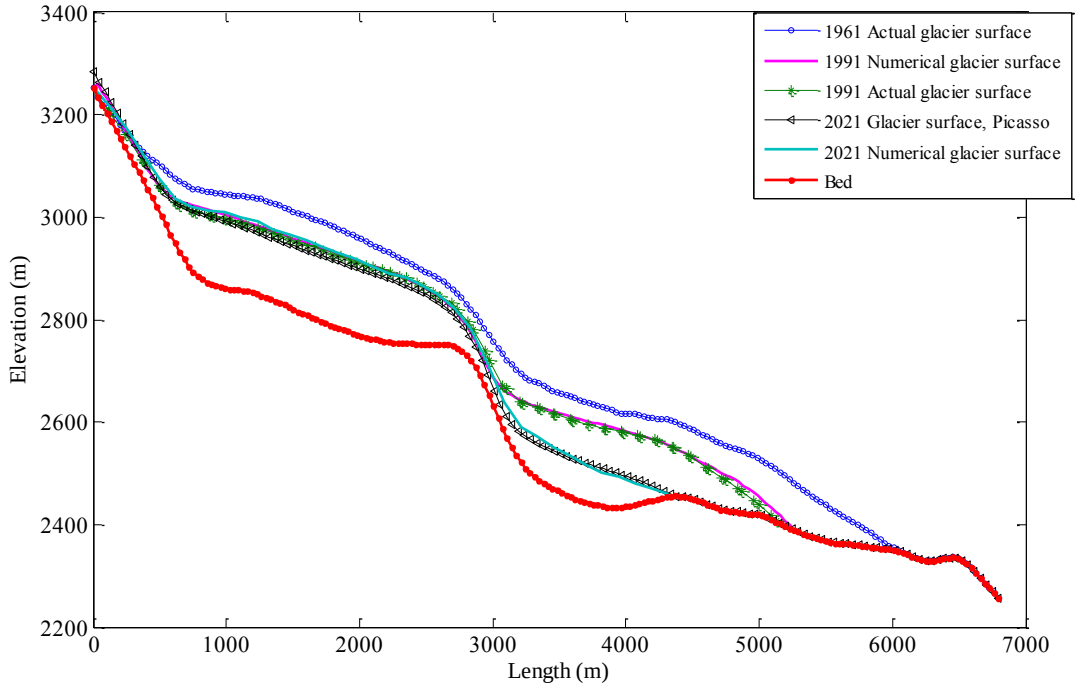


Figure 8.11: Gries glacier bedrock and surface elevation at different times. Comparison of actual and predicted profiles

As can be inferred from Figure 8.11, the 1991 glacier shape predicted by the numerical solution is in very good agreement with the actual measured glacier shape. Additionally, the 2021 glacier shape predicted is also in good agreement with the results published by Picasso and others, [109].

These results show that the numerical solution approach implemented for the forward problem is capable of solving steady and unsteady glacier flows for given steady or transient ablation/accumulation rates along with the initial and boundary conditions.

## 8.3. The inverse problem

The inverse problem consists of inferring the bedrock topographic elevation from a known glacier free surface elevation and a known ablation/accumulation distribution over the entire glacier. Many glaciers have been studied for many decades and there is sufficient data on the glacier free surface elevation and the ablation/accumulation function. Thus, it is possible to use particular data of a specific glacier in order to infer its bedrock. Like the forward problem the same SIA equation is used for the inverse problem analysis. In the following, two approaches are presented, the analytical and numerical, to infer the glacier bedrock topography.

### *8.3.1. Analytical reconstruction approach*

The analytical approach presented is based on the steady shallow ice approximation equations. Consider a known glacier surface elevation $S(x)$. Equation (8.1) can be rewritten in the following form

$$\frac{\partial H}{\partial t} = a + \frac{2(\rho g)^3}{5}\frac{\partial}{\partial x}(TM), \tag{8.9}$$

where $T = H^3\left(AH^2 + \frac{5}{2}\alpha A_s\right)$ . The variable $M = \frac{\partial s}{\partial x}\left|\frac{\partial s}{\partial x}\right|^2$ is known from the given glacier surface $S(x)$ . To solve the inverse problem, the knowledge of ablation/accumulation data, glacier free surface elevation data and its first derivative are the prerequisites . For the analytical solution approach, steady state frozen bed glaciers,

where no sliding exists, are considered. Thus, the sliding effect in equation (8.9) is neglected thus equation (8.9) simplifies to

$$0 = a + \frac{2A(\rho g)^3}{5}\frac{\partial}{\partial x}\left(H^5 M\right), \tag{8.10}$$

which can be solved analytically by

$$H = \left[ C_0 - \int_0^x a dx \left( \frac{2A(\rho g)^3}{5} M \right)^{-1} \right]^{1/5} \tag{8.11}$$

where $C_0 = \frac{2A(\rho g)^3}{5} H_0{}^5 M_0{}^2 + \int_0^{x_0} a dx$

is the constant of integration with $H_0 = H(x_0)$ and $M_0 = M(x_0)$. Although the inverse problem has an analytical solution it requires the knowledge of the value $H_0$ which corresponds to the glacier thickness at an arbitrary point. In some cases, however, this is impossible and the analytical solution cannot be employed.

The analytical solution using Equation (8.11) with a known $H_0$ is produced for test case-II in order to test the capability of the solution approach to reconstruct the bedrock constituting a bump and depression. The known glacier surface elevation data of test case-II of the forward problem is used as input parameter and the results of the reconstructed bedrock are shown in Figures 8.12 (c) and (d). The respective results of the reconstructed glacier thickness are shown in Figures 8.12 (a) and (b). Since the expression in equation (8.11) is an analytical solution of equation (8.10), a perfect agreement between the reconstructed bed and the actual bed is expected and it is confirmed in Figure 8.12.

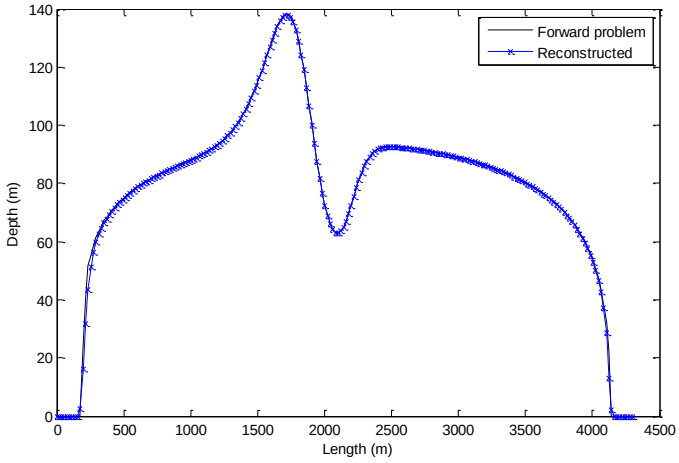


(a)

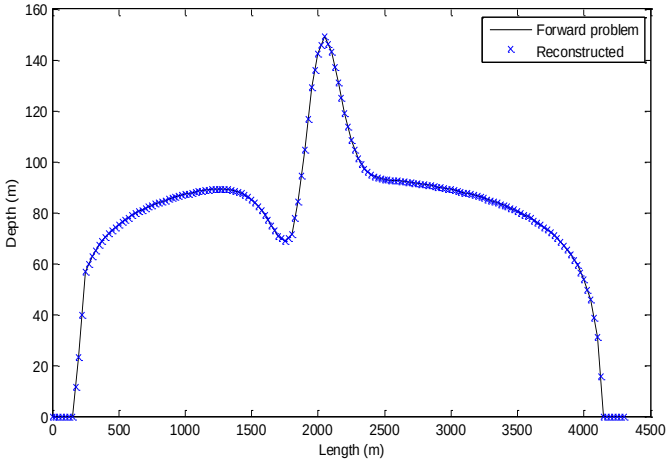


(b)

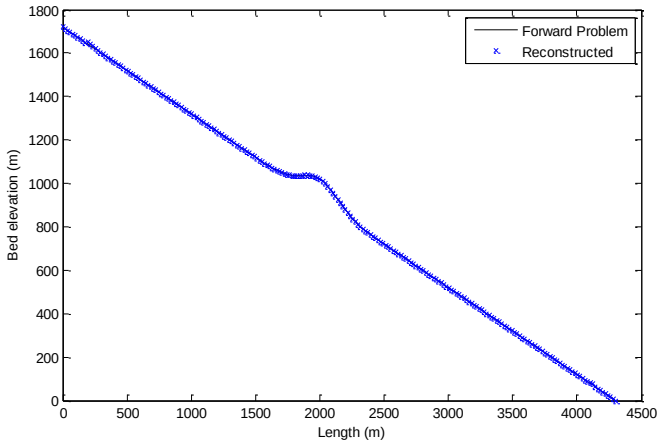


(c)

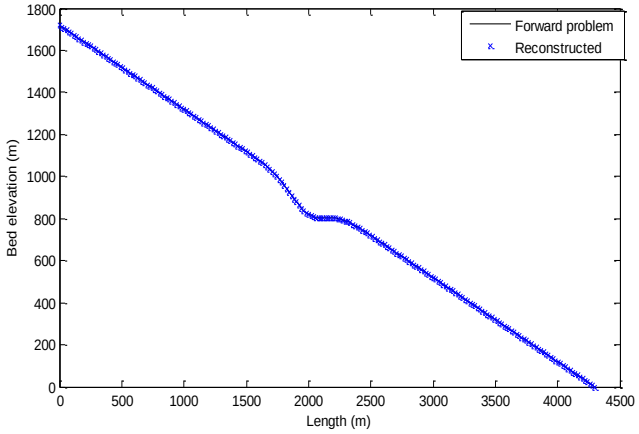


(d)

Figure 8.12: Analytical reconstruction of the glacier thickness (a), (b) and the bedrock (c), (d) for a given glacier shape. The other parameters are $\alpha = 0.4$ and $a_0 = 5\text{w.e.a}^{-1}$. The solid lines show the thickness of the glacier and the bedrock shape whereas the cross lines show the reconstructed bedrock profile.

### *8.3.2. The numerical approach*

In addition to the analytical solution, a numerical scheme is introduced to solve the governing equation of the glacier flows for the inverse problem. Again, the underlying idea is to solve the SIA directly for the unknown parameter. In other words, the inverse problem is governed by an explicit partial differential equation which can be solved using a direct solution approach analogous to the inverse problem of shallow water flows solved

in the previous chapters of the thesis. In comparison to the code developed for the forward problem, the inverse problem solution requires an implicit scheme because the explicit method is unstable in this case. Following the notation of the inverse analytical problem, the spatial derivative is discretized implicitly as follows:

$$\frac{\partial}{\partial x}(TM) = \frac{(TM)_{i+1/2}^{n+1} - (TM)_{i-1/2}^{n+1}}{\Delta x}, \tag{8.12}$$

Therefore, a nonlinear system of equations will be solved at each time step

$$\frac{H_{i+1}^{n+1} - H_{i+1}^{n}}{\Delta t} - = \frac{(TM)_{i+1/2}^{n+1} - (TM)_{i-1/2}^{n+1}}{\Delta x}. \tag{8.13}$$

The system of algebraic equations is solved numerically which usually converges within 10 iterations. It has to be noted that although an implicit method used, the steep gradient at the front and the back of the glacier leads to spurious oscillations. To avoid these oscillations a smoothing technique is applied at every time step. This is implemented by moving average smoothing over 3 to 5 grid points close to the front and to the back of the glacier.

To test this numerical algorithm, the known data from the forward problem is taken to reconstruct the bedrock shape of the glacier. Two examples are presented based on the bump and depression bedrock structures from Figures 8.4 and 8.7. A time step of $\Delta t = 1$a (year) and a spatial resolution of $\Delta x = 19.63$m are used. Figures 13 (a) and (b) show the reconstruction of the glacier thickness at different times (20a, 40a, 60a, 100a) and Figures 13 (c) and (d) show the final reconstructed bedrock shapes. It can be noted that the reconstruction perfectly matches the actual glacier bedrock elevation data.

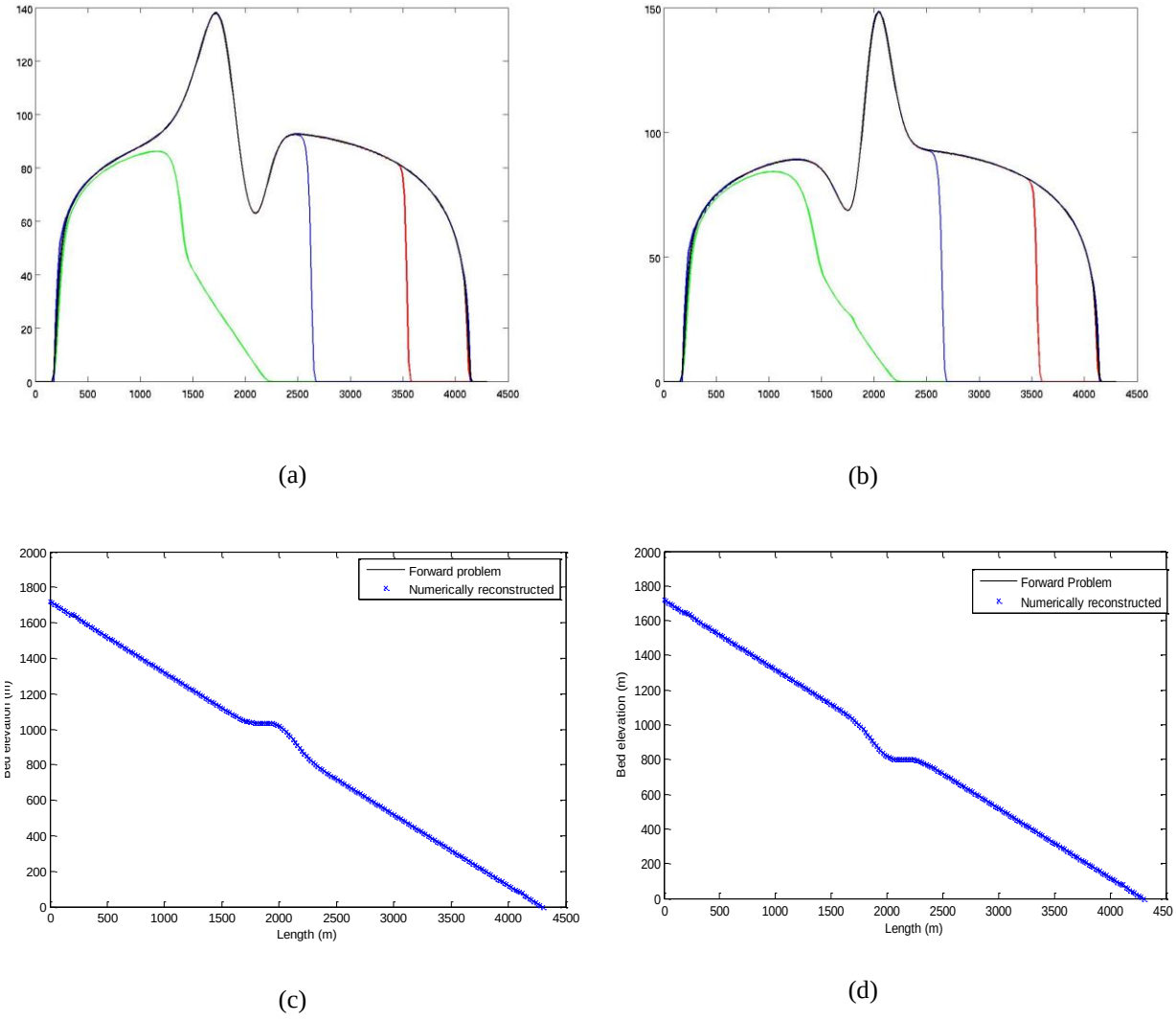


Figure 8.13: Reconstruction with the implicit numerical scheme. (a) and (b) show the intermediate depths of the glacier in the bedrock reconstruction process at different time steps 20, 40, 60 and 100 years. (c) and (d) compare the reconstructed with the initial bedrock for the cases of a bump and a depression, respectively.

### *Reconstruction based on experimental/actual glaciers*

Ultimately the value of the proposed approach is best tested on actual glacier data. This can be done by considering the topographical data of well studied glaciers. The analytical solution methodology, as mentioned above, requires additional depth data at an arbitrary point and neglects the effect of sliding which limits the reconstruction process. However, the numerical approach can accommodate the effect of sliding and does not require an

arbitrary glacier depth. Thus, in the following test cases the numerical approach is presented to infer the bedrock of Glacier de Saint-Sorlin and Gries Glacier.

The reconstruction of the bedrock elevation for test case-III is based on our forward problem analysis of Glacier de Saint-Sorlin. The resulting free surface from the forward problem along with the ablation/accumulation values are used to reconstruct the bedrock. A comparison of the reconstructed and the actual bedrock forms for this test case is presented in Figure 14.

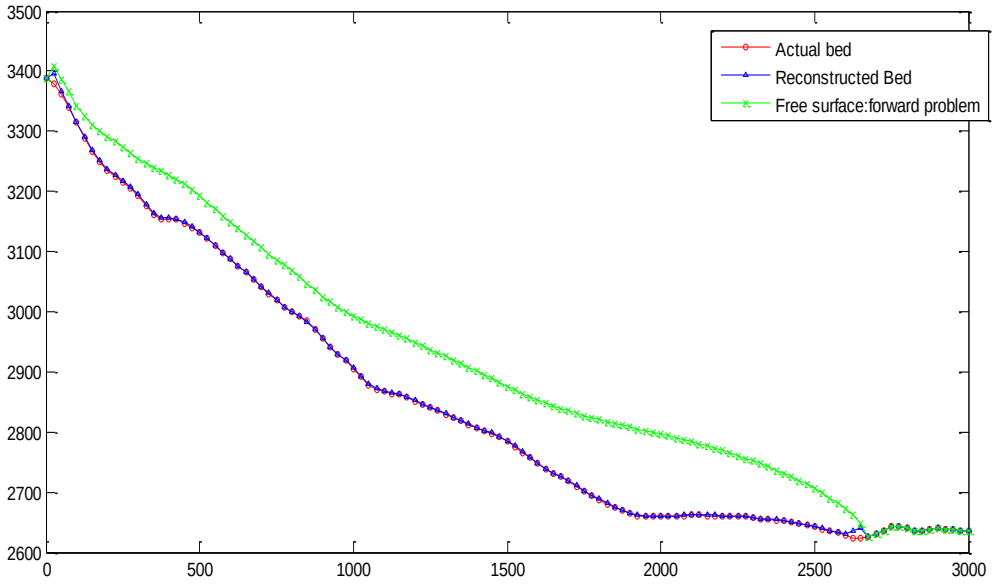


Figure 8.14: Comparison of reconstructed and actual bedrock forms of Glacier de Saint Sorlin

The results show good agreement between the reconstructed and actual bed forms. When, on the other hand, an actual free surface profile and average ablation/accumulation coefficient profiles are considered over the computational period, a considerable deviation from the actual bed topography was observed. This is due to the lack of accuracy of the ablation/accumulation profiles. The effect of ablation/accumulation coefficients, as in the case of the forward problem, is paramount in the inverse problem as well.

The other test case considered here is the reconstruction of bedrock topography of Gries Glacier along its centreline as presented in test IV of the forward problem. Ablation/accumulation values over 33 years from 1961-1993 along with 1993 measured free surface are considered for the reconstruction process. A time step of 1 year is used and steady results are generated after 300 years of computation time. For the first 33 years of the computation, actual ablation/accumulation time series are used, however, for the rest of the computational time an average value is used. This is due to the fact that there is no available data for the rest of the computational time.

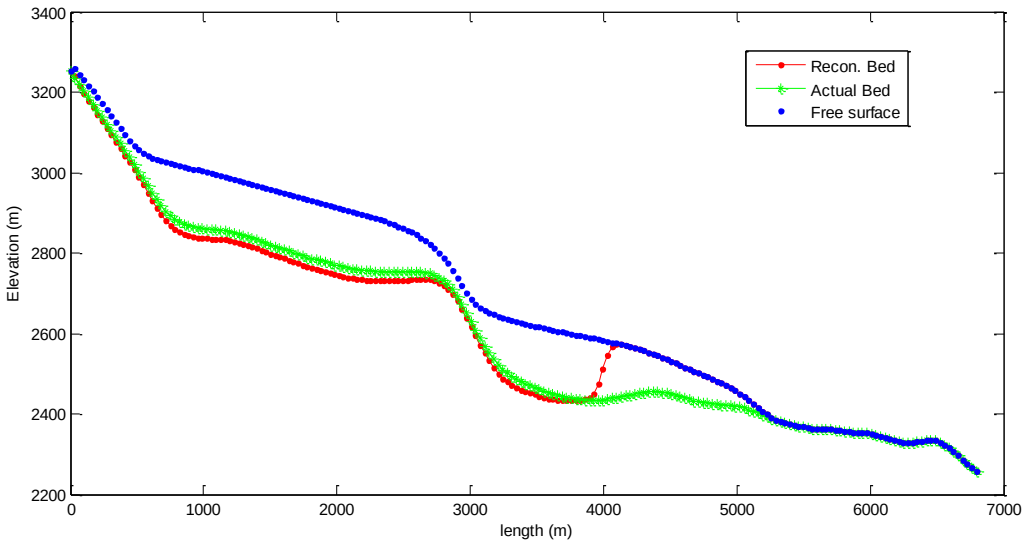


Figure 8.15: Comparison of the actual and reconstructed bedrock of Gries glacier

The results show good agreement in most parts of the computational domain; however the methodology ceased to reconstruct at the downstream end of the flow, Figure 8.15. This is due to the use of average ablation/accumulation value for the computation. If yearly average ablation/accumulation time series profiles were known for the full period of computational time, the approach would generate a good reconstruction. This is well addressed in the canonical test cases used above.

The analytical and the numerical approaches for the reconstruction process require accurate values of the glacier surface elevation and the mass balance distribution. There are some restrictions for the analytical bedrock reconstruction approach. These restrictions include that the annually averaged ablation/accumulation distribution should change very little over longer period of time, the depth of the glacier at any arbitrary location should be known prior to computation, and the analytical approach is valid for frozen glaciers where the sliding coefficient can effectively be neglected.

The numerical solution approach, as mentioned in the experimental test cases of the inverse problem, requires accurate accumulation/ablation over the period of computation. This may require the use of climate prediction tools to forecast the mass balance over the surface of the glacier over the years if possible.

## 8.4. Concluding remarks

New numerical and analytical algorithms to reconstruct the bedrock of glaciers from the free surface elevation in the context of one-dimensional SIA are presented. For the purpose of numerical verification of the inverse problem, the forward problem is solved using an explicit central difference technique. The reconstruction approaches are easy-to-implement and have the potential to overcome the shortcomings of traditional PDE-constrained optimization based reconstruction techniques, i.e. for quasi-steady glaciers.

The analytical approach is based on the steady SIA equation. It requires information of the depth at an arbitrary point on the glacier, the value of ablation/accumulation coefficients along with the boundary conditions. This approach is tested on the canonical experiment resulted from the forward problem. This approach works well for the ablation/ accumulation of glaciers that change slowly with time. This due to the fact that the

analytical solution approach is based on the steady SIA equation and thus the time dependency of ablation/accumulation coefficient is not accommodated.

To overcome the restrictions of the analytical approach, a numerical solution approach is also presented. This numerical approach is fully implicit to overcome the unstable nature of the SIA equation. The approach is a direct numerical technique which solves for the depth of the glacier from the given free surface elevation data and boundary conditions. Unlike the analytical approach, this approach requires the time series of the ablation/accumulation values in the computational domain. However, the ablation/accumulation time series should not be necessary slowly changing.

The numerical algorithm is tested against canonical and experimental test cases. Results show that, there is good agreement between the actual and reconstructed bedrock topographies in most of the test cases where accurate time series of the accumulation/ablation coefficients are available. In the reconstruction of the Gries glacier bedrock, the lack of full time series of ablation/accumulation coefficients results in the discrepancy of the results in the lower end of the glacier. To generate an accurate time series of the mass balance, a climate model to forecast the temperature and precipitation at the glacier surface could be used in future studies.

# 9. Conclusion

## Contents

## 9.1. Summary

This thesis explored the application of direct numerical reconstruction techniques to infer bed topography from known free surface data in geophysical flows, specifically open channel and glacier flows. Details of the key outcomes of the research are summarized below.

Easy to implement and efficient direct numerical and pseudo-analytical reconstruction algorithms are developed to infer the channel bed topographic elevation from known free surface elevation data for one-dimensional steady shallow water flows. The algorithms utilize one-dimensional shallow water equations along with the required boundary conditions and parameters, i.e. in addition to the free surface elevation data, the algorithms require the steady flow rate, the depth of the flow at the inlet, and the bed roughness for subcritical flows. Transcritical flows require an additional value of flow depth at the outlet boundary. It is found that the governing equations of the forward and the inverse problems are similar in form, which allows for the use of a similar discretization procedure for both problems. This gives a major advantage compared to conventional inverse problem methodologies based on PDE-constrained optimization which can lead to complex formulations and implementations. One-dimensional benchmark test cases are used to validate the algorithm and it is found that the one-dimensional algorithm works well and the results show that the underlying bed topography is reconstructed from noise-free and noisy free-surface data with only a small amplification of noise. The noise affects the reconstructed bed topography, confirming that in shallow water flows the free surface is sensitive to the bed topography and vice versa.

Experimental measurement of bed topographic elevation data is complex, time consuming, and costly. However, the measurement of free surface data (free surface elevation data and free surface velocity) is relatively easier. A numerical algorithm that utilizes the measured free surface velocity data to reconstruct the bed topography for one-dimensional shallow water flows is presented in this thesis. The algorithm requires that the steady state flow rate is known along with the flow depth at one location and the channel roughness value. Also the relationship between the free surface velocity and the depth-averaged velocity needs to be known. The value of the relationship can be determined from the flow conditions. The results show that when there is a hydraulic jump in the flow, deviations between the actual and the reconstructed beds is observed to be higher than that of the deviations in the case of subcritical flows where the bed is reconstructed with minimal error. The numerical approach is based on the one-dimensional steady version of the shallow water equations which can be integrated to obtain an integral equation explicitly which gives the bed topography as a function of the depth-averaged or free surface velocity. A simple marching method along with the trapezoidal rule is used to solve this integral equation. One particular advantage of this integral formulation is that noise in the input data, i.e. the free surface velocity, will not be amplified by the reconstruction approach. Its applicability is demonstrated on a range of benchmark problems. The good agreement between the reconstructed and actual bed forms even for mildly noisy experimental data indicate the “well-posed” behaviour of the proposed technique.

The idea of bed topography reconstruction from known free surface elevation data in one-dimensional flows is extended to the two-dimensional flow case where two algorithms are developed: one for a zero-inertia two-dimensional flow and the other for full two-dimensional shallow flows with the inertia term included.

1. The zero-inertia, two-dimensional shallow water equations govern open channel flows having dominant roughness values and steep beds where the effect of inertia can be conveniently neglected. A new governing equation for the inverse problem is derived from the mass conservation and momentum equations of the zero-inertia shallow water equations. This equation relates the free surface and the bed topography elevation of shallow waters flow in an open channel.

   The MacCormack solution methodology is adopted to determine the free surface profile for the forward problem analysis, while the inverse problem is solved by using the method of characteristics to reconstruct the channel bed topography from known free surface elevation data. Interestingly, unlike the reconstruction algorithm implemented for one-dimensional shallow water flow, the analysis shows that knowledge of the channel bed roughness is not required for the reconstruction algorithm. This is because the Manning's roughness coefficient disappears in the reformulation of the governing equations and it is only required if the velocity field is required to be determined. However, determination of velocity fields is not necessary as the modified governing equation of the inverse problem allows a computation of depth of the flow without the simultaneous calculation of the velocity field which reduces the computational effort of the algorithm.

   The reconstruction algorithm provides the depth of the flow along the characteristic curves in the computational domain from the given free surface elevation data and depth at the inlet boundary. The canonical test case results show good agreement between the reconstructed and actual bed forms. The algorithm handles the introduction of noise in the free surface data and results show no noise amplification. This proves the robustness of the implemented approach.

2. The full two-dimensional shallow water equations are used to reconstruct channel bed topographic elevation from known three-dimensional free surface elevation data. The methodology implemented is based on an explicit finite difference scheme and requires a steady flow rate, knowledge of the roughness coefficient, and the depth of the flow at the inlet boundary in addition to the free surface elevation data.

   The algorithm is tested on a set of benchmark test cases and encouraging results are found. The bed topography is well reconstructed with a deviation of 3% or less. The numerical methodology is easy-to-implement and produces a fast solution but has a CFL restriction because of its explicit nature.

   In practice, the measured free surface contains noise. The presented methodology is found to be capable of reconstructing the channel bed topography from noisy data. When tested on a set of noisy numerical data, the methodology was found to introduce no noise amplification in all test cases considered.

The reconstruction algorithms developed for open channel flows are suitable for steady open channel flows for which the shallow water approximation holds where the signal due to the existence of the underlying bed topography is captured by the free surface measurement technique. All approaches, except the one for the zero-inertia case, require information of the steady flow rate, bed roughness and flow depth at the boundary. While the algorithm developed for the zero-inertia shallow water flow only requires the depth of the flow at the upstream boundary. These approaches fall in the category of the very few inverse problems which are one-shot, easy to implement, fast, accurate, and direct approaches which make them dominant over the conventional PDE-constrained optimization based approaches which call for relatively higher computational cost.

However, the direct approach is not always possible for all inverse problems. The form of the governing equations and the nature of the parameters dictate its appropriateness.

Finally, analogous to the approaches developed for the inverse problem of shallow water flows, new numerical and analytical algorithms to reconstruct the bedrock of glaciers from the free surface elevation in the context of one-dimensional shallow ice approximation are developed. The reconstruction approaches are easy-to-implement and have the potential to overcome the shortcomings of traditional PDE-constrained optimization based reconstruction techniques. The analytical approach requires a depth value at an arbitrary point on the glacier and the value of ablation/accumulation coefficients along with the boundary conditions. The analytical approach does not accommodate the time dependency of the ablation/accumulation coefficient. To overcome this, a fully implicit numerical solution approach is developed to accommodate time dependency of ablation/accumulation coefficients. The numerical algorithm is tested against canonical and experimental test cases. Results show that there is good agreement between the actual and reconstructed bedrock topographies in most of the test cases where accurate time series of the accumulation/ablation coefficients were available. In the reconstruction of the Gries glacier bedrock, the lack of a full time series of ablation/accumulation coefficients results in discrepancies in the results at the lower end of the glacier.

## 9.2. Suggestions for future work

The developed algorithms presented in this thesis would benefit from further investigation. The following aspects are suggested for future work.

1. Development of a two-dimensional reconstruction algorithm using known free surface velocity to infer the underlying bed topographic elevation data using two-dimensional shallow water equations.
2. The numerical test cases presented in part-I are mostly canonical, thus further investigation based on real experimental free surface data would have significant relevance.
3. The use of channel bed roughness for reconstruction algorithms as well as for forward problems is paramount. Thus, algorithms to infer channel bed roughness from measureable quantity in shallow water flows would be of great importance.
4. Development of two-dimensional reconstruction algorithms from known free surface elevation data to infer the underlying bedrock elevation data for two-dimensional glaciers.

# References


1. J.C. McWilliams, *Fundamentals of Geophysical Fluid Dynamics*. 2006, Los Angeles: Cambridge University Press.
2. D.R. Montgomery, K.M. Schmidt, W.E. Dietrich, and J. McKean, *Instrumental record of debris flow initiation during natural rainfall: Implications for modeling slope stability.* Journal of geophysical research, 2009. **114**.
3. R.H. Norris and M.C. Thomas, *What is river health?* Freshwater biology, 1999. **41**: p. 197-209.
4. M. Acreman and M.J. Dunbar, *Defining environmental river flow requirements - a review.* Hydrology and Earth System Sciences 2004. **8**(5): p. 861-876.
5. J.A. Cunge, F.M. Holly, and A. Verwey, *Practical aspects of computational river hydraulics*. 1980, London: Pitam Publishing.
6. M.H. Chaudhry, *Open-channel flow*. 2 ed. 2007, New York: Springer.
7. R.C. Hilldale and D. Raff, *Assessing the ability of airborne LiDAR to map river bathymetry.* Earth Surface Processes and Landforms, 2008. **33**: p. 773-783.
8. K. Marks and P. Bates, *Integration of high-resolution topographic data with floodplain flow models.* Hydrological Processes 2000. **14**: p. 2109 - 2122.
9. R.M. Westaway, S.N. Lane, and D.M. Hicks, *The development of an automated correction procedure for digital photogrammetry for the study of wide, shallow, gravel-bed rivers.* Earth Surface Processes and Landforms, 2000. **25**: p. 209-225.
10. H. Roux and D. Dartus. *Estimating hydraulic parameters and geometric characteristics of a river from remote sensing data using optimization methods* in *The Second International Conference on Fluvial Hydraulics* 2004. Napoly, Italy A. A. BALKEMA.

11. R.M. Westaway, S.N. Lane, and D.M. Hicks, *Remote sensing of clear-water, shallow, gravel-bed rivers using digital photogrammetry.* Photogrammetric Engineering & Remote Sensing, 2001. **67**(11): p. 1271-1281.
12. Y. Hirose and Y. Imai, *Airborne remote sensing for river environmental assessment* The International Archives of the Photogrammetry, Remote Sensing and Spatial Information Sciences, 2008. **37**: p. 1149-1152.
13. K. Hutter, *Theoretical Glacieology*. 1983, Dordrecht: D. Reidel Publishing Company.
14. J. Oerlemans, B. Anderson, A. Hubbard, P. Huybrechts, T. Johannesson, W.H. Knap, M. Schmeits, A.P. Stroeven, R.S.W. vandeWal, J. Wallinga, and Z. Zuo, *Modelling the response of glaciers to climate warming.* Climate Dynamics, 1998. **14**: p. 267-274.
15. J. Oerlemans, *Glaciers and climate change*. 2001, Tokyo: Balkema
16. D. Farinotti, *Simple methods for inferring glacier ice-thickness and snow-accumulation distribution*. 2010, ETH ZURICH.
17. D. Farinotti, M. Huss, A. Bauder, M. Funkand, and M. Truffe, *A method to estimate ice volume and ice-thickness distribution of alpine glaciers.* Journal of Glaciology, 2009. **55**(191): p. 422-430.
18. P. Huybrechts and T. Payne, *The EISMINT benchmarks for testing ice-sheet models.* Annals of Glaciology, 1996. **23**.
19. M. Schäfer, O. Gagliardini, F. Pattyn, and E.L. Meur, *Applicability of the Shallow Ice Approximation inferred from model inter-comparison using various glacier geometries.* The Cryosphere Discussions, 2008. **2**: p. 557-599.

20. E.L. Christensen, N. Reeh, R.Forsberg, J.H. Jorgensen, N. Skou, and W. Woelders, *A low-cost glacier-mapping system.* Journal of Glaciology 2000. **46**(154): p. 531-537.

21. K. Keller, G. Casassa, A. Rivera, R. Forsberg, and N. Gundestrup, *Airborne laser altimetry survey of Glaciar Tyndall, Patagonia.* Global and Planetary Change 2007. **59**: p. 101-109.

22. T.W. Sturm, *Open Channel Hydraulics*. McGraw-Hill Series in Water Resources and Environmental Engineering. 2001: McGraw-Hill Higher Education.

23. R.H. Frénch, *Open-channel hydraulics*. 1985, New York: McGraw-Hill.

24. H. Roux and D. Dartus, *Sensitivity analysis and predictive uncertainty using inundation observations for parameter estimation in open-channel inverse problem.* Journal of Hydaulic Engineering, 2008 **134**: p. 541-549.

25. M. Honnorat, J. Monnier, and F.-X. LeDimet, *Lagrangian data assimilation for river hydraulics simulations.* Computing and Visualization in Science, 2009. **12**: p. 235-246.

26. W. Castaings, D. Dartus, M. Honnorat , F.X. LeDimet, and Y. Loukili, *Automatic differentiation: a tool for variational data assimilation and adjoint sensitivity analysis for flood modelling* Lecture Notes in Computational Sciences 2006 **50**( 249-262 ).

27. R.L. Hooke, *Principles of Glacer Mechanics* Second ed. 2005, New York: Cambridge University Press.

28. A. Mangeney and F. Califano, *The shallow ice approximation for anisotropic ice-formulation and limits.* Journal of geophysical research, 1998. **103**: p. 691-705.

29. J. VanDenBerg, R.S.W. VanDeWAL, and J. Oerlemans, *Effects of spatial discretization in ice-sheet modelling using the shallow-ice approximation.* Journal of Glaciology, 2006. **52**(176): p. 89-98.

30. E. LeMeur, O. Gagliardini, T. Zwinger, and JuhaRuokolainen, *Glacier flow modelling: a comparison of the Shallow Ice Approximation and the full-Stokes solution.* Comptes Rendus Physique, 2004. **5**: p. 709-722.

31. O. Soucek and Z. Martinec, *Iterative improvement of the shallow-ice approximation.* Journal of Galciology, 2008. **54**(188): p. 812-822.

32. M. Schäfer and E. LeMeur, *Improvement of a 2-D SIA ice-flow model: application to Glacier de Saint-Sorlin, France.* Journal of Galciology, 2007. **53**(183): p. 713 - 723.

33. M. Schäfer and E. LeMeur. *A new numerical scheme for a two-dimensional shallow ice-flow model applied to an alpine glacier*. in *Geophysical Research Abstracts*. 2006.

34. A.H. Jarosch and C.G. Schoof. *A new shallow ice scheme for alpine glaciers*. in *European Geosciences Union. General Assembly 2009*. 2009. Vienna, Austria.

35. L. Michel, M. Picasso, D. Farinotti, A. Bauder, M. Funk, and H. Blatter, *Estimating the ice thickness of mountain glaciers with an inverse approach using surface topography and mass-balance.* Inverse Problems, 2013. **29**(3).

36. D.N. Goldberg and O.V. Sergienko, *Data assimilation using a hybrid ice flow model.* The Cryosphere, 2011. **5**: p. 315-327.

37. P. Hiembach and V. Bugnion, *Greenland ice-sheet volume sensitivity to basal, surface and initial conditions derived from an adjoint model.* Annals of Glaciology 2009. **50**(52): p. 67-80.

38. A. Tarantola, *Inverse problem theory and methods for model parameter estimation*. 2005, Society for Industrial and Applied Mathematics: Philadelphia p. 342.

39. G.M. Smart, J. Bind, and M.J. Duncan. *River bathymetry from conventional LiDAR using water surface returns* in *18th World IMACS/MODSIM Congress*. 2009. Cairns, Australia.

40. E.D. Zaron, M.-A. Pradal, P.D. Miller, A.F. Blumberg, N. Georgas, W. Li, and J.M. Cornuelle, *Bottom Topography Mapping via Nonlinear Data Assimilation.* Journal of Atmospheric and Oceantic Technology 2011. **28**: p. 1606-1622.

41. M. Honnorat, J. Monnier, N. Rivière, É. Huot, and F.-X. LeDimet, *Identification of equivalent topography in an open channel flow using Lagrangian data assimilation.* Computing and Visualization in Science, 2010. **13**(3): p. 111-119

42. W. Cheng and G. Liu, *Analysis of nonlinear channel friction inverse problem.* Frontiers of Architecture and Civil Engineering in China, 2007. **1**(2): p. 205-210.

43. H.T. Nguyen and J.D. Fenton, *Identification of Rouhgness in Open Channels* Advances in Hydro-Science and Engineering, 2004. **VI**.

44. H.T. Nguyen and J.D. Fenton. *Identification of Roughness for Flood Routing in Compound Channels*. in *31st IHAR Congress, International Association of Hydraulic Engineering and Research*. 2005. Seoul Korea.

45. M.T. Ayvaz and Ö. Genç. *Optimal Estimation of Manning's Roughness in Open Channel Flows Using a Linked Simulation-Optimization Model*. in *BALWOIS 2012* 2012. Ohrid, Republic of Mecedonia.

46. R. Ramesh, B. Datta, S.M. Bhallamudi, and A. Narayana, *Optimal Estimation of Roughness in Open-Channel Flows.* Journal of Hydraulic Engineering, 2000. **126**(4).

47. Y. Ding and S.S.Y. Wang, *Identification of Manning's roughness coefficients in channel network using adjoint analysis.* International Journal of Computational Fluid Dynamics, 2005. **19**(1): p. 3-13.

48. R. Hostache, X. Lai, J. Monnier, and C. Puech, *Assimilation of spatially distributed water levels into a shallow-water flood model. Part II: Use of a remote sensing image of Mosel River.* Journal of Hydrology and Hydromechanics, 2010. **390**: p. 257-268.

49. H. Abida, *Identification of compound channel flow parameters.* Journal of Hydrology and Hydromechanics 2009. **57**(3): p. 172-181.

50. M. Sellier, *Substrate design or reconstruction from free surface data for thin film flows.* Physics of Fluids, 2008. **20**(6).

51. M. Sellier and S. Panda, *Beating capillarity in thin film flows.* International journal for numerical methods in fluids 2009. **63**: p. 431-448.

52. C. Heining and N. Aksel, *Bottom reconstruction in thin-film flow over topography: Steady solution and linear stability.* Physics of Fluids, 2009. **21**.

53. C. Heining, *Velocity field reconstruction in gravity-driven flow over unknown topography.* Physics of Fluids, 2011. **23**.

54. M.S. Horritt, *Stochastic modelling of 1-D shallow water flows over uncertain topography.* Journal of Computational Physics 2002. **180** p. 327-38.

55. C.J. Legleiter and P.C. Kyriakidis, *Spatial prediction of river channel topography by kriging.* Earth Surface Processes and Landforms, 2008. **33** p. 841-867.

56. X. Ying, A.A. Khan, and S.S.Y. Wang, *Upwind conservative scheme for the Saint Venant equations.* journal of hydraulic engineering 2004. **130**(10): p. 977-987.

57. A. Saint-Venant, *Theorie du mouvement non permanent des eaux, avec application aux crues des rivieres et a l'introduction de marees dans leurs lits.* Comptes rendus des seances de l'Academie des Sciences, 1871.

58. P. Novak, V. Guinot, A. Jeffrey, and D.E. Reeve, *Hydraulic Modelling- an introduction principles, methods and applications*. 2010, London: Spon Press.

59. C. Aricò and T. Tucciarelli, *A marching in space and time (MAST) solver of the shallow water equations. Part I: the 1 D model* Advances in Water Resources, 2007. **30**: p. 1236-1252.

60. C. Hirsch, *Numerical computation of internal and external flows. Volume 1: Fundamentals of computational fluid*

*dynamics*. Second ed. 2007: John Wiley & Sons, Ltd.

61. J.-M. Hervouet, *Hydrodynamics of Free Surface Flows: Modelling with the Finite Element Method* 2007, Chichester: John Wiley & Sons.

62. *HEC-RAS (The Hydraulic Engineering Center River Analysis System)*. Available from: http://www.hec.usace.army.mil/software/hec-ras/.

63. P. Bates, M. Horritt, M. Wilson, and N. Hunter, *LISFLOOD-FP User manual and technical note* in *code release 2.6.2*. 2005, University of Bristol.

64. Hydronia. *RiverFLO-2D*. Available from: http://www.hydronia.net/.

65. Halcrow. *ISIS*. Available from: http://www.halcrow.com/isis/isisfree.asp.

66. Y. Sadi, *One-Dimensional Hydrodynamic Modelling for River Flood Forecasting.* Civil Engineering Dimension 2008. **10**(1).

67. M. Hicks, R. Westaway, and S. Lane, *A bird's-eye assessment of gravel movement in large braided rivers.* Water & Atmosphere 2003. **11**(1).

68. R.J. Connell, D.J. Painter, and C. Beffa, *Two-dimensional flood palin flow. II; Model validation* Journal of Hydraulic Engineering, 2001: p. 406-415.

69. M.S. Horritt and P.D. Bates, *Evaluation of 1D and 2D numerical models for predicting river flood inundation.* Journal of Hydrology 2002. **268**: p. 87-99.

70. W. Wu, *Computational River Dynamics* 2007: Taylor & Francis

71. M.J. Castro-Diaz, E.D. Fernandez-Nieto, and A.M. Ferreiro, *Sediment transport models in Shallow Water equations and numerical approach by high order finite volume methods.* Computers & Fluids, 2008. **37**: p. 299-316.

72. M. Honnorat, J. Marin, J. Monnier, and X. Lai, *DassFlow v1.0: a variational data assimilation software for 2D river flows*. 2007, Institut National de Recherche en Informatique et en Automatique (INIRA)

73. R.A. Yahia-Djouadi, D. Hernane-Boukari, and D. Teniou, *A study of the inverse of a free surface problem.* Abstract and Applied Analysis, 2005. **2005**( 2): p. 159-171.

74. Q. Liang and A.G.L. Borthwick, *Adaptive quadtree simulation of shallow flows with wet-dry fronts over complex topography.* Computers & Fluids 2009. **38**: p. 221-234.

75. Y. Xing and C.-W. Shu, *High order finite dierence WENO schemes with the exact conservation property for the shallow water equations.* Journal of Computational Physics, 2005. **208**: p. 206-227.

76. D.E. Alsdorf and D.P. Lettenmaier, *Tracking fresh water from space.* Science, 2003. **301**: p. 1491-1494.

77. D.E. Alsdorf, E. Rodriguez, and D.P. Lettenmaier, *Measuring surface water from space.* Reviews of Geophysics, 2007. **45**(2).

78. L.C. Smith and T.M. Pavelsky, *Estimation of river discharge, propagation speed, and hydraulic geometry from space: Lena River, Siberia.* Water Resource Research, 2008. **44**.

79. P.Y. Julien, *River mechanics*. 2002, New York: Cambridge University Press

80. W.J. Plant, W.C. Keller, K. Hayes, and K. Spicer, *Streamflow properties from time series of surface velocity and stage.* Journal of Hydraulic Engineering 2005. **131**: p. 657-664.

81. J.-S. Lee and P.Y. Julein, *Electromagnetic wave surface velocimetry.* Journal of Hydraulic Engineering, 2006. **132**: p. 146-153.

82. M. Muste, J. Schöne, and J.-D. Creutin, *Measurement of free-surface flow velocity using controlled surface waves.* Flow Measurment and Instrumentation, 2005. **16**: p. 47-55.

83. V. Weitbrecht, G. Kühn, and G.H. Jirka, *Large scale PIV-measurements at the surface of shallow water flows.* Flow Measurement and Instrumentation 2002. **13**: p. 237-245.

84. M. Muste, I. Fujita, and A. Hauet, *Large-scale particle image velocimetry for measurements in riverine environments.* Water Resource Research, 2008. **44**.

85. N.-S. Cheng, *Power law index for velocity profiles in an open channel flows.* Advances in Water Resources, 2007. **30**: p. 1775-1784.

86. H. Chanson, *The hydraulics of open channel flows: an introduction - basic principles, sediment motion, hydraulic modelling, design of hydraulic structures*. 2nd ed. 2004, Burlington: Elsevier Butterworth-Heinemann.

87. H. Bonakdari, F. Larrarte, L. Lassabatere, and C. Joannis, *Turbulent velocity profile in fully developed open channel flows.* Environmental Fluid Mechanics, 2008. **8**: p. 1-17.

88. S.-Q. Yang, W.-L. Xu, and G.-L. Yu, *Velocity distribution in a gradually accelerating free surface flow.* Advances in Water Resources, 2006. **29**: p. 1969-1980.

89. S.-Q. Yang, S.-K. Tan, and S.-Y. Lim, *Velocity distribution and dip-phenomenon in smooth uniform open channel flows.* Journal of Hydaulic Engineering 2004. **130**: p. 1179-1186.

90. C.-L. Chiu and C.A. Abidin-Said, *Maximum and mean velocities and entropy in open-channel flow,.* Journal of Hydaulic Engineering, 1995. **121**: p. 26-35.

91. S. Nikmehr and J. Farhoudi, *Estimation of velocity profile based on Chiu's equation in width of channels.* Research Journal of Applied Sciences, Engineering and Technology, 2010. **2**: p. 476-479.

92. C. Polatel, *Large-scale roughness effect on free-surface and bulk flow characteristics in open-channel flows*, in *Civil and Environmental Engineering* 2006, University of Iowa.

93. R. Balachandar, K. Hagel, and D.Blakely, *Velocity distribution in decelerating flow over rough surfaces.* Canadian Journal of Civil Engineering, 2002. **29**: p. 211-221.

94. M.N. Hunter, D.P. Bates, S.M. Horritt, and D.M. Wilson, *Simple spatially-distributed models for predicting flood inundation: A review.* Geomorphology, 2007. **90**: p. 208-225.

95. J.M. Shultz, C.E. Crosby, and A.J. McEnery, *Kinematic wave technique applied to hydrologic distributed modeling using stationary storm events: an application to synthetic rectangular basins and an actual watershed.* Hydrology days, 2008: p. 116-126.

96. R.M. Li, B.D. Simons, and A.M. Stevens, *Nonlinear kinematic wave approximation for water routing.* Water Resource Research, 1975. **11**(2): p. 245-252.

97. T. Moramarco, C. Pandolfo, and P.V. Singh, *Accuracy of kinematic wave and diffusion wave approximations for flood routing. I: Steady analysis.* Journal of Hydaulic Engineering, 2008. **13**(11): p. 1089-1096.

98. A.W. Heemink, E.E.A. Mouthaan, M.R.T. Roest, E.A.H. Vollebregt, K.B. Robaczewska, and M. Verlaan, *Inverse 3D shallow water flow modelling of the continental shelf.* Continental Shelf Research, 2002. **22**(3): p. 465-484.

99. F.M. Henderson, *Open channel flow*. 1966, New York: Macmillan.

100. A.P. Willsman, T. Chinn, J. Hendrikx, and A. Lorrey, *New Zealand Glacier Monitoring: End of Summar Snowline Survey 2010*. 2010, National Institute of Water & Atmospheric Research Ltd (NIWA): Christchurch, New Zealand

101. A. Bauder, C. Frei, M. Funk, M. Hoelzle, M. Huss, G. Kappenberger, and F. Paul, *The Swiss Glaciers 2003/2004 and 2004/2005 Glaciological Report*, A. Bauder and R. Ruegg, Editors. 2009: Zurich, Switzerland. p. 41-44.

102. F. Pattyn, *A new three-dimensional higher-order thermomechanical ice sheet model: Basic sensitivity, ice stream development, and ice flow across sub glacial lakes.* Journal of Geophysical research, 2003. **108**(B8).

103. Elmer. *Elmer Manuals* 2006; Available from: http://www.csc.fi/english/pages/elmer.

104. A. Fowler, *Mathematical Geoscience (Interdisciplinary Applied Mathematics)*. 2011, New York: Springer.

105. D.R. Baral, K. Hutter, and R. Greve, *Asymptotic theories of large-scale motion, temperature, and moisture distribution in land-based polythermal ice sheets: A critical review and new developments.* Applied Mechanics Reviews 2001. **54**(3): p. 215-257.

106. E. LeMeur and C. Vincent, *A two-dimensional shallow ice-flow model of Glacier de Saint-Sorlin, France.* Journal of Galciology 2003. **49**(167): p. 527-538.

107. A.E. Racoviteanu, M.W. Williams, and R.G. Barry, *Optical Remote Sensing of Glacier Characteristics: A Review with Focus on the Himalaya.* Sensors, 2008. **8**: p. 3355 - 3383.

108. C. Heining, M. Sellier, and N. Aksel, *The inverse problem in creeping film flows* Acta Mechanica, 2012. **3**.

109. M. Picasso, J. Rappaz, A. Reist, M. Funk, and H. Blatter, *Numerical simulation of the motion of a two dimensional glacier.* International journal for numerical methods in engineering, 2000.

110. C. Vincent, M. Vallon, L. Reynaud, and E.L. Meur, *Dynamic behaviour analysis of glacier de Saint Sorlin, France, from 40 years of observations, 1957-97.* Journal of Galciology, 2000. **46**(154): p. 499-506.

111. IAHS/UNESCO, *Fluctuations of Glaciers 1990-1995 Volume VII*. 1998: Zurich: World Glacier Monitoring Service.